

Z (1996)

MICHIGAN STATE UNIVERSITY LIBRARIES

This is to certify that the

dissertation entitled

Nonlinear Optical Studies of Polydiacetylenes

presented by

Selezion Afeworki Hambir

has been accepted towards fulfillment of the requirements for

Ph.D. degree in Analytical Chemistry

Date September 26, 1995

LIBRARY Michigan State University

PLACE IN RETURN BOX to remove this checkout from your record. TO AVOID FINES return on or before date due.

	DATE DUE	DATE DUE
MON O S TENS		
MAGIC 2 AR 2 8 1999		
DEC WAY 2801 20	5	

MSU is An Affirmative Action/Equal Opportunity Institution excited stated as pm3-p.1

NONLINEAR OPTICAL STUDIES OF POLYDIACETYLENES

By

Selezion Afeworki Hambir

A DISSERTATION

Submitted to
Michigan State University
in partial fulfillment of the requirements
for the degree of

DOCTOR OF PHILOSOPHY

Department of Chemistry

1995

ABSTRACT

NONLINEAR OPTICAL STUDIES OF POLYDIACETYLENES

by

Selezion Afeworki Hambir

The main objective of this dissertation is the investigation of conjugated polymers as potential photonic switching materials. Present day information transfer is done by means of electronic signal processing. Faster information transfer will require replacement of electrons with photons as information carrying units. Such an application requires efficient switching devices and an efficient switching techniques. Polydiacetylenes (PDAs) are promising candidate photonic switching materials because of their large third order nonlinear optical response. Before these materials can be incorporated into optical switching devices, their energy relaxation pathways and ability to be processed into devices has to be investigated.

This dissertation is composed of two parts. The first part (chapters 2 & 3) were conducted to evaluate the feasibility of storing energy in a polydiacetylene with carbazole side groups, PDA-DCHD. Polydiacetylene DCHD was studied both at 300K and 10K and we found that energy deposited on the side groups migrates rapidly (<10ps) to the PDA backbone. Relaxation of this excitation has the same spectral and temporal signatures as relaxation of the backbone excitonic resonance. Comparison of these data to the electroabsorption response of DCHD confirms excitation transfer rather than charge transfer. This energy transfer is consistent with a Förster through-space mechanism. At

low temperature the slow population recovery signal seen subsequent to excitation transfer to the polymer backbone shows an excitation energy dependence that is indicative of the existence of different conformers under the excitonic envelope. Thus, long term optical energy storage in PDAs does not appear to be feasible.

The second part of this thesis (chapters 4 & 5) was conducted to investigate systematically how the nonlinear optical response of the polydiacetylene poly(4BCMU) varies as its morphology is adjusted from crystalline to highly disordered materials. A pump-probe method of accessing $\chi^{(3)}$ which makes use of the large linear absorption of the conjugated polymers was developed. This nondegenerate wave mixing technique (inverse Raman spectroscopy) is very sensitive to subtle chemical structure and thus provides opportunity to investigate a novel switching scheme by altering polymer morphology. The magnitude of $\chi^{(3)}$ is related to the oscillator strength of the exciton that dominates the absorption edge in PDAs and our pump-probe measurement scheme couples vibrational modes to the exciton to enhance the nonlinear optical response. The dynamic Stark effect has been measured both in the crystalline form of poly(4BCMU) and in films possessing varying degrees of disorder. The macroscopic alignment of the polymer chain in these films is controlled by stretch orientation. After characterizing the linear optical properties of these materials, the coupling between the vibrational and electronic structure of these systems was measured using stimulated inverse Raman Scattering. In PDAs disorder can be used to enhance the nonlinear response by a factor of ~2 per chromophore unit. Stretch orientation of disordered films aligns individual chromophores and thereby a nonlinear response comparable to that of the highly ordered crystalline polymer can be achieved.

Acknowledgments

I would like to thank my advisor, Dr. Gary J. Blanchard for his valuable advice, patience and time he took to walk me through the tough experiments and most of all for maintaining friend-friend type of relationship during my graduate career. I would also like to extend my sincere gratitude to my committee members Dr. G. T. Babcock, Dr. J. S. Ledford and G. L. Baker. Special thanks goes to Dr. G. L. Baker for providing me with all the polymers I needed for this project. My thanks also go to the members of the Blanchard group, past and present. I really enjoyed working with you, and wish all the best of luck in what you do. I wish to thank the people in the machine shop and electronic shop for their efficient and prompt reply to my needs. My special thanks go to Tom Carter for helping me with computer whenever I am stuck. Finally, I would like to thank my brothers, sisters and friends for their understanding, support and love.

To:

Eritrean martyrs.

TABLE OF CONTENTS

LIST OF TABLES	ix
LIST OF FIGURES	x
INTRODUCTION	1
Chapter 1. SYNCHRONOUS PUMPING OF TWO DYE LASERS USING A SINGLE UV EXCITATION SOURCE	9
1.1. Introduction	10
1.2. Experimental	11
1.2.1. Source laser	11
1.2.2. Dye lasers	12
1.2.3. Time domain measurements	12
1.2.4. Frequency domain measurements	13
1.3. Results and Discussion	14
1.4. Conclusions	22
1.5. Literature Cited	23
Chapter 2. EXCITATION MIGRATION IN THE	
POLYDIACETYLENE DCHD	25
2.1. Introduction	26
.2. Experimental	29
2.3. Results and Discussion	31
2.4. Conclusion	42
2.5. Literature Cited	43

Chapter	3. LOW TEMPERATURE TRANSIENT OPTICAL SPECTROSCOPY OF POLYDIACETYLENE DCHD. EVIDENCE FOR A DISTRIBUTION	A L
	OF SIDE GROUP ORIENTATIONS	45
	3.1. Introduction	46
	3.2. Experimental	47
	3.2.1. Materials and temperature control	47
	3.2.2. Pump-probe spectroscopy	48
	3.3. Results and Discussion	50
	3.4. Conclusion	61
	3.5. Literature Cited	62
Chapter	4. DISORDER INDUCED ENHANCEMENT OF	
	THE THIRD ORDER OPTICAL NONLINEAR	
	IN A CONJUGATED POLYMER	64
	4.1. Introduction	65
	4.2. Theory	69
	4.3. Experimental	73
	4.3.1. Laser spectroscopy	73
	4.3.2. Material processing	75
	4.4. Results and Discussion	76
	4.5. Conclusion	90
	4.6. Literature Cited	91
Chapter	5. THE EFFECT OF STRETCH ORIENTATION	I
	ON THE LINEAR AND NONLINEAR OPTICA	AL
	RESPONSE OF POLY(4-BCMU) FILMS	93
	5.1. Introduction	94
	5.2. Experimental	95
	5.2.1. Nonlinear laser spectroscopy	95
	5.2.2. Linear spectroscopy	96
	5.2.3. Material processing	96
	5.2.4. Substrate	97
	5.3. Results and Discussion	98
	5.4. Conclusion	125
	5.5 Literature Cited	126

Chapter 6. FEASIBILITY STUDY OF DEGENERATE	
FOUR WAVE MIXING	129
6.1. Introduction	130
6.2. Experimental	132
6.3. Discussion	
6.3.1. Unit Conversions	134
6.3.2. Magnitude of the Expected Signal	135
6.3.3. Expected Signal to Noise Ratio	137
6.4. Literature Cited	139
Chapter 7. SUGGESTED FUTURE STUDIES	140
Literature Cited	142

LIST OF TABLES

Table 1.1.	Output parameters of stilbene and coumarin dye lasers modeled by the noise burst model.	17
Table 1.2.	Cross correlation widths for different dye laser wavelength combinations. Wavelengths for the two lasers are indicated on top and side. Cross correlation time widths are from fits of the data to a Gaussian function.	20
Table 4.1.	Experimental v-X transition cross-sections and maximum $\Delta T/T$ values for backbone double and triple bond stretching resonances in crystalline and spin cast films of poly(4BCMU).	87
Table 4.2.	Experimental frequencies of C=C and C=C stretching resonances for spin cast film poly(4BCMU) as a function of excitation energy.	88
Table 5.1.	Cross sections for ground state vibration-to-excited electronic state transitions in poly(4BCMU).	119
Table 5.2.	Comparison of elongation ratio and optical dichroism at 2.29 eV.	121
Table 5.3.	Excitation energy dependence of vibrational resonance frequencies of spin-cast and aligned poly(4BCMU) films.	124
Table 6.1.	Conversion table between $\chi_{esu}^{(3)} \left(\frac{cm^4}{sC^2} \right)$ and $\chi_{SI}^{(3)} \left(\frac{C^4m}{J^3} \right)$.	135
Table 6.2.	Average and peak E ₄ values for $\ell = 10^{-7} \text{m}$ and different $\chi^{(3)}$ values.	137

LIST OF FIGURES

Figure 1.1.	Gain curves for five laser dyes spanning the wavelength range between 405 nm and 555 nm. Conversion efficiency is defined here as the ratio of the input average power to the output average power.	15
Figure 1.2.	(a) Frequency spectrum for a stilbene 420 dye laser operating at 440nm presented with a best fit Gaussian function for the spectrum. (b) frequency spectrum for a coumarin 460 dye laser operating at 485 nm, presented with a best fit Gaussian function.	16
Figure 1.3.	(a) Autocorrelation trace corresponding to the frequency profile shown in Figure 2a, presented with a fit to Equation 2. Parameters of the fits are presented in Table I. (b) Autocorrelation trace corresponding to the frequency profile shown in Figure 2b, presented with a fit to Equation 2.	18
Figure 1.4.	Unidirectional cross correlation for the two pulses detailed in Figures 2 and 3 together with a fit of the data to symmetric Gaussian function.	21
Figure 2.1.	Structure of polydiacetylene DCHD. The long axis of the carbazole side group is tilted 81° and the short axis 43.3° with respect to polymer backbone in the crystal. The arrows indicate the transition dipole moment directions.	27
Figure 2.2.	Linear absorption spectrum of a ~1600Å thick crystal of DCHD in the region of the polymer backbone excitonic transition.	30
Figure 2.3.	Transient response of DCHD for excitation at 1.908 eV, direct excitation of the exciton. The fast response (0 ps, ■) is scaled to the linear absorption spectrum. Slow responses are shown for 30 ps (●) and 125 ps (▲) delay times.	33
Figure 2.4.	Transient fast (0 ps, ■) and slow (30 ps, ●; 125 ps, ▲) responses of the DCHD excitonic transitions for excitation at 4.13 eV, the long axis polarized transition localized on the carbazole side group.	34

Figure 2.5.	Transient fast (0 ps, ■) and slow (30 ps, ●; 125 ps, △) responses of the DCHD excitonic transition for excitation at 3.57 eV, the short axis polarized transition localized on the carbazole side group.	35
Figure 2.6.	Time-scan of the pump-probe signal for excitation at 1.908 eV and probing at 1.879 eV. The magnitude of the slow absorptive signal decays exponentially with a time constant of 3.3 ± 0.3 ns.	37
	Comparison of the slow response reported here (solid line with data points) with the electroabsorption response of DCHD, taken from reference 16 (dotted line). Signal intensity scales are arbitrary.	40
Figure 3.1.	Linear absorption spectrum obtained from Kramers-Kronig transformation of the reflection spectrum of a thick crystal of DCHD (≈ 100µm) in the region of the polymer backbone excitonic transition at (a) 300 K and (b) 10 K.	49
Figure 3.2.	Time scan of the pump-probe signal for excitation at 1.937 eV and probing at 1.925 eV.	53
Figure 3.3.	Transient response of DCHD for excitation at 1.937eV direct excitation of the exciton transition. Fast response (0 ps, ■) and slow response (30 ps, ●; 125 ps, ▲) are shown.	54
Figure 3.4.	Transient responses of the DCHD excitonic transition for excitation at 3.57eV, the short axis polarized on the carbazole side group. Fast response (0 ps, ■) and slow responses (30 ps, ●; 125 ps, ▲) are shown.	55
Figure 3.5.	Transient responses of the DCHD excitonic transition for excitation at 4.13eV, the long axis polarized on the carbazole side group. Fast response (0 ps, ■) and slow responses (30 ps, ●; 125 ps, ▲) are shown.	56
Figure 4.1.	Poly[5,7-dodecadiyne-1,12-diolsbis(n-butoxycarbonymethylurethane] or Poly(4BCMU). The dashed lines indicates hydrogen bonding between the side groups.	67
Figure 4.2.	Schematic three level system.	70
Figure 4.3.	Nonlinear susceptibility as a function of potential well displacement.	74
Figure 4.4.	Linear absorption spectra of crystalline and spin cast film forms of poly(4BCMU). For the crystalline polymer, $\omega_{ox} = 1.96 \text{ eV}$	

	and for the spin cast film, $\omega_{ox} = 2.29 \text{ eV}$.	77
Figure 4.5.	Experimental data points and calculated fit (solid line) for a) stimulated inverse Raman spectrum of crystalline poly(4BCMU) for $\omega_p = 1.774 eV$ and b) for $\omega_p = 1.741 eV$.	80
Figure 4.6.	Experimental data points and calculated fit (solid line) for a) stimulated inverse Raman spectrum of crystalline poly(4BCMU) for $\omega_p = 1.701 eV$ and b) for $\omega_p = 1.653 eV$.	81
Figure 4.7.	Experimental data points and calculated fit (solid line) for a) stimulated inverse Raman spectrum of spin cast poly(4BCMU) for $\omega_p = 2.141 eV$ and b) for $\omega_p = 2.113 eV$.	82
Figure 4.8.	Experimental data points and calculated fit (solid line) for a) stimulated inverse Raman spectrum of spin cast poly(4BCMU) for $\omega_p = 2.083 eV$ and b) for $\omega_p = 1.978 eV$.	83
Figure 5.1.	Linear absorption of a poly(4BCMU) film cast on FEP for elongation ratio: (a) $\ell/\ell_o = 5$ (b) $\ell/\ell_o = 1$.	101
Figure 5.2.	Linear absorption of (a) crystalline poly(4BCMU) (b) freshly prepared spin cast poly(4BCMU) on a quartz substrate and (c) elongation to $\ell/\ell_o = 5$ for a poly(4BCMU) film cast on FEP copolymer substrate.	103
Figure 5.3.	Experimental data points and calculated fit (solid line) for a) stimulated inverse Raman spectrum of spin cast poly(4BCMU) for $\omega_p = 2.141eV$ and b) for $\omega_p = 2.113eV$.	104
Figure 5.4.	Experimental data points and calculated fit (solid line) for a) stimulated inverse Raman spectrum of spin cast poly(4BCMU) for $\omega_p = 2.083 eV$ and b) for $\omega_p = 1.978 eV$.	105
Figure 5.5.	Experimental data (points) and calculated fit (solid line) of the stimulated inverse Raman spectrum of a spin cast film poly(4BCMU) on a FEP copolymer substrate, $\ell/\ell_o=1$, for (a) $\omega_{pump}=2.142$ eV and (b) $\omega_{pump}=2.109$ eV.	107
Figure 5.6.	Experimental data (points) and calculated fit (solid line) of the stimulated inverse Raman spectrum of a spin cast film poly(4BCMU) on a FEP copolymer substrate, $\ell/\ell_o=1$, for (a) $\omega_{pump}=2.077$ eV and (b) $\omega_{pump}=1.978$ eV.	108

Figure 5.7.	Experimental data (points) and calculated fit (solid line) of the stimulated inverse Raman spectrum of a spin cast film poly(4BCMU)	
	on a FEP copolymer substrate, $\ell/\ell_0=1.5$, for (a) $\omega_{pump}=2.142$ eV and (b) $\omega_{pump}=2.109$ eV.	109
Figure 5.8.	Experimental data (points) and calculated fit (solid line) of the stimulated inverse Raman spectrum of a spin cast film	
	poly(4BCMU) on a FEP copolymer substrate, $\ell/\ell_0=1.5$, for (a) $\omega_{pump}=2.077$ eV and (b) $\omega_{pump}=1.978$ eV.	110
Figure 5.9.	Experimental data (points) and calculated fit (solid line) of the stimulated inverse Raman spectrum of a spin cast film	
	poly(4BCMU) on a FEP copolymer substrate, ℓ/ℓ_o =3, for (a) ω_{pump} = 2.142 eV and (b) ω_{pump} = 2.109 eV.	111
Figure 5.10	D. Experimental data (points) and calculated fit (solid line) of the stimulated inverse Raman spectrum of a spin cast film poly(4BCMU) on a FEP copolymer substrate, $\ell/\ell_o=3$, for (a) $\omega_{pump}=2.077$ eV and (b) $\omega_{pump}=1.978$ eV.	112
Figure 5.11	1. Experimental data (points) and calculated fit (solid line) of the stimulated inverse Raman spectrum of a spin cast film poly(4BCMU) on a FEP copolymer substrate, $\ell/\ell_o=5$, for (a) $\omega_{pump}=2.142$ eV and (b) $\omega_{pump}=2.109$ eV.	113
Figure 5.12	2. Experimental data (points) and calculated fit (solid line) of the stimulated inverse Raman spectrum of a spin cast film poly(4BCMU) on a FEP copolymer substrate, $\ell/\ell_o=5$, for (a) $\omega_{pump}=2.077$ eV and (b) $\omega_{pump}=1.978$ eV.	114
Figure 5.13	3. Experimental data (points) and calculated fit (solid line) of the stimulated inverse Raman spectrum of a freshly prepared spin cast poly(4BCMU) on quartz substrate for $\omega_{pump} = 1.978$ eV including in the calculation (a) two excitonic resonances ($\omega_x = 2.02$, 2.29 eV) (b) single excitonic resonance ($\omega_x = 2.29$ eV).	117
Figure 5.14	4. $\Delta\alpha$, the nonlinear response, normalized for sample thickness and laser intensities for the various forms of poly(4BCMU) as a function of stretching ratio for different excitation frequencies.	123
Figure 6.1.	Schematics of the optical beam geometry in the plane of the sample for the folded boxcars geometry.	131
Figure 6.2.	DFWM schematic energy level for the experiments.	133

Introduction

It is expected that the next century will see a wide applications of optical technology for transmitting, receiving and processing information. At present, the well established technology is one in which electrical signal are converted into pulses of light by rapidly turning semiconductors laser on and off. The resultant optical signal is then sent down optical fibers and received at the other end by a solid-state detector. The optical signal carried on the optical fiber is converted to an electrical signal for manipulation and decoding. Subsequent switching and signal processing is, by and large, performed by conventional electronic means. Therefore, in today's information transfer mechanism, optical signal finds use only in the transmission of information through fiber optics.

For faster information transfer one obvious thing to do is to replace electronic devices with their optical analogs. This would provide a direct means of switching optical signal without conversion back to electronic signal. An all-optical switch, which processes light by light, would circumvent this conversion complexity, without sacrificing the speed of light transport by the signal. An optical switch must function macroscopically much like a mechanical switch. The setting corresponding to "on" must allow light to pass through while "off" blocks transmission.

Photonics are expected to be superior to electronics for the following reasons: 1) a photonic switching cycle can, in principle, take place within femtoseconds, thus providing a gain of speed over that of the electronic process; 2) working at optical frequencies provides tremendous gain in the bandwidth of the information processing devices; 3) optical processing functions are generally free from interference by electrical or magnetic sources; 4) freedom from cross-talk *i.e.* two beams of photons can pass through one another with negligible interaction. The same is obviously not true for electrons flowing in crossed wiring. It is the combination of massive parallelism, and cross-talk and interference-free interconnection, that gives optics its greatest advantage over electronics.

The most critical need in this field today involves finding materials to carry out the active switching functions of optical devices. These materials will be used to construct photonic devices and are to photonics what semiconductor materials are to electronics. Optical switches and amplifiers will perform the functions now performed by transistors in electronic devices. All-optical devices rely on nonlinear optical materials. A nonlinear optical material may be defined as any material that changes any of its optical properties as result of illumination. These changes can be quantified by observing the behavior of the optical constants upon photoexcitation. These constants describe the optical response of a material and are the frequency-dependent real and imaginary parts of the complex dielectric response of the material, n and k.

Nonlinear optics (NLO) is primarily concerned with response of a dielectric material to a strong electromagnetic field. The electric field associated with incident light induces a

polarization P in the material of interest which is, in the simplest case, linearly related to the amplitude of the electric field by the proportionality constant χ . For sufficiently large electric fields, however, the general observation has been that the microscopic charges comprising matter fail to respond to the applied field in a strictly linear way. The polarization can more generally be expressed in expanded powers of E, $^{[1,2]}$

$$P = P^{o} + \chi^{(1)}E_{j} + \chi^{(2)}E_{j}E_{k}^{*} + \chi^{(3)}E_{j}E_{k}E_{l}^{*}$$
 [1]

where P is the induced polarization, P° is the permanent polarization, $\chi^{(1)}$ is the linear optical susceptibility, $\chi^{(2)}$ and $\chi^{(3)}$ are the second and third order nonlinear susceptibilities, respectively. All-optical nonlinear optical phenomena are described by the fourth-rank tensor $\chi^{(3)}$.

The macroscopic NLO behavior of organic conjugated polymers originates from the polarization response of the π -electrons. The molecular polarization behavior can be expressed as^[1,2]

$$\mu_i = \mu_i^O + \alpha_{ij} E_j + \beta_{ijk} E_j E_k + \gamma_{ijkl} E_j E_k E_l$$
 [2]

where μ_i is the dipole moment of the molecule induced by an electric field, μ_i° is the permanent dipole moment, α_{ij} is the polarizability, β_{ijk} and γ_{ijkl} are the first and second hyperpolarizabilities, respectively. When molecules are immobile in the applied electrical

or optical fields (which is the case with most solid samples) $\chi^{(3)}$ results directly from molecular γ . Thus optimizing the molecular structure for large γ results in optimization of $\chi^{(3)}$ of solid NLO materials.

It is important to make the distinction between resonant and nonresonant nonlinear optical effects. Resonant effects are large and are the direct result of elementary excitations created in a material by the absorption of incident light. Excitations so created are considered "real" in the sense that they have a discrete lifetime and result in the permanent exchange of energy out of the light field and into the material. Nonresonant nonlinear optical effects are smaller in magnitude and differ in that elementary excitations are created only "virtually" and hence no light is absorbed. These excitations result from the spontaneous distortion of the electronic wave functions in the presence of the laser field. Once the field is turned off, the electrons revert to their unperturbed configuration. Nonresonant response times are necessarily limited by the duration of the incident electric field.

All-optical switching devices are required to operate at very high speeds and need to have switching speeds (both on and off) of less than ~10ps if they are to compete with existing electronic devices. Resonant optical nonlinearities have, so far, failed to provide a satisfactory mechanism, despite extensive investigation. There are several reasons for this, which include the saturation of the resonant nonlinearity, the relatively slow recovery of the nonlinearity due to the population of stationary states and heating associated with

absorption, which introduces undesirable thermal effects and eventually can lead to material degradation.

However, nonresonant optical nonlinearities have been employed for all-optical switching. Nonresonant nonlinearities are, in general, several orders of magnitude smaller than resonant nonlinearities. If they are to be employed in all-optical switching, then they require an efficient switching mechanism such as inverse Raman scattering. All materials exhibit a third order nonlinear optical response. [1,2] The power of the optical field required to observe these effects depends on the nature of the electronic structure of the medium, its dynamical behavior, symmetry and geometrical arrangements in the medium. From the device point of view, important nonlinear optical materials are in solid form and must meet a variety of requirements for practical use. In general, they have to have stability with respect to ambient conditions and high intensity light sources. These materials will have to meet many processing requirements as well.

Recently the scope of synthesis and characterization of third order nonlinear materials has expanded tremendously. The incentive for this increased interest has been a search for a basic understanding of the "structure-property" relationships for third order optical nonlinearities and the technological interest in all-optical signal processing provided by third order processes. Although studies of third order optical nonlinearities go back as far as the 1960s, this field has shown only limited progress. Hermann *et. al.* [3] conducted the first systematic investigation of third order optical nonlinearity in a conjugated system on trans β -carotene. This work inspired considerable interest in conjugated systems and resulted in a theoretical analysis by Rustagi and Ducuing, [4] who predicted the importance

of π conjugation in determining the third order nonlinear optical properties. Sauteret *et.* $el.^{[5]}$ reported the first investigation of the polydiacetylene PTS where they studied third harmonic generation. This work clearly showed that the value of $\chi^{(3)}$ depends strongly on the extent of π conjugation in the nonlinear chromophore. As a result, conjugated polymers have emerged as the most widely studied class of $\chi^{(3)}$ organic materials.

No symmetry requirement exists for a material to exhibit a third order nonlinear response. All kinds of materials are potential candidates: liquids, thin films, glasses, and crystals. In the solid state one can use various forms such as crystalline materials, amorphous polymers, glasses and Langmuir-Blodgett films, for example amorphous polymers or glasses are particularly useful media for third order nonlinear processes because they can be readily processed into device structures.

Polydiacetylenes are one of the most widely investigated class of conjugated polymers for their third order nonlinear optical effects. The general structure of this polymer is,

$$R_2$$
 R_1
 R_1
 R_1

Polydiacetylenes (PDA) are prepared by the solid state polymerization of the corresponding monomers. ^[6] A large variety of PDAs with different properties can be prepared depending on the nature of the side groups R_1 and R_2 . PDAs offer significant opportunities to study conformational effects, effects of conjugation length and the role of the side groups on third order nonlinearities. Polydiacetylenes have been extensively studied for their large nonlinear optical susceptibilities^[7-15] with an ultrafast response time. ^[8] The quasi-one dimensional conjugated backbone structures coupled with chemical identity of the side groups (R_1 and R_2) are responsible for these unique characteristics. The $\chi^{(3)}$ values for a large number of PDAs have been investigated in crystals, ^[10,11] solution cast film, ^[12] Langmuir-Blodgett films, ^[13] solutions ^[14] and spin cast films ^[15] by using different measurement techniques.

Literature Cited

- 1. P. N. Prasad, D. J. Williams, Introduction to Nonlinear Optical effects in Molecules and Polymers, Wiley Interscience, 1991.
- 2. Y. R. Shen Principles of Nonlinear Optics, Wiley Interscience, 1984.
- 3. J. D. Hermann, D. Richard, Ducuing J., Appl. Phys. Lett., 23, 178(1973).
- 4. K. C. Rustagi, Ducuing J., Opt. Commun., 10, 258(1974).
- 5. C. Saureret, J. P. Hermann, R. Frey, F. Pradere, J. Ducuing, R. H. Baughman, R. R. Chance, *Phys. Rev. Lett.*, 36, 956(1976).
- 6. M. Schott, G. Wegner in D. S. Chemla, J. Zyss (Eds.), Nonlinear Optical Properties of Organic Molecules and Crystals, Vol. 2 Academic, New York, 1987, p.3.
- 7. Polydiacetylenes, NATO ASI series E, Vol. 102, Edited by D. Bloor, R. Chance (Nijhoff, Dordrecht, 1985).
- 8. G. M. Carter, J. Opt. Soc. Am. B, 4, 1018(1987).
- 9. T. Kanetake, T. Hasegawa, K. Ishikawa, T. Koda, T. Takeda, M. Hasegawa, K. Kunodera, H. Kobayashi, *Appl. Phys. Lett.*, **54**, 2287(1989).
- G. M. Carter, Y. G. Chen, M. F. Rubner, D. J. Sandman, M. K. Thakur, S. D. Tripathy in D. S Chemla, J. Zyss (Eds.), Nonlinear Optical Properties of Organic Molecules and crystals, Vol. 2, Academic, New York, 1987, p. 85.
- 11. D. N. Rao, P. Chopra, S. K. Ghodhal, J. S. Swiatkiewicz, P. N. Prasad, J. Chem. *Phys.*, **84**, 7049(1986).
- 12. G. Y. Berkvic, Y. R. Shen, P. N. Prasad, J. Chem. Phys., 87, 1897(1987).
- 13. F. Kajzar, J. Messier in D. S. Chemla, J. Zyss (Eds.), Nonlinear Optical Properties of Organic Molecules and Crystals, Vol. 2 Academic, New York, 1987, p.51.
- 14. J. Lemoigne, A. Thierry, P. A. Chollet, F. Kajzar, J. Messier, J. Chem. Phys., 88, 6647(1988).
- 15. a) G. L. Baker, J. A. Shelburne III, P. D. Townsend, Materials for Linear and nonlinear Optics, Institute of Physics Conference Series, 103, 227(1990).
 - b) J. S. Patel, D. S. Lee, G. L. Baker, J. S. Shelburne, Appl. Phys. Lett., 56, 131(1990).

CHAPTER 1

Synchronous Pumping of Two Dye Lasers Using a Single UV Excitation Source

Abstract

The synchronous pumping of two cavity dumped CW dye lasers operating in the wavelength range of 405 nm to 555 nm with a single mode-locked UV pump source has been studied. The pulses obtained from each dye laser are described quantitatively by using the noise burst model. The cross correlation between the two laser pulse trains indicates that the relative temporal stability is approximately one pulsewidth.

1.1. Introduction

The synchronously pumped dye laser^[1] has proven to be an extremely useful light source for a wide range of time and frequency domain spectroscopies.^[2] The primary advantage of synchronous pumping compared to passive mode locking techniques is the inherent timing stability attainable with gain modulation. Synchronously pumped dye lasers can be tuned over a much wider frequency range than passively mode locked dye lasers, and in addition, it is possible to synchronize two or more dye lasers using a single pump source. [3] The output pulse characteristics of synchronously pumped dye lasers have been examined extensively, and it is generally recognized that, without the addition of a bandwidth restricting element to the dye laser cavity, it is not possible to achieve transform limited behavior. [4,5] The pulses produced by the synchronously pumped dye laser have been described quantitatively using a "noise burst" model. [6] and, operating under optimum conditions, it is possible to achieve pulses that are well within a factor of two of the transform limit. Pulses that are not transform limited pose a serious problem only for experiments where shot noise limited behavior is required or where a coherent process. such as vibrational dephasing, is under investigation.

The excitation sources used most widely for the synchronously pumped CW dye laser are mode locked ion lasers or frequency doubled CW mode locked Nd³⁺:YAG lasers. These pump lasers operate either in the green or the red and, as a consequence, the practical blue limit for the simultaneous operation of more than one synchronously pumped dye laser is ~550 nm. While the operation of two dye lasers below 550 nm is possible using the mode-

locked blue or violet lines of ion lasers as a pump source, ^[7] the wavelengths and low efficiency of these lines limit the tuning range available. Recent advances in Nd³⁺:YAG laser technology have, however, allowed these limitations to be lifted and the tuning range for simultaneous operation of two dye lasers can be extended to wavelengths as low as 405 nm. The third harmonic of a CW mode locked Nd³⁺:YAG laser was used to pump two cavity dumped dye lasers synchronously. These dye lasers are independently tunable between 405 nm and 555 nm using five different laser dyes. Conversion efficiency for these lasers lies in the range of 1% to 25%, depending on the dye and wavelength of operation.

1.2. Experimental

1.2.1. Source laser. The pump laser for these experiments is a CW mode locked Nd³⁺:YAG laser (Coherent Antares 76-S). The output of this laser is ~30 W average power at 1.064 μ m, with ~100 ps pulses at 76 MHz repetition rate. The 1.064 μ m output is frequency doubled using a type I temperature tuned LBO crystal (7 mm) to produce ~3 W average power at 532 nm, with the same pulse characteristics as for the fundamental. The residual fundamental and collinear second harmonic light are mixed in an angle tuned Type I BBO crystal (7 mm) to produce \geq 1 W average power at 355 nm, again with the same pulse width and repetition rate as the fundamental. Stability of this source is \geq 6 hours once thermal equilibrium is established within the laser head.

- 1.2.2. Dye lasers. The third harmonic output of the source laser was divided using a ~50% beam splitter and routed to two cavity dumped dye lasers (Coherent 702) operating with three plate birefringent filters and no saturable loss. The dye circulating in each laser was cooled to ~2°C to increase the viscosity of the dye solutions and to reduce the rate of thermal degradation of the dyes. Low frequency noise present on the output of the dye lasers was reduced noticeably as a result of cooling the dye solutions. Five dyes were used to achieve the tuning range reported in here. Stilbene 1 (405 nm - 450 nm), stilbene 420 (425 nm - 470 nm), coumarin 490 (480 nm - 525 nm) and coumarin 500 (505 nm - 555 nm) were purchased from Exciton Chemical Co. Coumarin 460 (460 - 490 nm) was purchased from Aldrich Chemical Co. For all dyes except stilbene 1 either benzyl alcohol or methanol was used as the premix and ethylene glycol was used as the carrier solvent. Stilbene 1 was dissolved directly in warm ethylene glycol. It was necessary to use three different mirror sets for the dye lasers to cover the wavelength range between 405 nm and 555 nm. The dye lasers were cavity dumped at ~8 MHz instead of the more commonly used 4 MHz. Cavity dumping at 4 MHz yielded autocorrelation traces with obvious substructure even at the synchronous cavity length, while a cavity dumping rate of 8 MHz produced smooth autocorrelation traces without excess depletion of cavity gain. The single pass gain for the coumarin dyes was insufficient to allow CW (76 MHz) operation.
- 1.2.3. Time domain measurements. Background-free, noncollinear autocorrelation traces were recorded on a storage oscilloscope from the output of a scanning autocorrelator (Spectra-Physics model 409) modified for operation between 410 and 555 nm. The modifications consisted of using two different BBO SHG crystals cut for type I

second harmonic generation of 450 nm and 532 nm fundamental light, replacement of the photomultiplier with a solar blind detector (Hamamatsu R166) and use of interference filters (Inrad) to block the laser fundamental and pass the second harmonic to the detector. Calibration of the time scale was accomplished by using a calibrating etalon mounted in the autocorrelator. The hard copy output from the storage oscilloscope was subsequently digitized with a commercial hardware and software package (Jandel Scientific).

Noncollinear cross correlation measurements were performed in a different manner. The cross correlation was measured as a pump-probe signal by varying unidirectionally the differential arrival time of the two dye laser pulses at a (type I) BBO sum frequency generation crystal. Sum frequency light was detected as a function of time delay between the two pulses using radio frequency modulation/synchronous demodulation technology. [8] The output signal from the experiment was sent directly to a computer and no intermediate digitization steps were required. Because of the unidirectional nature of the measurement scheme the width of the cross correlation trace is a *direct* measure of the convolution of the two laser pulse envelopes.

1.2.4. Frequency domain measurements. The frequency spectra of the dye lasers were measured by using a Heath EU-700 0.3 m scanning monochromator with $2\mu m$ slits. The band pass of this monochromator is ≤ 0.03 nm. The output of the PMT detector was converted to a voltage and output to an X-Y recorder, and this trace was digitized.

1.4. Results and Discussion

The fundamental wavelength range accessible to synchronously pumped dye lasers is limited by the wavelength of the source laser. Extending the tuning range of this class of laser further to the blue would allow access to a wide range of interesting chemistry and physics. Earlier reports have shown that either the mode locked UV lines of an Ar⁺ or Kr⁺ laser. [9,10] or the third harmonic of a mode locked Nd³⁺:YAG laser [11] can be used to excite a single dve laser. There is no report on the literature where a single CW mode locked UV source has been used to pump two dye lasers simultaneously. It was found that 400 to 500 mW of average UV power is sufficient to pump each dye laser, and the tuning curves for five dyes spanning the wavelength range between 405 nm and 555 nm are shown in Figure 1. We note that the efficiencies for the stilbene dyes are substantially higher than those for the coumarins. In constructing these gain curves we attempted operation with several other coumarin dyes, but their thresholds for laser operation were higher than the ~400-500 mW average power available to each dye laser. We also demonstrated operation with coumarin 450 but have not included its gain curve here because stilbene 420 offers coverage of the same wavelength range with higher conversion efficiency.

The temporal and frequency profiles of pulses produced from the coumarin 460 and stilbene 420 lasers determine collectively how close their performance is to the transform limit. These data are summarized in Table 1.1. Figure 1.2a shows a representative

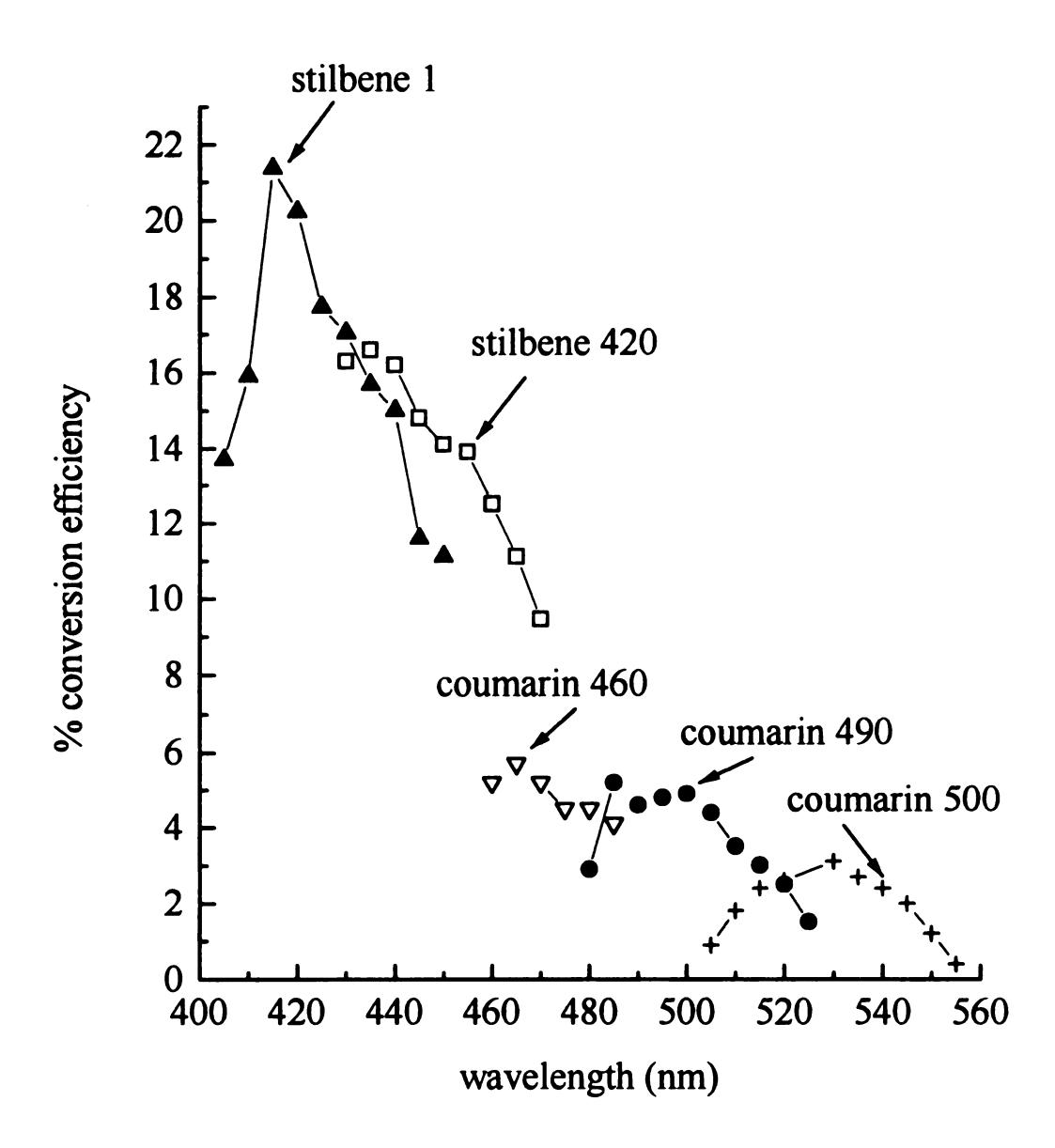
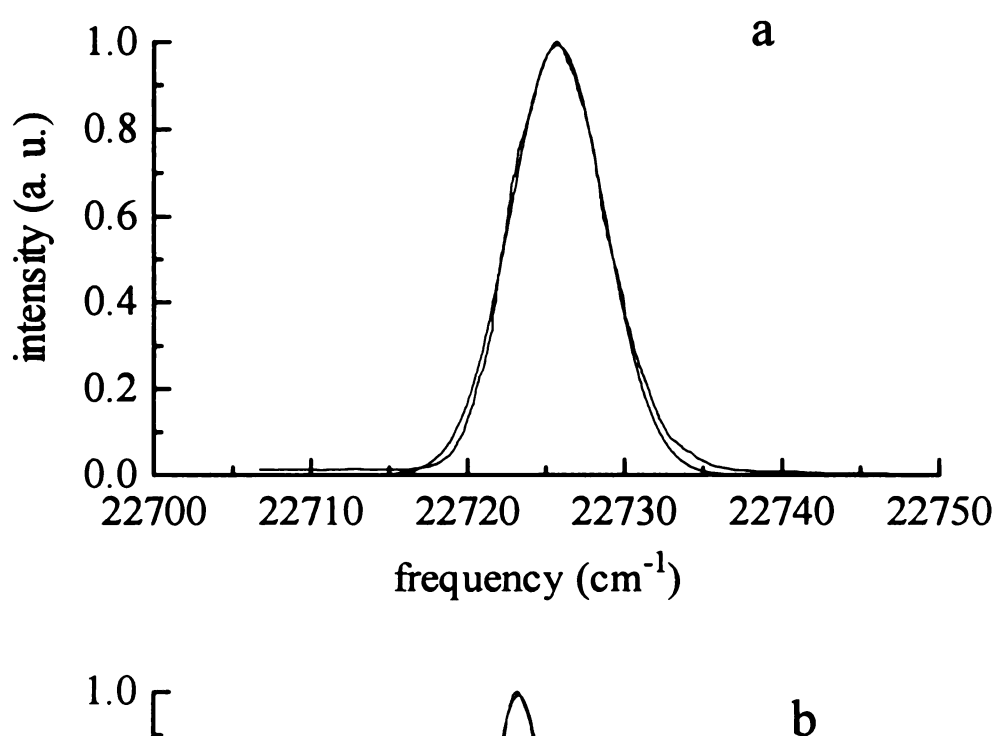


Figure 1.1. Gain curves for five laser dyes spanning the wavelength range between 405 nm and 555 nm. Conversion efficiency is defined here as the ratio of the input average power to the output average power.



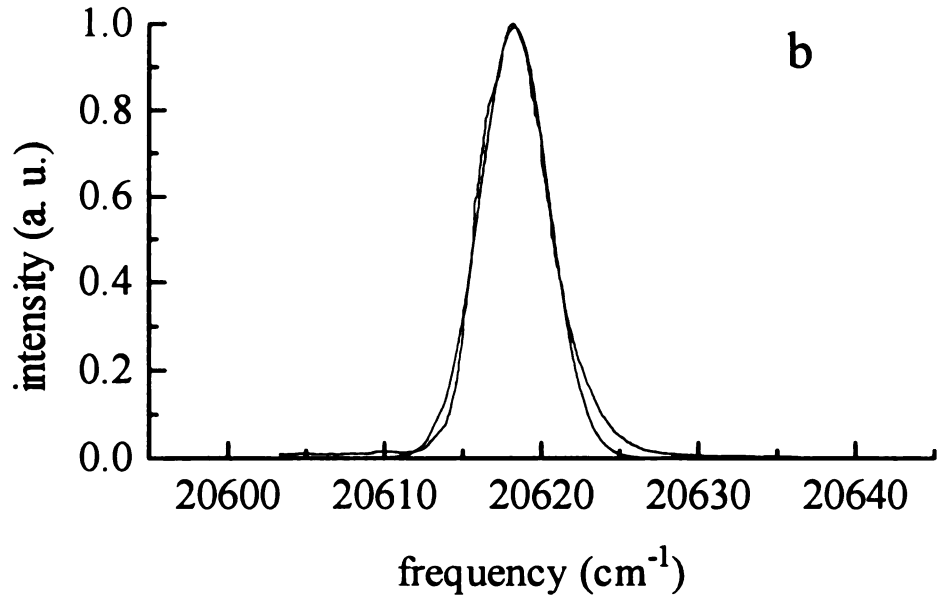


Figure 1.2. (a) Frequency spectrum for a stilbene 420 dye laser operating at 440 nm presented with a best fit gaussian function for the spectrum. (b) Frequency spectrum for a coumarine 460 dye laser operating at 485 nm, presented with a best fit gaussian function.

Table 1.1. Output parameters of stilbene and coumarin dye lasers modeled by the noise burst model.

laser dye	λ (nm)	Δv (cm ⁻¹)	$\Delta \nu \Delta au_n$	ΔνΔτ _e	
stilbene 420	430	4.43	0.408	0.801	
*	440	4.29	0.400	0.748	
**	465	4.07	0.305	0.629	
coumarin 460	460	3.02	0.340	0.466	
"	473	3.11	0.321	0.489	
"	485	3.10	0.302	0.490	

frequency spectrum for operation with stilbene 420 at 440 nm and Figure 1.2b shows a frequency spectrum for operation with coumarin 460 at 485 nm. While there are slight deviations, these spectra are represented well by a Gaussian profile, and this fit is shown in Figures 1.2. The corresponding autocorrelation traces for these frequency spectra are shown in Figures 1.3a and 1.3b. If the output of these lasers is transform limited it is expected that the autocorrelation functions would be fit well by a Gaussian profile. [12] Experimentally this is not observed. However, it was found that these pulses can be modeled quantitatively using the noise burst model. [6] In this model, the laser pulse is separable into two parts; a bandwidth limited pulse of thermal radiation (noise) and a slower temporal envelope.

$$E(t) = T(t)A(t)$$
 [1]

where A(t) is the stochastic profile of the thermal radiation and T(t) is the temporal envelope. For a pulse described by this model, an autocorrelation of the form

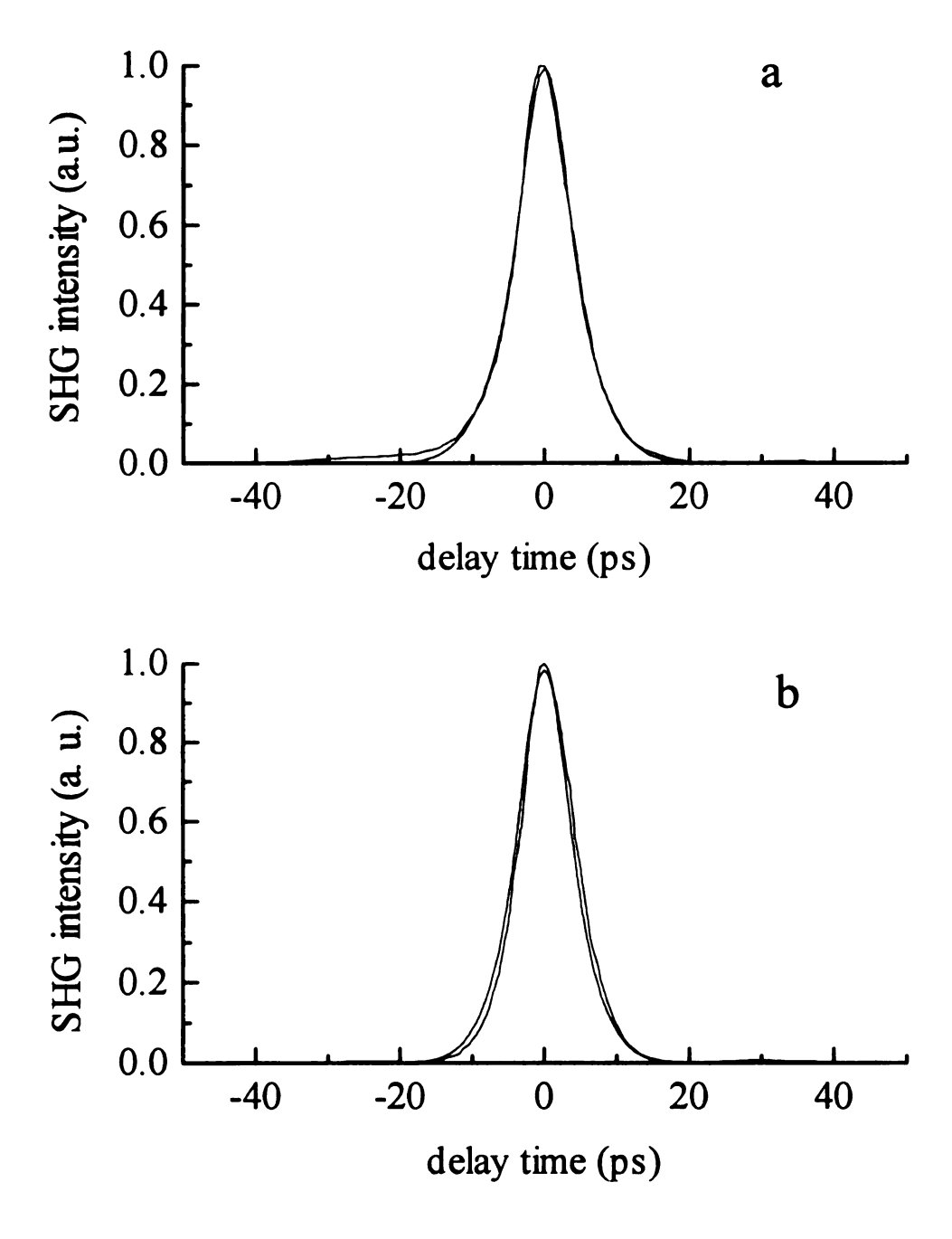


Figure 1.3. (a) Autocorrelation trace corresponding to the frequency profile shown in Figure 2a, presented with a fit to Equation 2. Parameters of the fits are presented in Table I. (b) Autocorrelation trace corresponding to the frequency profile shown in Figure 2b, presented with a fit to Equation 2.

$$G(t) = G_{\mathfrak{o}}(t) [1 + G_{\mathfrak{o}}(t)]$$
 [2]

is expected, where Ge(t) is the component of the autocorrelation arising from the function T(t) and $G_n(t)$ is the component of the autocorrelation determined by A(t). [13,14] If this model describes the data adequately then the time bandwidth product $\Delta \nu \Delta \tau_n \sim 0.44$ should be observed. The quantity $\Delta \tau_n$ is the actual pulse width and is inferred from the autocorrelation trace ($\sqrt{2}\Delta\tau_n$ for a Gaussian). The autocorrelation data was fit to Equation 1.2 assuming a Gaussian functionality for both $G_e(t)$ and $G_n(t)$, and the results of these fits are presented in Table 1.1 and Figures 1.3. For all of the wavelengths studied it was found that the quantity $\Delta\nu\Delta\tau_n\sim 0.4$ and $\Delta\nu\Delta\tau_e\sim 0.75.$ The actual value of $\Delta\nu\Delta\tau_n$ varies with wavelength and this might be due to slight deviations from a Gaussian frequency profile. The output of these lasers is clearly not transform limited, $\Delta \nu \Delta \tau_e > 0.4$, but is well within a factor of two of the transform limit (see Table 1.1). This deviation from transform limited behavior is typical of the output of a synchronously pumped dye laser where no additional bandwidth restricting elements have been introduced into the laser cavity. [14] We expect that, if an etalon or other bandwidth restricting element were introduced into the dye laser cavities, it would be possible to achieve transform limited performance.[4]

One of the most important properties of a laser system like the one reported here is the relative temporal stability of the pulse trains of the two dye lasers. Experimental measurement of the cross correlation of the two laser pulse trains provides a direct measurement of this jitter if the pulse envelope is known. The time width of the cross

shown in Table 1.2, and the cross correlation for the pulses shown in Figures 1.2 and 1.3

Table 1.2. Cross correlation widths for different dye laser wavelength combinations.

Wavelengths for the two lasers are indicated on top and side. Cross correlation time widths are from fits of the data to a Gaussian function.

laser wavelength	460 nm	473 nm	485 nm	
430 nm	12.6 ps	13.1 ps	14.2 ps	
440 nm	12.3 ps	14.6 ps	14.7 ps	
465 nm	11.6 ps	12.4 ps	11.6 ps	

is shown in Figure 1.4. The results of these measurements demonstrate that, in general, a cross correlation width that is on the order of twice that of the individual pulses, implying approximately one pulsewidth of instability between the two pulse trains can be expected. The measured jitter is consistent with results for this same system when it is pumped by the second harmonic of the Nd³⁺:YAG laser and operated with red dyes, suggesting that the relative temporal stability of the laser pulse trains is determined by the noise characteristics of the source laser instead of the gain characteristics of the dye lasers. In Figure 1.4, a fit of the cross correlation data to a Gaussian function is shown. Because of the unidirectional nature of the cross correlation measurement, asymmetry in the individual laser pulses can produce asymmetry in the cross correlation. The data shown in Figure 1.4 is typical of this system; all of the cross correlation data are fit best by a symmetric Gaussian function, suggesting the individual laser pulses are symmetric.

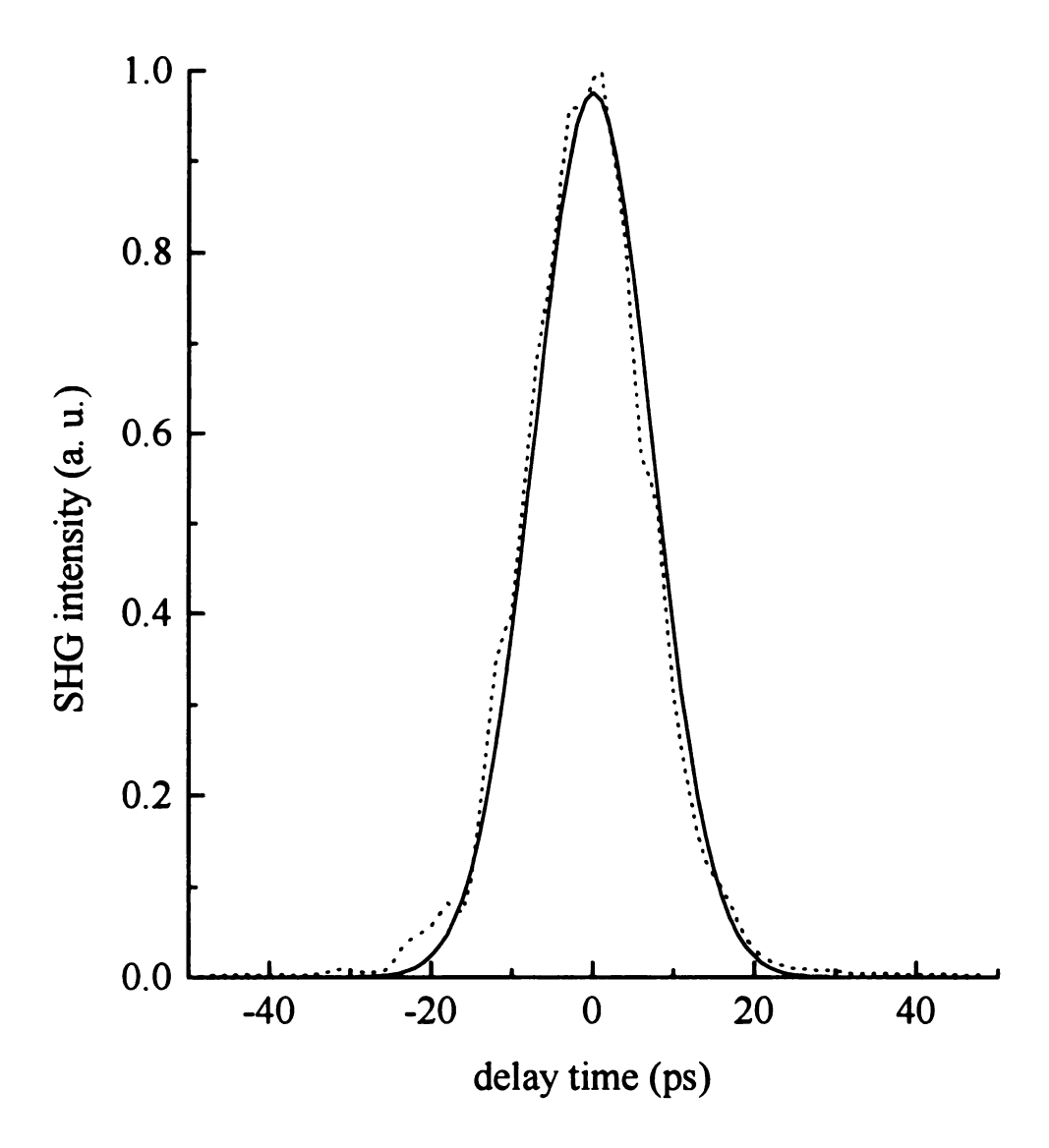


Figure 1.4. Unidirectional cross correlation for the two pulses detailed in Figures 2 and 3 together with a fit of the data to symmetric Gaussian function.

1.5. Conclusions

The operation of two CW synchronously pumped cavity dumped dye lasers with a single UV excitation source has been described. This advance extends the fundamental tuning range of this class of lasers to cover the spectrum between 405 nm and $\sim 1 \mu m$ with no gaps. The pulse characteristics of this system are described quantitatively by the noise burst model and are consistent with other synchronously pumped dye lasers operating at longer wavelengths. Instability between the dye laser pulse trains is on the order of one pulsewidth, demonstrating that pump-probe measurements previously restricted to wavelengths longer than ~ 550 nm can be performed in the blue. It is expected that, as with other synchronously pumped systems, the addition of saturable loss to the dye lasers will result in better absolute time resolution. This extended spectral range has been used to study the ultrafast stimulated emission response of perylene in dilute solution^[15] and for the study of excitation migration in conjugated polymers (see chapter 2 and 3)^[16] and stimulated inverse Raman scattering studies of the $\chi^{(3)}$ response of poly(4BCMU) (see chapters 4 and 5).^[17,18]

Literature Cited

- 1. J. M. Harris, R. W. Chrisman and F. E. Lytle, Appl. Phys. Lett., 26, 16 (1975).
- 2. see "Chemical Applications of Ultrafast Spectroscopy", by G. R. Fleming, Oxford, 1986, and references therein.
- 3. (a) R. K. Jain and J. P. Heritage, Appl. Phys. Lett., 32, 41 (1978). (b) J. Kuhl and D. von der Linde in "Picosecond Phenomena III", ed. by K. B. Eisenthal, R. M. Hochstrasser, W. Kaiser and A. Laubereau, Springer, Berlin, 1982, p.201.
- 4. G. J. Blanchard and M. J. Wirth, Opt. Commun., 53, 394 (1985).
- 5. B. F. Levine and C. G. Bethea, IEEE J. Quant. Electron, QE-16, 85 (1980).
- 6. H. A. Pike and M. Hercher, J. Appl. Phys., 41, 4562 (1970).
- 7. E. P. Economou, R. R. Freeman, J. P. Heritage and P. F. Liao, Appl. Phys. Lett., 36, 21 (1980).
- P. Bado, S. B. Wilson and K. R. Wilson, Rev. Sci. Instrum., 53, 706 (1982); L. Andor,
 A. Lorincz, J. Siemion, D. D. Smith and S. A. Rice, Rev. Sci. Instrum., 55, 64 (1984);
 G. J. Blanchard and M. J. Wirth, Anal. Chem., 58, 532 (1986).
- 9. J. N. Eckstein, A. I. Ferguson, T. W. Hänsch, C. A. Minard and C. K. Chen, *Opt. Commun.*, 27, 466 (1978).
- 10. A. I. Ferguson, Opt. Commun., 38, 387 (1981).
- 11. T. P. Carter, private communication.
- 12. K. L. Sala, G. A. Kenney-Wallace and G. E. Hall, *IEEE J. Quant. Electron.*, QE-16, 990 (1980).
- 13. D. B. McDonald, D. Waldeck and G. R. Fleming, Opt. Commun., 34, 127 (1980).
- 14. D. B. McDonald, J. L. Rossel and G. R. Fleming, *IEEE J. Quant. Electron.*, QE-17, 1134 (1981).
- 15. S. A. Hambir, Y. Jiang and G. J. Blanchard, J. Chem. Phys., 98, 6075(1993).
- 16. S. A. Hambir, T. Yang, G. J. Blanchard and G. L. Baker, *Chem. Phys. Lett.*, 201, 521(1993).
- 17. S. A. Hambir, G. J. Blanchard and G. L. Baker, J. Chem. Phys., 102, 2295(1995).
- 18. S. A. Hambir, D. Wolfe, G. J. Blanchard and G. L. Baker, in preparation.

CHAPTER 2

Excitation Migration in the Polydiacetylene DCHD

Abstract

Ultrafast spectroscopic results on excitation migration in the polydiacetylene DCHD, a crystalline conjugated polymer with carbazole side groups has been investigated. It was found that excitations created initially on the carbazole side group migrate rapidly (≤10 ps) to the polydiacetylene backbone. Relaxation of this excitation has the same spectral and temporal signature as relaxation of the backbone excitonic resonance. Comparison of these data to the electroabsorption response for DCHD confirms excitation transfer and not carrier transfer. The rapid excitation transfer measured is consistent with a Förster through-space mechanism. The excitonic transition localized to the polymer backbone decays nonradiatively into side group vibrational modes that have a characteristic (e⁻¹) lifetime of ~3.3 ns.

2.1. Introduction

Conjugated polymers have been studied extensively over the past decade because of their characteristically large third order nonlinear optical response, $\chi^{(3)}$. This response is thought to originate from the extensively delocalized π electron system found in conjugated polymers, but the molecular level understanding of the hyperpolarizability responsible for the observed optical nonlinearity is incomplete. A significant experimental limitation to gaining this understanding is the disorder present in many conjugated polymers. Most conjugated polymers are disordered to the extent that it is difficult to distinguish between inter-chain effects and intra-chain effects. One class of conjugated polymers, the polydiacetylenes, can be synthesized as large single crystals, where interchain and intra-chain effects can be effectively distinguished. The side groups of polydiacetylenes determine their morphological properties and, for crystalline forms, separate the individual polymer backbones from one another so that these materials behave as model 1-dimensional systems. [2] Despite these advantageous materials properties, our understanding of the dynamics of optical excitation and subsequent relaxation in these systems remains limited.

Poly[1,6-di(N-carbazolyl)-2,4-hexadiyne], [3-6] (DCHD, Figure 2.1) a polydiacetylene with N-methylcarbazole side groups was studied to understand the role that these side groups play in optical energy storage, excitation migration and relaxation in polydiacetylenes.

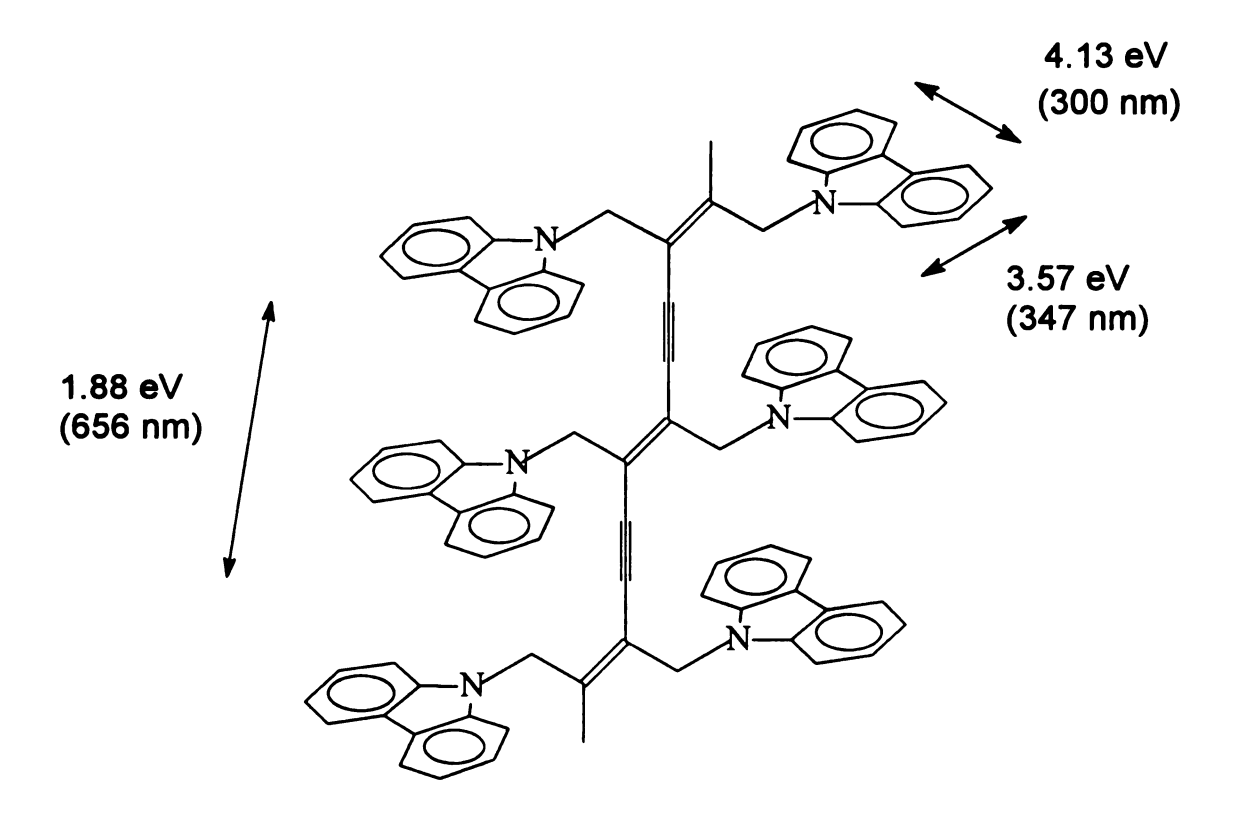


Figure 2.1. Structure of poly[1,6-di (N-carbazolyl)-2,4-hexadiyne] (DCHD). The long axis of the carbazole side group is tilted 81° and the short axis 43.3° with respect to polymer backbone in the crystal. The arrows indicate the transition dipole moment directions.

DCHD was chosen for several reasons. First, it possesses the lowest energy excitonic transition of any crystalline polydiacetylene reported to date. [3] implying a stable and highly ordered polydiacetylene backbone, and second, its side groups can be excited optically. [4] allowing the direct study of excitation transfer between the polymer side groups and backbone. In addition, the photoconductivity of DCHD has been reported to be substantially greater than that seen in other polydiacetylenes, suggesting the possible role of the carbazole side groups in carrier injection onto the polymer backbone. [5] The carbazole side group possesses two allowed transitions at energies in the near UV, one polarized along the chromophore short axis (3.57 eV) and the other polarized along the chromophore long axis (4.13 eV).^[4] It was found that, for excitation of either side group transition, the excitation migrates to the polymer backbone in less than the 10 ps. experimental time resolution of the spectrometer. Further, the excitonic transition localized on the polymer backbone relaxes rapidly (≤10 ps) and a slow, energy-dependent response is observed. The energy dependence of this slow response is the same, within experimental uncertainty, regardless of how the excitation is produced initially. Because this slow response differs from the electroabsorption response for DCHD, [7] the data presented here are consistent with excitation transfer rather than carrier injection from the polymer side group to the backbone. The slow response arises from dipolar coupling between side groups and the conjugated diacetylene backbone, analogous to that seen previously for PTS, a polydiacetylene with p-toluene sulfonate side groups. [8,9]

2.2. Experimental

Polydiacetylene DCHD was prepared by exposing crystalline 1,6-di(N-carbazolyl)-2,4 hexadiyne to 50 Mrad of 60 Co γ -radiation. ^[4] The resulting polymer crystals were typically several microns thick. Thin crystalline sheets of DCHD were separated from the crystals using masking tape, deposited on Pyrex substrates and washed with tetrahydrofuran to remove residual adhesive from the delamination operation. The resulting crystals were estimated to be several hundred Å thick. The linear absorption spectrum of a somewhat thicker crystal of DCHD is presented in Figure 2.2. The thickness of this crystal was estimated to be 1600Å, based on the value of $\alpha_{\text{max}} = 5 \times 10^5 \text{ cm}^{-1}$. ^[4]

Ultrafast pump-probe spectroscopic measurements were made on DCHD by using a spectrometer that was described in detail in chapter 1. [10] Briefly, a mode-locked Nd:YAG laser (Coherent Antares 76-S) was used to produce 100 ps pulses at 76 MHz repetition rate. The second harmonic of output from this laser (2W average, 532 nm) was used to pump synchronously two cavity dumped dye lasers (Coherent 701-3) operating with either LDS698 or DCM laser dyes (Exciton). The output of the pump laser was ~150 mW average power at 8 MHz repetition rate, 7 ps pulse width. The probe laser output was ~50 mW average power at 8 MHz repetition rate, 5 ps pulse width. A typical cross correlation measurement yielded a 10 ps FWHM response. For experiments pumping the carbazole side groups, the pump laser pulse train was frequency doubled using a 2 mm angle tuned LiIO3 SHG crystal. Average pump power at the sample was ≤ 1 mW for all experiments, and the average probe power was ~150 µW. Detection of all pump-probe signals was

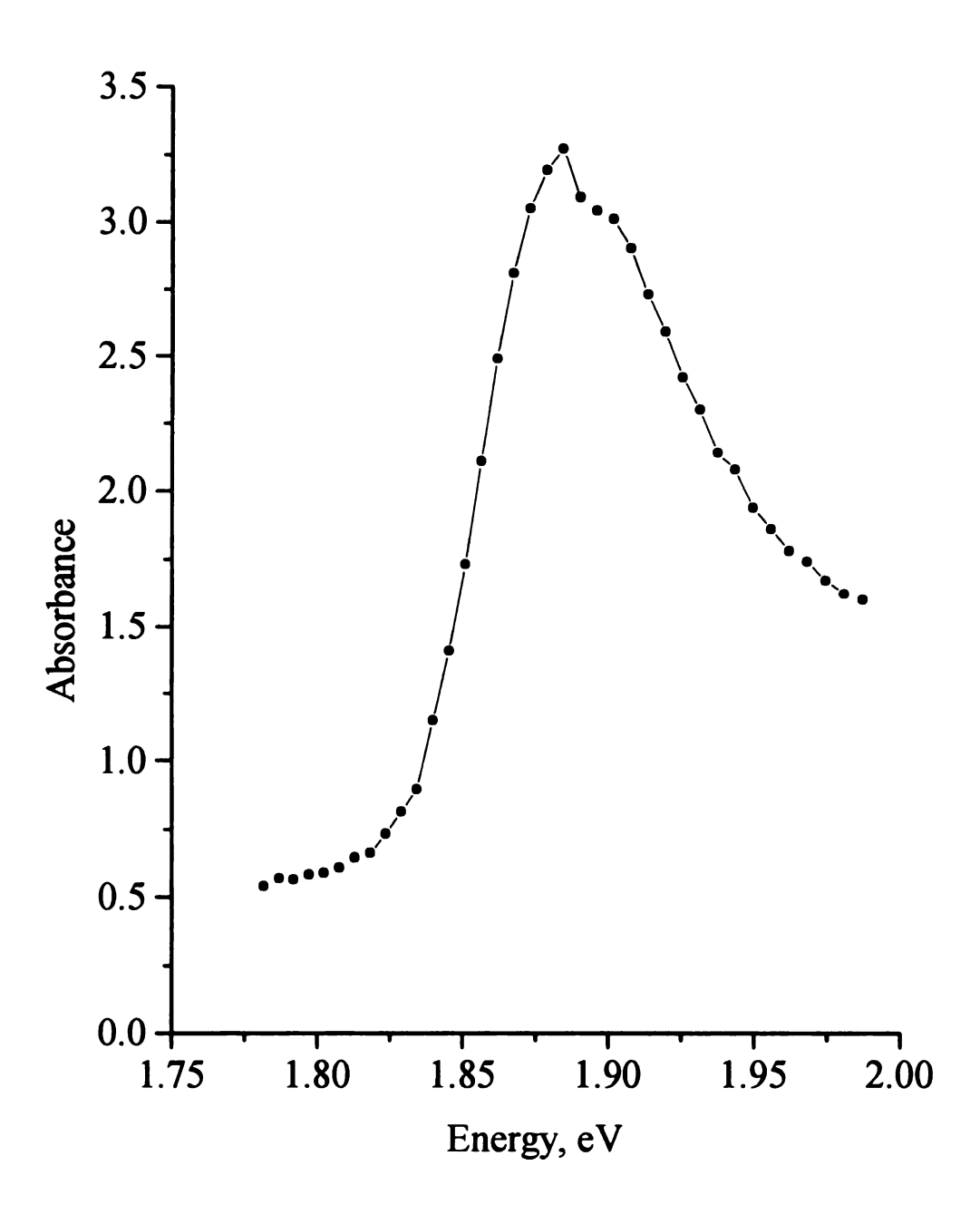


Figure 2.2. Linear absorption spectrum of a ~1600Å thick crystal of DCHD in the region of the polymer backbone excitonic transition.

accomplished by using a radio and audio frequency triple modulation, shot noise limited detection system.^[11]

2.3. Results and Discussion

Much of the work on polydiacetylenes has focused on the optical properties of the polymer backbone because it is thought to be the dominant linear and nonlinear chromophore. The role that the polymer side group plays in the material optical response can be profound, however. For example, crystalline polydiacetylene poly(4BCMU) has an excitonic resonance at 1.95 eV. Unlike most other polydiacetylenes, this crystalline polymer can be disordered to a limited extent or dissolved because of the labile nature of its side groups. Exposing poly(4BCMU) crystals to solvent vapors or heat causes a 0.3 eV blue shift and broadening of the excitonic resonance due to increased disorder on the length scale of the exciton. [12] Even for rigid crystalline systems, the side groups play an important role in energy relaxation subsequent to optical excitation. [8,9] For PTS, a crystalline polydiacetylene. the exciton lifetime is ~2 ps^[13] and there is a slow energydependent optical response subsequent to excitonic decay. [8,9] The optical energy introduced in the form of an exciton is dissipated vibrationally, with the dominant relaxation pathway being through the side groups. Because the side groups possess a significant permanent dipole moment they are coupled strongly to the side groups of neighboring polydiacetylene chains. Vibrational motions on side groups from one chain couple to side groups on adjacent chains, which in turn modulate the energy of the

backbone π system to which they are attached. Thus the identity of the polymer side group can play a deterministic role in the observed optical response of the polymer backbone.

The optical response of the polymer backbone of the polydiacetylene DCHD following excitation of the carbazole side groups and direct excitation of the excitonic transition has been studied. It was found that the excitonic transition responds identically to each of these different modes of excitation. Excitation transport from the side group to the backbone occurs in less than 10 ps. These data are consistent with the excitation transfer proceeding by a Förster through-space mechanism. The reasons for this assertion are detailed below.

Relaxation of the excitation on the polymer backbone involves several steps, with markedly different time constants. Figures 2.3-2.5 show the energy dependence of the fast and slow responses of the excitonic absorption of DCHD subsequent to direct backbone excitation and side group excitation. The limited spectral ranges reported for excitation of the side groups, presented in Figures 2.4 and 2.5, reflect the small signal size encountered in these experiments. Over the spectral ranges examined, however, the slow response is the same for all modes of optical excitation that were used. In all experiments the fast response arises from a uniform bleaching of the excitonic transition due to a phase-space filling mechanism. The raw data were recorded as time scans at a series of fixed pump and probe laser energies. The spectral responses presented in Figures 2.3-2.5 were reconstructed from individual time scans with the phase space filling response for calibration. The zero-time responses were scaled to correspond in intensity to the linear

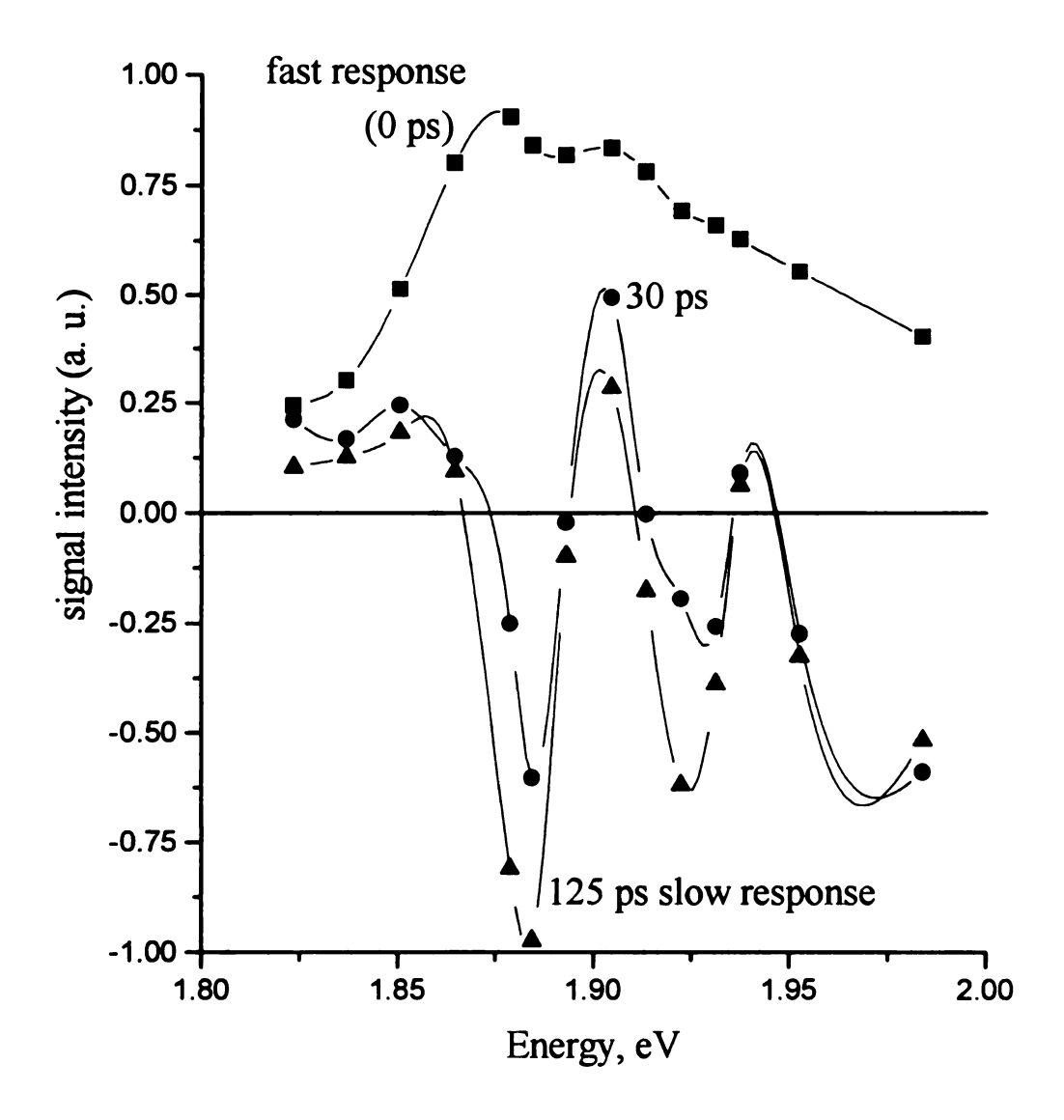


Figure 2.3. Transient response of DCHD for excitation at 1.908 eV, direct excitation of the exciton. The fast response (0 ps, ■) is scaled to the linear absorption spectrum. Slow reponses are shown for 30 ps (●) and 125 ps (▲) delay times.

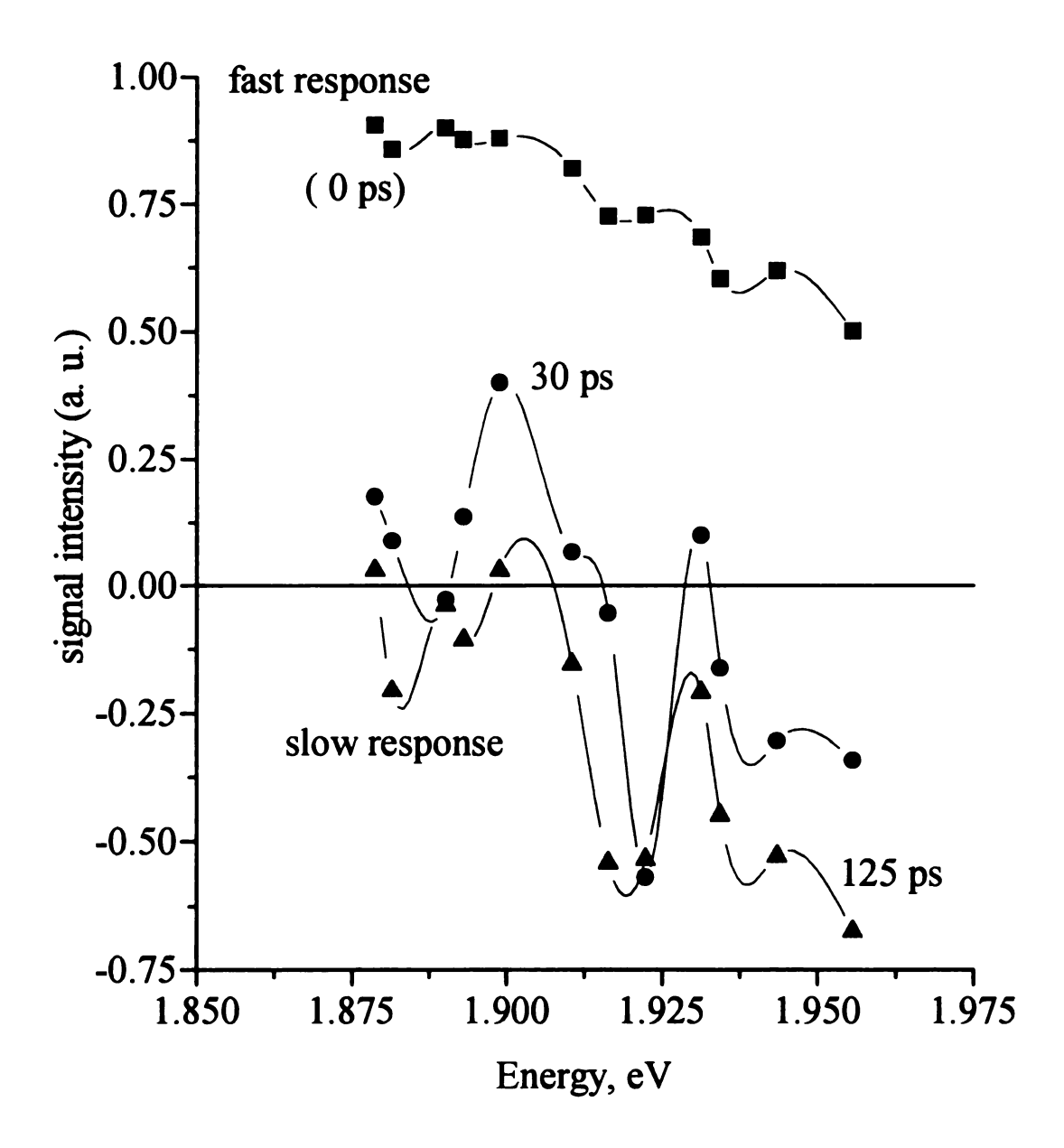


Figure 2.4. Transient fast (0 ps, ■) and slow (30 ps, ●; 125 ps, ▲) responses of the DCHD excitonic transitions for excitation at 4.13 eV, the long axis polarized transition localized on the carbazole side group.

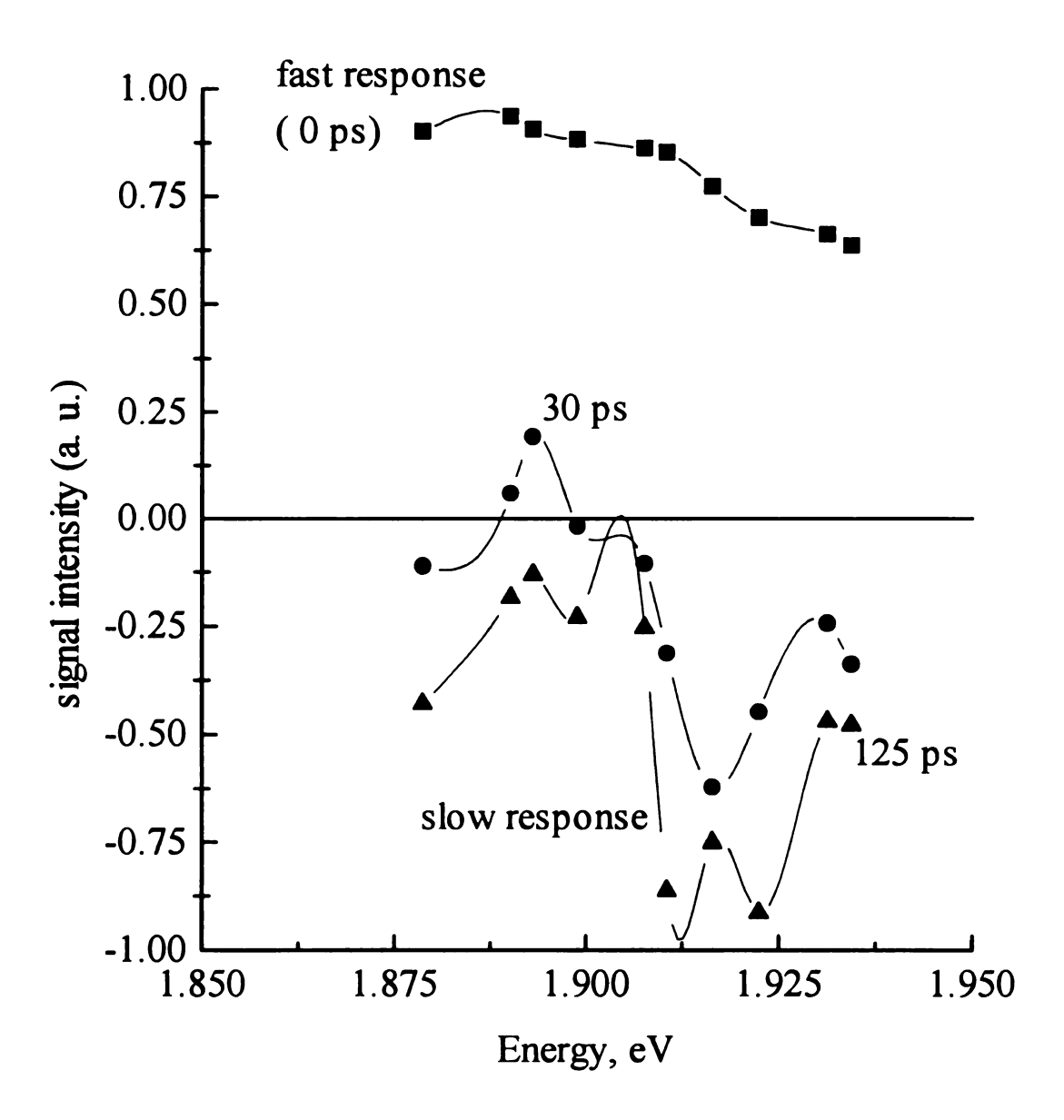


Figure 2.5. Transient fast (0 ps, ■) and slow (30 ps, ●; 125 ps, △) responses of the DCHD excitonic transition for excitation at 3.57 eV, the short axis polarized transition localized on the carbazole side group.

absorption spectrum because the samples used were not sufficiently uniform to determine absolute signal intensities. The slow response is attributed to modulation of the backbone excitonic transition by side group vibrational motion. This response has the same physical origin as the slow relaxation seen in the polydiacetylene PTS^[9] but for DCHD the time constant of the exponential population decay was measured to be 3.3 ± 0.3 ns at 300 K (Figure 2.6). The corresponding relaxation time for PTS is 130 ps.^[18] This difference is attributed to the density of bath mode states available to the different side groups in these two crystalline polydiacetylenes.

The ultrafast energy transfer from the carbazole side group to the polydiacetylene backbone is the same for transfer from either of the two accessible transitions localized on the side groups. The two side group transitions occur at 3.57 eV and 4.13 eV, and are polarized along the carbazole short axis and long axis, respectively. The carbazole side group is planar and its long and short axes make angles of 81° and 43.3°, respectively, with the polydiacetylene backbone. ^[6] This geometric arrangement permits energy transfer to occur via a Förster mechanism. The rate constant for Förster energy transfer is given by, ^[15]

$$k_{DA} = \frac{3\kappa^2 R_0^6}{2\tau_D R^6} \tag{1}$$

where τ_D is the lifetime of the excited carbazole chromophore in the absence of the polydiacetylene backbone. For N-methylcarbazole, τ_{fl} =18.3 ns. [16] R₀ is the critical

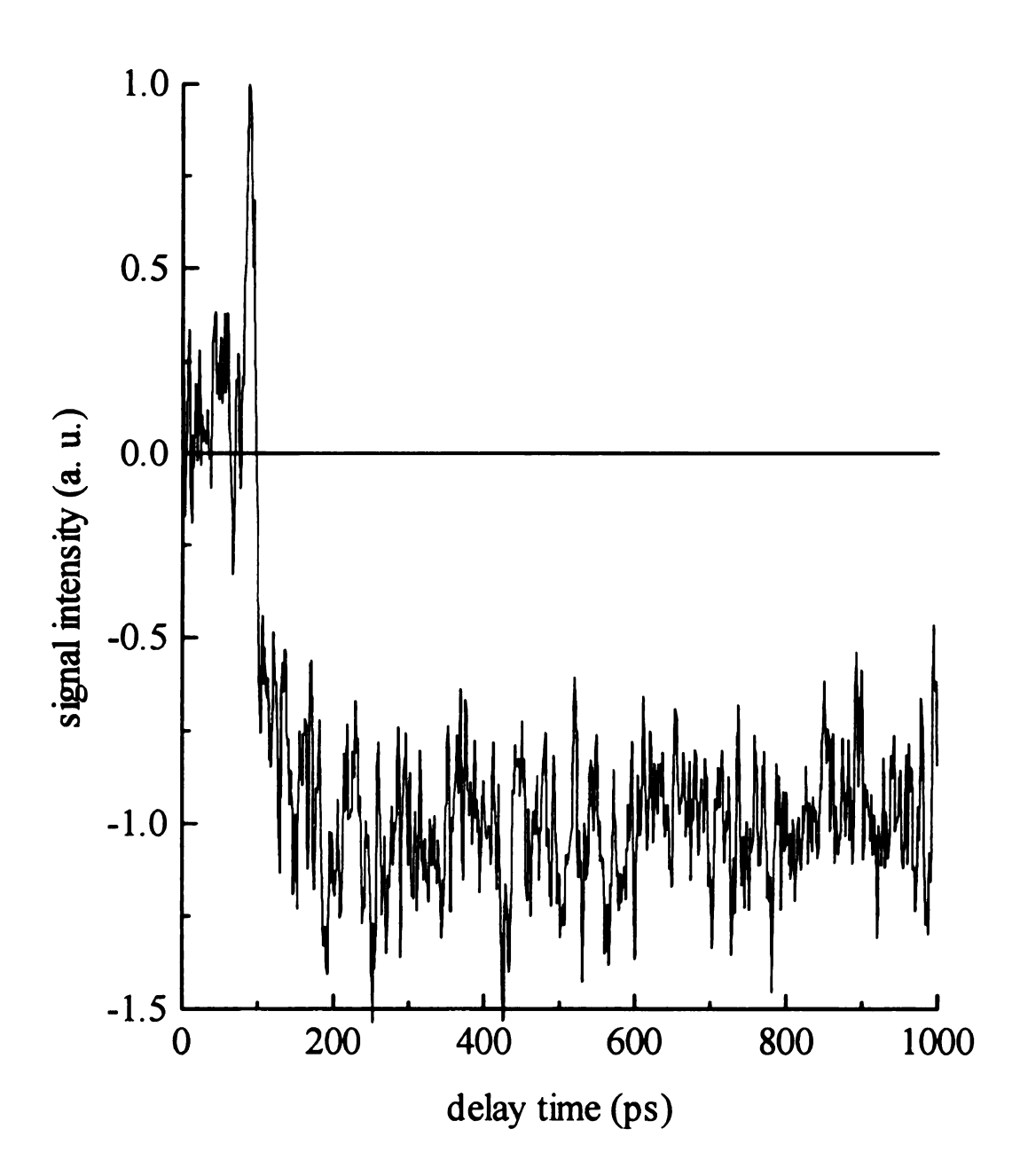


Figure 2.6. Time-scan of the pump-probe signal for excitation at 1.908 eV and probing at 1.879 eV. The magnitude of the slow absorptive signal decays exponentially with a time constant of 3.3 ± 0.3 ns.

transfer distance, a quantity related to the spectral overlap between the donor and acceptor chromophores and the donor fluorescence quantum yield. For the 3.57 eV transition R_0 was calculated to be 26Å and for the 4.13 eV transition R_0 was calculated to be 29Å, the difference arising from a v^4 dependence in the spectral overlap term. From X-ray crystallography data, R was estimated to be 3.26Å. The term κ^2 in Equation 1, the geometry factor, is given by

$$\kappa^2 = (\sin \theta_D \sin \theta_A \cos \phi - 2\cos \theta_D \cos \theta_A)$$
 [2]

The terms θ are the angles of the transition dipole moments for the donor and acceptor with respect to the vector joining the two chromophores, and ϕ is the azimuthal angle between them. κ^2 was calculated to be 0.16 for the short axis polarized transition (3.57 eV) and 0.10 for the long axis polarized transition based on the X-ray crystal structure of DCHD. Thus we expect $k_{DA} \sim 6.5 \times 10^{12} \, \text{s}^{-1}$ for the carbazole short axis transition and $k_{DA} \sim 2 \times 10^{12} \, \text{s}^{-1}$ for the long axis transition. The experimental observation that the excitation transfer proceeds in ≤ 10 ps is consistent with dipolar coupling being the dominant mechanism.

The slow response observed for DCHD exhibits both an energy dependence and a time-dependence. These two features will be addressed separately. Before the possible origins of the slow response are discussed, however, it is important to compare the observed energy dependence to other data on DCHD. DCHD is known to exhibit a high

photoconductivity compared to other polydiacetylenes.^[5] This high photoconductivity is thought to be related to carrier injection onto the backbone from the side groups. The spectral response of a polymer backbone perturbed by the presence of a local electric field is seen in electroabsorption experiments. Kawabe *et al.* have reported the electroabsorption spectrum for DCHD,^[7] and their data has been compared to the slow response in Figure 2.7. Clearly the slow response reported here does not correspond to an electroabsorption signal for DCHD. Excitation of the carbazole side groups with little excess spectroscopic energy does not produce a carrier population on the polymer backbone. These data are dominated by excitation transfer rather than carrier injection.

The energy dependence of the slow response is strongly suggestive of substructure within the exciton envelope. Modulation of the polydiacetylene backbone by sidegroup vibrational motions will produce either a blue-shift or a red-shift of the excitonic resonance, just as has been reported for PTS. [8,9] If the excitonic response in DCHD was comprised of a single feature one would expect a single zero-crossing in the energy dependence. For such a feature, a blue-shift would produce a transmissive response for energies below the excitonic maximum and an absorptive response at energies higher than the maximum. The several zero-crossings observed in the slow response indicate the presence of more than one feature. The character of this response can be reproduced by shifting three overlapped Lorentzian lines, although agreement with this simple model is by no means proof of this mechanism. It would be expected to find evidence for excitonic substructure in the linear response of DCHD (Figure 2.1). There are several factors that obviate this possibility, however. Near the excitonic maximum, the imaginary part of the

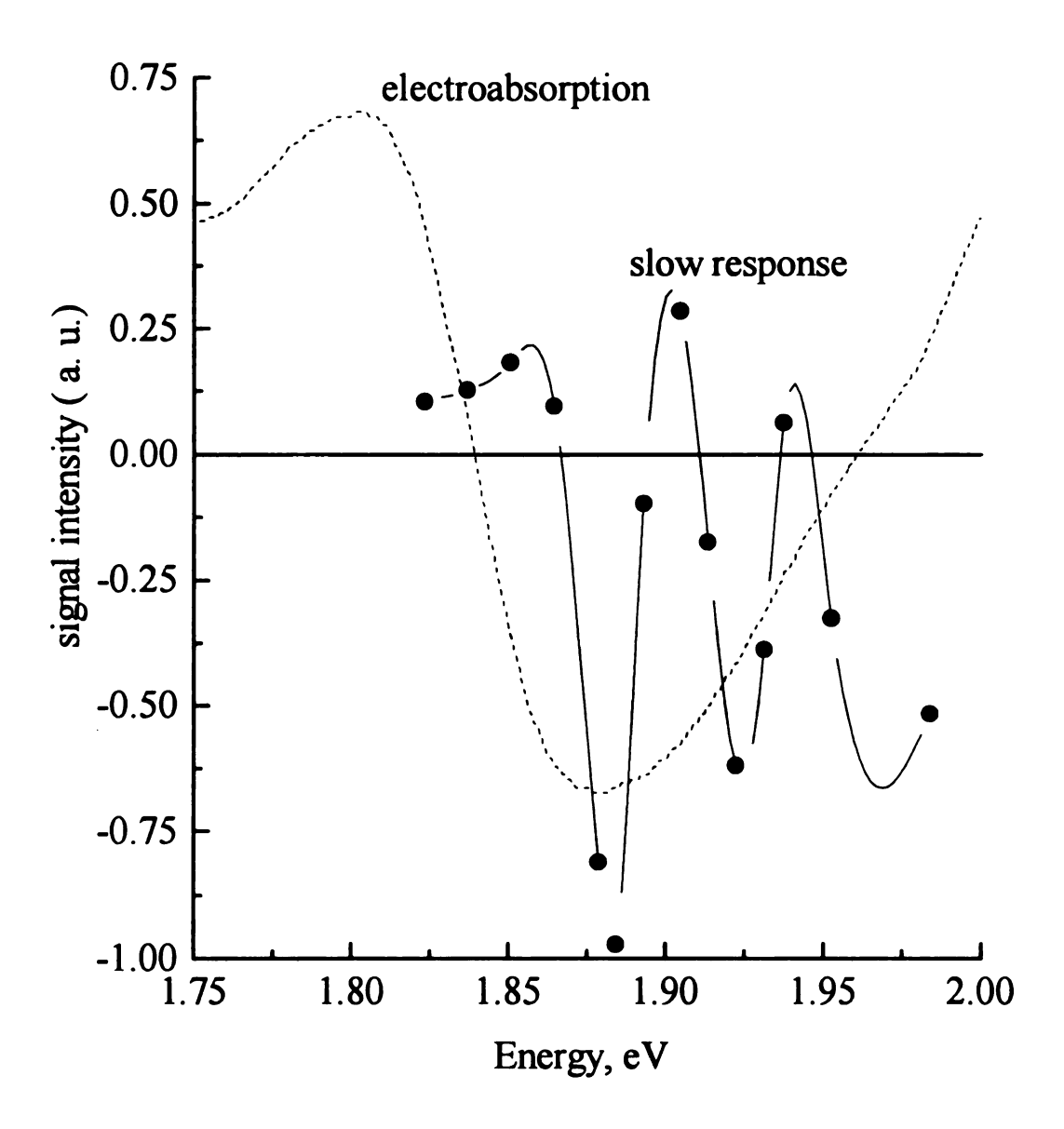


Figure 2.7. Comaprison of the slow response reported here (solid line with data points) with the electroabsorption response of DCHD, taken from reference 7 (dotted line). Signal intensity scales are arbitrary.

complex dielectric response of crystalline polydiacetylenes is $\epsilon \approx 25$. For systems with such a high dielectric response the linear absorption spectrum is not a direct measure of the intrinsic spectral linewidth. Attempts to infer underlying line shapes from absorption measurements can thus be misleading. The second problem with this approach is that the observed linear response for DCHD is essentially identical to the room temperature absorption spectrum of PTS. The room temperature slow response of PTS exhibits a markedly different spectral signature, however, indicating that there is not a simple correlation between the excitonic absorption band shape and the slow response in these materials.

Two explanations for the existence of more than one excitonic feature in DCHD could be suggested. The first is the possibility of more than one allowed orientation of the carbazole side groups within the polydiacetylene crystal. The potential energy surface for rotation of the carbazole side groups about their tethering bond may not be smooth, and may possess several local minima. This is not unknown in polydiacetylenes; the potential energy surface for side group rotation in PTS exhibits minima at ±8° from its room temperature equilibrium position, and the barrier heights for these local minima are ~200 K. Similarly, energy deposited into the side groups from excitonic relaxation may be sufficient to overcome a side group rotation barrier in DCHD. It is also possible that the second feature corresponds to partially oxidized DCHD. Oxygen-induced spectral features in PTS are known^[17] and, because of the thin films studied, any oxidized material on the surface of the crystal could contribute significantly to the overall spectral response. Obtaining the x-ray crystal structure of the crystals used for the optical experiments would allow the

evaluation of these possibilities. Unfortunately, the crystalline domain sizes of these thin crystals are too small for x-ray diffraction measurements to be performed. The second feature in the slow response is its time evolution. Although subtle, the response at 30 ps delay time differs from the response at 125 ps delay (Figures 2.3-2.5). Most probably this difference is related to the time required for energy to migrate to the vibrational modes of the side groups. [9] Low temperature measurements to examine this relaxation process are discussed in greater detail in the next chapter.

2.4. Conclusion

Ultrafast energy transfer between the side groups and backbone of a conjugated polymer at room temperature were investigated. This effect is manifested by a transient bleaching of the polydiacetylene backbone excitonic feature immediately following excitation. The rate of excitation transfer is consistent with a Förster through-space mechanism. The slow decay following the exciton bleaching response is strongly energy dependent, but is not commensurate with electroabsorption data. The energy dependence of this slow response is the same for excitation of either the backbone or the side group, and is observed to "build up" in time, likely due to the rate at which vibrational energy accumulates in the polymer side groups. While the complex nature of the slow signal indicates more than one spectral feature within the excitonic envelope, it was not possible to identify definitively the origin of these several features. Further experiments including low temperature spectroscopic and x-ray diffraction measurements will reveal their origin. It is clear from these data, however, that direct excitation of the DCHD carbazole side

groups with little excess spectroscopic energy does not result in carrier injection onto the polydiacetylene backbone.

Literature Cited

- 1. Nonlinear Optical Properties of Organic Molecules and Crystals, Vol. 2, ed. by D. S. Chemla and J. Zyss, Academic Press, 1987.
- 2. G. J. Blanchard, J. P. Heritage, A. C. Von Lehmen, M. K. Kelly, G. L. Baker and S. Etemad, *Phys. Rev. Lett.*, 63, 887 (1989).
- (a) M. E. Morrow and C. J. Eckhardt, Chem. Phys. Lett., 144, 65 (1988).
 (b) L. Sebastian and G. Weiser, Phys. Rev. Lett., 46, 1156 (1981).
 (c) L. Sebastian and G. Weiser, Chem. Phys., 62, 447 (1981).
- 4. R. J. Hood, H. Müller, C. J. Eckhardt, R. R. Chance and K. C. Yee, *Chem. Phys. Lett.*, 54, 295 (1978).
- 5. U. Seiferheld, B. Ries and H. Bässler, J. Phys. C., 16, 5189 (1983).
- 6. P. A. Apgar and K. C. Yee, Acta. Cryst., B34, 957 (1978).
- 7. Y. Kawabe, F. Jarka, N. Peyghambarian, Dandan Guo, S. Mazumdar, S. N. Dixit and F. Kajzar, Synth. Metals, 49-50, 517 (1992).
- 8. G. J. Blanchard, J. P. Heritage, G. L. Baker and S. Etemad, Chem. Phys. Lett., 158, 329 (1989).
- 9. M. J. Nowak, G. J. Blanchard, G. L. Baker, S. Etemad and Z. G. Soos, *Phys. Rev. B*, **B41**, 7933 (1990).
- 10. Y. Jiang, S. A. Hambir and G. J. Blanchard, Opt. Commun., 99, 216(1993).
- (a) G. J. Blanchard and M. J. Wirth, Anal. Chem., 58, 532 (1986).
 (b) P. Bado, S. B. Wilson and K. R. Wilson, Rev. Sci. Instrum., 53, 706 (1982).
 (c) L. Andor, A. Lorincz, J. Siemion, D. D. Smith and S. A. Rice, Rev. Sci. Instrum., 55, 64 (1984).
- 12. M. J. Nowak, G. J. Blanchard, G. L. Baker, S. Etemad and Z. G. Soos, in *Conjugated Polymeric Materials; Opportunities in Electronics, Opto-Electronics and Molecular Electronics*, ed. by J. L. Brédas and R. R. Chance, NATO ASI Series E, 182, Kluwer Academic Publishers, Dordrecht, 1990, 412.
- 13. G. M. Carter, J. V. Hryniewicz, M. K. Thakur, Y. J. Chen and S. E. Meyler, *Appl. Phys. Lett.*, 49, 998 (1986).
- 14. S. Schmitt-Rink, D. S. Chemla and D. A. B. Miller, Adv. Phys., 38, 89 (1989).
- 15. G. R. Fleming, Chemical Applications of Ultrafast Spectroscopy, Oxford University Press, 1986, 218-223.

- 16. I. B. Berlman, *Handbook of Fluorescence Spectra of Aromatic Molecules*, Academic Press, 1971, p. 208.
- 17. G. J. Blanchard and J. P. Heritage, Chem. Phys. Lett., 177, 287 (1991).

CHAPTER 3

Low Temperature Transient Optical Spectroscopy of Polydiacetylene DCHD. Evidence for a Distribution of Side Group Orientations

Abstract

The transient optical response of the polydiacetylene DCHD at low temperature was investigated. Ultrafast pump-probe spectroscopic measurements reveal that excitation of the polymer N-methyl carbazolyl side group results in instantaneous (<10 ps) excitation transfer to the polymer backbone at 10 K. The slow population recovery signal seen subsequent to excitation transfer to the polymer backbone exhibits an excitation energy dependence that is indicative of the existence of multiple conformers. The energy barriers between these conformers is inferred to be < 0.5 kcal/mol.

3.1. Introduction

Research over the past decade on conjugated polymers has shown that this family of materials is potentially useful for photonic signal processing applications. In addition, conjugated polymers have proven to be nearly ideal model systems for fundamental investigations of the nonlinear response of strongly coupled three-level systems. A limiting problem, inherent to many studies on the optical response of polymers, has been the ability to distinguish between interchain and intrachain relaxation processes. Several polydiacetylenes have been used as prototypical conjugated polymers because of their high degree of crystallinity and the substantial physical separation between individual polymer backbones. These favorable material properties preclude the occurrence of a host of intermolecular relaxation processes and allow direct examination of the linear and nonlinear optical processes intrinsic to a single polymer backbone. An added advantage of using polydiacetylenes is that the identity of the side groups can be controlled synthetically while maintaining the same backbone structure, so that interactions between the polymer backbone and its side groups can be evaluated systematically.

Understanding the interaction between the polymer backbone and side groups using the polydiacetylene DCHD was the focus of this investigation. This particular system was chosen because it is highly crystalline and the N-methyl carbazole side groups of DCHD can be excited selectively. In the previous chapter, it was demonstrated that excitation of either of the DCHD side group transitions resulted in a fast transfer of the excitation to the polymer backbone, and subsequent slow relaxation of the backbone excitation into the

ground state vibrational modes of the side groups. [8] The relaxation of energy into the side groups was manifested by a long-lived modulation of the backbone excitonic resonance arising from dipole-induced dipole coupling between the side group and the polymer backbone. These results demonstrated that the side group excited electronic states are coupled strongly to those of the polymer backbone, but two fundamental questions remained to be answered. First, excitation transfer between the excited side group and the polymer backbone was observed to occur in less than 10 ps at 300 K, but it was not possible to resolve this rate. These data suggested, but did not prove, the dominance of a Förster process. Second, the presence of sub-features within the slow relaxation envelope of the side group vibrational motions could not be explained unambiguously for lack of structural information and the amount of thermal energy present at 300 K. For these reasons it was necessary to undertake a series of measurements on DCHD at 10K. The results obtained do not clarify the nature of the fast excitation transfer between the excited side group and the polymer backbone, but the data presented here provide insight into the reasons for the spectral profile of the slow responses. These results show that several subtly different conformers are present in crystalline DCHD, and the energetic barriers between these conformers are small, i. e. <0.5kcal/mol.

3.2. Experimental

3.2.1. Materials and Temperature Control. Polydiacetylene DCHD was polymerized from crystalline 1,6-di(N-carbazolyl)-2,4-hexadiyne monomer with 50 Mrad of ⁶⁰Co γ-

radiation.^[7] Sheets of crystalline DCHD polymer were delaminated from thick (~100 μm) crystals using masking tape and were subsequently transferred to a pyrex substrate. The supported thin crystals (≤ 1000Å) were washed with tetrahydrofuran to remove any remaining adhesive from the crystal surface. The pyrex substrate was mounted in a flowing He(*I*) cryostat (Janis ST-100). The absorption spectra of DCHD at 300 K and 10K were obtained from their corresponding reflectance spectra by means of Kramers-Kronig transformation.^[9-11] For these reflection measurements, thick DCHD crystals were mounted in the cryostat. These data are presented in Figure 3.1a and 3.1b.

3.2.2. Pump-probe spectroscopy: The pump-probe measurements presented in this chapter can be divided into two classes; direct excitation of the polymer backbone and interrogation of its excitonic optical response, and excitation of the polymer side group followed by interrogation of the backbone excitonic response. Only a brief description of the pump-probe spectrometer will be given here because it has been described in detail chapter 1. A CW mode locked Nd:YAG laser (Coherent Antares 76-S) produces 30W average power at 1064 nm with 100 ps pulses at 76 MHz repetition rate. The output of this laser is frequency doubled to produce 2W average power at 532 nm. This second harmonic output pumps synchronously two cavity damped dye lasers (Coherent 701-3) operating with either DCM or LDS698 laser dyes (Exciton). The output of the pump laser is 100 to 150 mW average power at 8 MHz repetition rate, 5 to 7 ps pulse width, depending on the dye and wavelength of operation. The probe laser output is ~50 mW average power at 8 MHz repetition rate, ~5 ps pulse width. For excitation of either of the

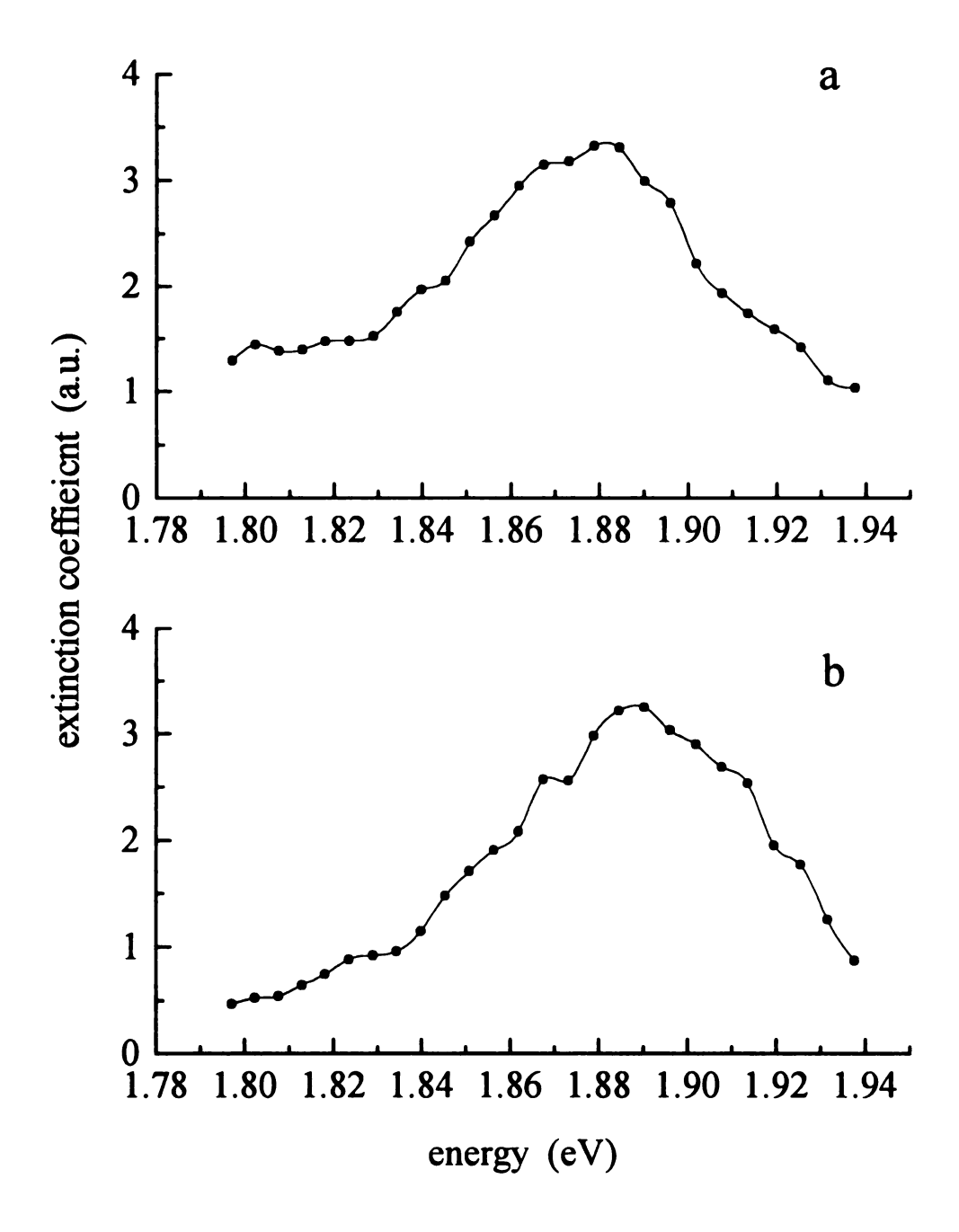


Figure 3.1. Linear absorption spectrum obtained from Kramers-Kronig transformation of the reflection spectrum of a thick crystal of DCHD (≈ 100μm) in the region of the polymer backbone excitonic transition at (a) 300 K and (b) 10 K.

carbazol side group transitions, the output of the pump laser was frequency doubled with a Type I LiIO₃ second harmonic generation crystal. Average pump power (either red or UV) at the sample is <1 mW for all of the experiments reported here, and the average probe power was $\sim 150 \mu W$. The pump-probe signal is detected with a radio and audio frequency triple modulation shot noise limited detection system. [13]

3.3. Results and Discussion

Crystalline polydiacetylenes exhibit a narrow (~50 meV FWHM), intense excitonic absorption due to the π - π * transition localized along the conjugated polymer backbone. The cross section of this excitonic transition is large; α ~10⁵ cm⁻¹ [3] The exact energy of this resonance depends sensitively on the chemical identity of the side group attached to the polymer backbone. PTS, a polydiacetylene with p-toluene sulfonate side groups, exhibits an absorption maximum at 1.98 eV, [2] whereas DCHD, with N-methyl carbazolyl side groups, shows an absorption maximum at 1.90 eV. [8] This difference in the position of the excitonic absorption maximum is presumed to arise from differences in crystalline packing forces for these materials, although there has been no direct proof of this assertion. The excitonic absorption band in crystalline polydiacetylenes exhibits substantial phonon side structure that persists for several hundred meV above the excitonic absorption maximum, and these features can be modeled quantitatively based on the resonance Raman response of the polymer backbone. [14] The excitonic absorption manifold is coupled strongly to the ground state vibrations in polydiacetylenes, typical of

many organic compounds, and this coupling is a crucial material property for multifrequency optical switching processes. The strength of this coupling depends sensitively on the extent of structural disorder or any electronic perturbation to the polymer backbone. Such an electronic perturbation can arise either as a consequence of oxygen adsorption,^[15] or from coupling to the side groups. It is therefore important to understand the nature of the coupling between the polymer backbone and its side groups from both a structural and electronic perspective.

PTS has received the majority of the experimental attention on polydiacetylenes because of its comparative ease of synthesis and the many earlier works that have served to characterize its structure and relaxation properties. The ultrafast relaxation processes of PTS both at room temperature and 10K has been investigated. [16] PTS, and other polydiacetylenes, exhibit a characteristic optical response on two distinct timescales and with different spectral signatures. A fast response, which follows the laser cross correlation (~10 ps), and a slow, energy dependent response, with a characteristic decay time of hundreds of picoseconds to nanoseconds, is observed subsequent to direct excitation of the backbone excitonic transition. PTS is considered unique among polydiacetylenes because the excitonic absorption splits into two resonances separated by 40 meV below 200 K. [16-18] The reason for the observed excitonic splitting is that PTS undergoes a structural phase transition at 200 K wherein the crystal unit cell doubles and the p-toluene sulfonate side groups undergo alternate $\pm 8^{\circ}$ rotations from their high temperature conformation. [19] These two side group orientations yield two inequivalent polymer backbone environments, resulting in two excitonic resonances. It was this

optical response seen in pump-probe experiments on PTS. The slow response exhibited a spectral profile corresponding to the first derivative of the excitonic transitions, and this derivative character has proven to be a sensitive indicator of substructure within the absorption band of polydiacetylenes. A featured slow response has been observed for DCHD at 300 K and this response was investigated in detail at 10 K. It is likely that the origin and energy-dependence of the slow response observed for DCHD is fundamentally the same as that observed in PTS.

The previous chapter discusses the room temperature pump-probe response of DCHD focused on the ultrafast transfer of excitation from the N-methyl carbazolyl side group to the polymer backbone. The N-methyl carbazolyl side group exhibits two allowed transitions, one along the carbazole long axis (300 nm, 4.13 eV), and the other along the carbazole short axis (347 nm, 3.57 eV). The transient response of both excitations showed a fast bleaching signal followed by a slow, energy dependent recovery. The fast response follows the laser cross correlation and arises from phase space filling. Earlier work on PTS has shown that the slow response is due to the modulation of the polymer backbone by dipolar coupling to vibrational motion of the side groups. [16]

The data presented here, taken at 10 K, are shown in Figures 3.2-3.5. The excitonic transition responds similarly to excitation of either side group transition (3.57 eV, 4.13 eV) or direct excitation of the polymer backbone (1.90 eV). A fast (< 10 ps) bleaching response followed by a slow energy dependent recovery was observed (Figure 3.2). The

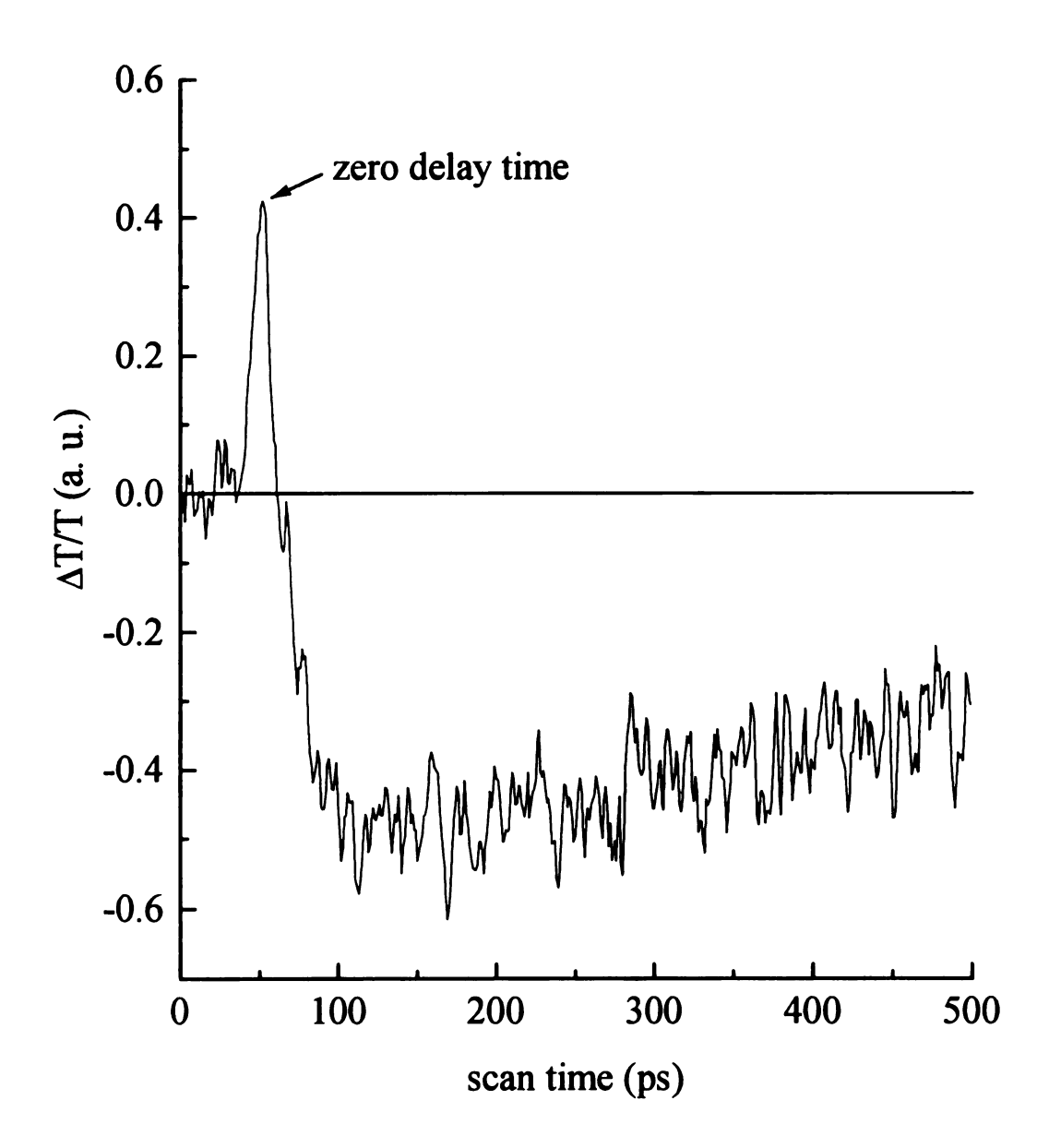


Figure 3.2. Time scan of the pump-probe signal for excitation at 1.937 eV and probing at 1.925 eV.

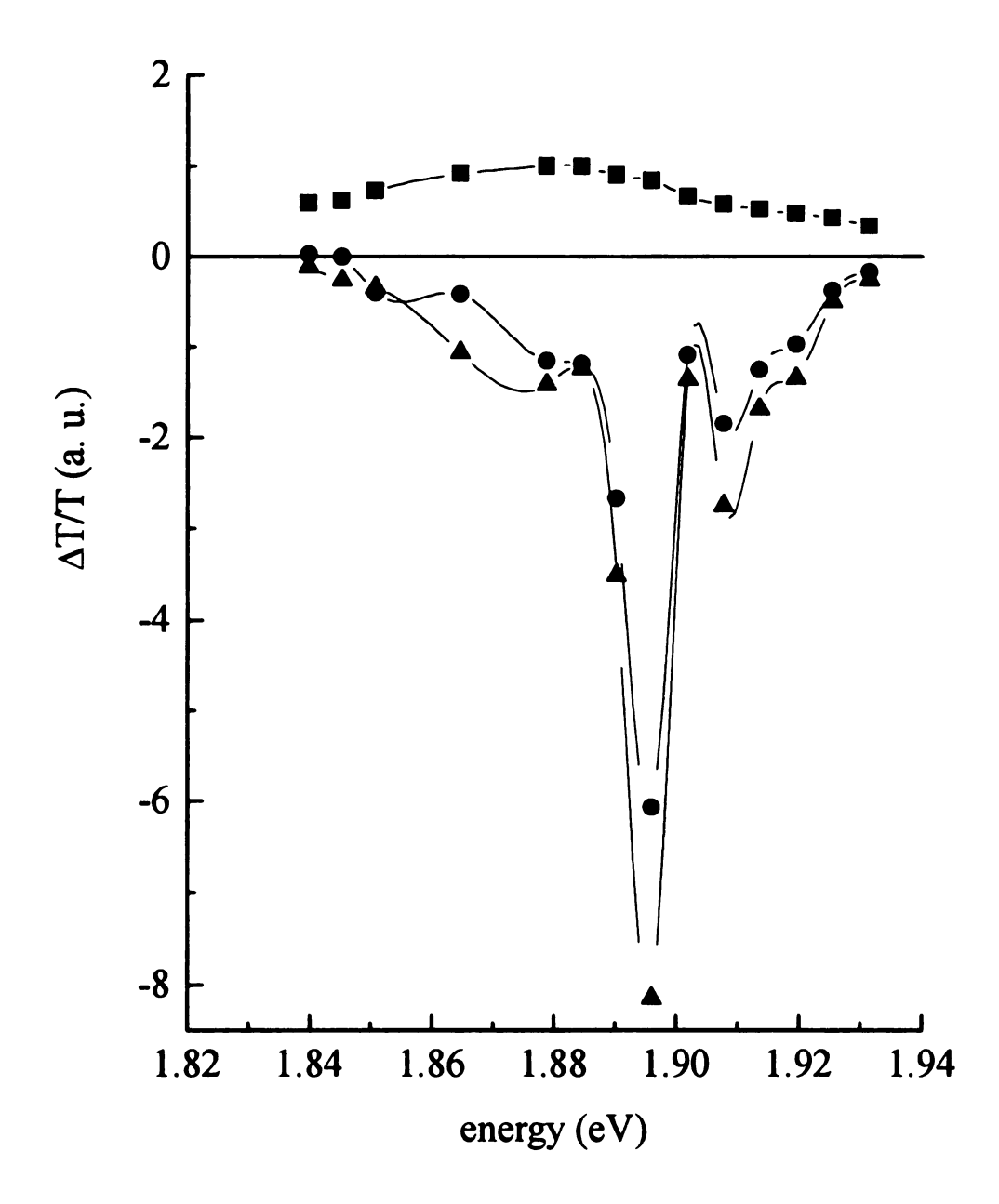


Figure 3.3. Transient response of DCHD for excitation at 1.937eV direct excitation of the exciton transition. Fast response (0 ps, ■) and slow response (30 ps, ●; 125 ps, ▲) are shown.

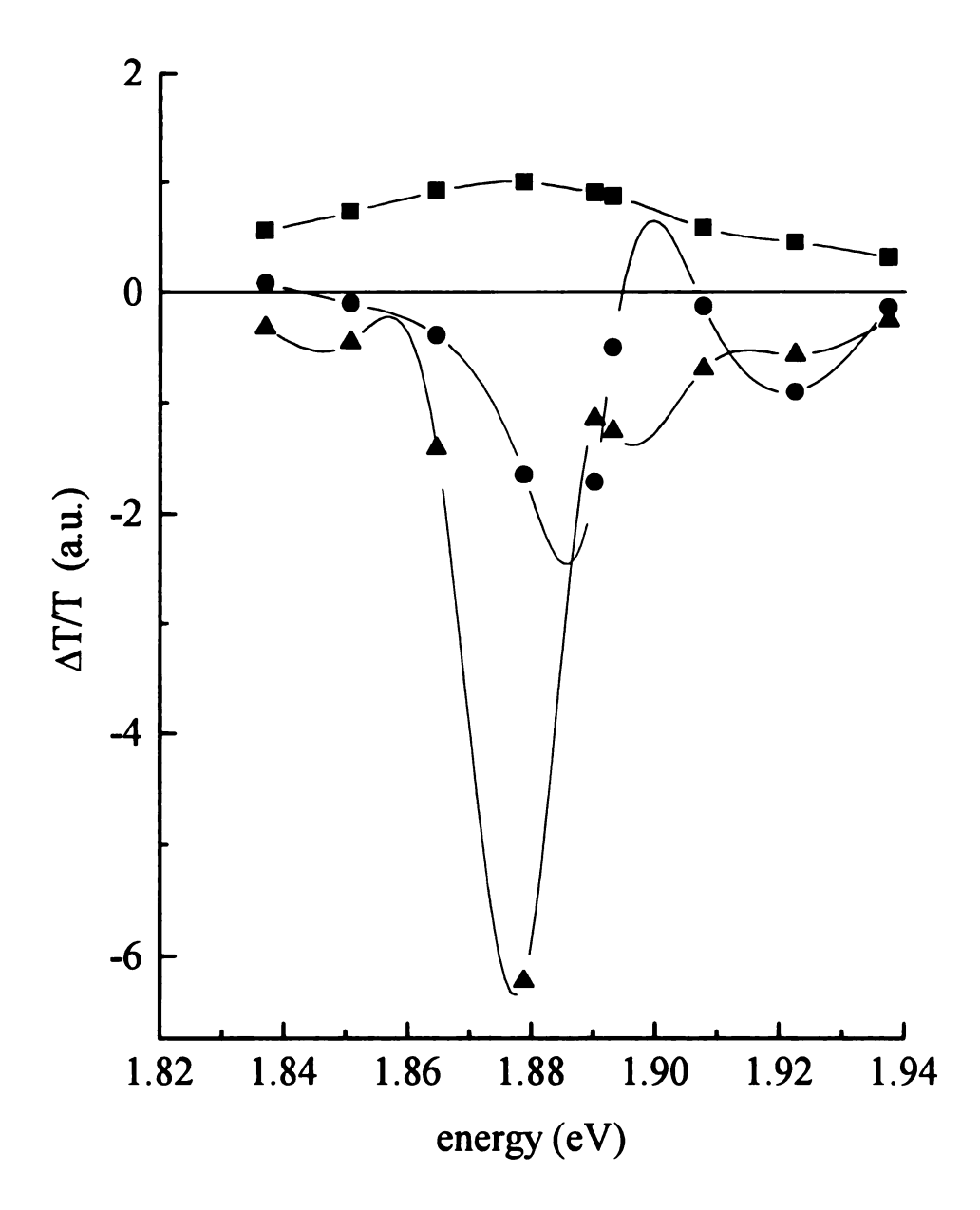


Figure 3.4. Transient responses of the DCHD excitonic transition for excitation at 3.57eV, the short axis polarized on the carbazole side group. Fast response (0 ps,) and slow responses (30 ps,); 125 ps,) are shown.

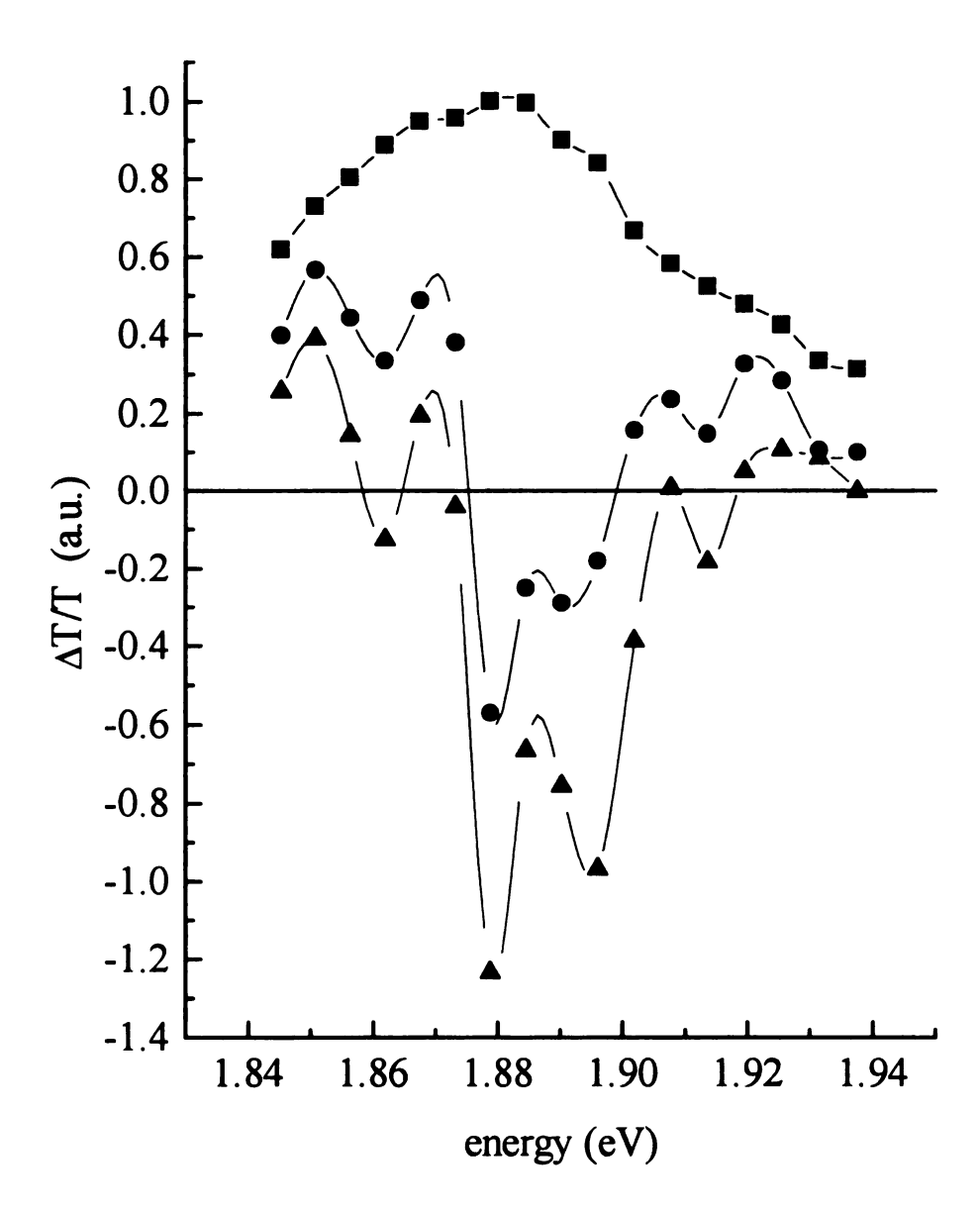


Figure 3.5. Transient responses of the DCHD excitonic transition for excitation at 4.13eV, the long axis polarized on the carbazole side group. Fast response (0 ps, ■) and slow responses (30 ps, ●; 125 ps, ▲) are shown.

information contained in both of these responses provides insight into the structural and energetic couplings in DCHD, and it is the structural information contained in these data that is the primary focus of this chapter.

One motivation for performing these experiments at low temperature was to attempt to resolve the fast excitation transfer from the side group to the polymer backbone. The excited state lifetime of the side group, τ_D , can, in principle, exhibit a temperature dependence, and this lifetime appears in the denominator of the expression for the excitation transfer rate constant in the Förster model. [8]

$$k_{DA} = \frac{3\kappa^2 R_o^6}{2\tau_D R^6}$$
 [1]

If the fast excitation transfer from the side group to the polymer backbone could be slowed by increasing τ_D , then the rate could be measured. The data for the fast response of DCHD at 10 K remain inconclusive in the sense that the transfer of excitation from the side group to the polymer backbone occurs in <10 ps. Nonetheless, the fast excitation transfer observed remains consistent with the predictions of the Förster energy transfer mechanism.

DCHD exhibits a temperature dependent optical response fundamentally different than that of PTS. The linear reflection spectra of DCHD both at room temperature and 10 K was measured and, using the Kramers-Kronig transformation, [9-11] converted these data to

absorption spectra (Figure 3.1a,b). The 10 K extinction spectrum of DCHD is red shifted by ~15 meV from that of the room temperature spectrum. Neither phase transition nor splitting of the absorption peak was observed as is seen for PTS. The observed substructure within the slow pump-probe response suggests the presence of more subtle structural heterogeneity in DCHD than has been measured for PTS. The Wegner group has, through their polymerization studies of polydiacetylenes, shown that the packing of the side groups determines the crystal structure of the polymer. Their work also shows that there is a large void volume in the DCHD crystalline monomer and strain introduced during polymerization process causes the side groups to reside in a variety of (slightly) different orientations. The results presented here serve to reinforce this assertion, and the pump-probe spectroscopic technique used senses the dynamical rather than static components of this structural heterogeneity.

An energy dependent slow response for all modes of excitation was observed (Figures 3.3-3.5). The most important aspect of these data is that the spectral profile of this slow response depends on the excitation energy, and this energy-dependence can be understood according to the amount of excess energy remaining in the system subsequent to electronic relaxation. The greater the energy difference between the excitation energy and the excitonic transition energy, the more features are observed in the slow response. The distinct features in the slow response are each separated by ~20 meV in DCHD, whereas the corresponding separation in PTS is ~40 meV. [16,17] It can be inferred that the structural variability in DCHD that gives rise to these individual features perturbs the

electronic structure of the backbone to a significantly smaller extent than the $\pm 8^{\circ}$ ring rotation seen for PTS.

The number of features seen in the slow response are related to the excess spectroscopic energy imparted to the system on excitation. Excitation of the side groups requires 3.57 or 4.13 eV, depending on the transition accessed. The backbone excitonic resonance is 1.90 eV. Excitation transfer from the side group to the backbone leaves either 1.67 or 2.23 eV of spectroscopic energy to be dissipated amongst the available degrees of freedom. Ultimately, the majority of this excess energy must be distributed into the vibrational modes of both the side groups and the polymer backbone. After excitation of the side groups and subsequent excitation transfer to the backbone, the side groups are vibrationally hot. Direct excitation of the backbone imparts no such excess energy in the side groups. Because dipolar coupling of the side groups to the polymer backbone gives rise to the slow optical response, the extent to which side group vibrational modes are populated will determine the number of species that can modulate the backbone resonance. It is fair to question whether these backbone modulations are side group vibrational mode-specific for a fixed side group orientation or are related to a distribution of side group orientations. From measurements on PTS it is known that the individual features in the slow response correspond to structurally distinct moieties rather than modulations from multiple vibrational modes. If it is assumed that this relationship holds for DCHD as well, then the excess vibrational energy remaining in the side groups is sufficient to distribute the side group among several slightly different orientations. For direct excitation of the polymer backbone, one resonance dominates the slow response

(Figure 3.3). For excitation at 3.57 eV, a different and broader resonance is seen, with at least two others discernible. Excitation at 4.13 eV yields four resonances in the slow response. Because it is unknown how the individual electronic states of the N-methyl carbazole moiety couple to the available vibrational degrees of freedom, i.e. ground state side group vibrational modes, it is not possible to predict how the excess vibrational energy will be partitioned, especially when the time scale of the observation is similar to the expected vibrational population relaxation times of organic molecules. [21] Measurement of the resonance Raman excitation profiles of both side group transitions would provide the information necessary to resolve this question. [14] However, the amount of excess energy remaining in the system could be correlated with the extent of observed structural heterogeneity. If it is assumed that the excess energy is distributed into all modes uniformly, the temperature rise in the DCHD crystal resulting from excitation of the side groups could be estimated. Assuming the thickness of the crystal to be 1000Å, the diameter of the beam spot at the crystal surface to be 25µm, and the excitation pulse to be functionally instantaneous, excess energies of 2.23 eV and 1.67 eV would change the temperature of the sample by ~9K and 7K, respectively, for these experimental conditions. These temperature increases are at least qualitatively consistent with the results obtained, but the differences in the slow responses for 1.67 eV and 2.23 eV excess energy (Figures 3.4 and 3.5, respectively) suggest different pathways for disposal of the excess energy from the two side group excited electronic states.

3.4. Conclusion

The pump-probe spectroscopic data on DCHD at 10 K show the rate of excitation transfer from the side group to the polymer backbone remains unresolvably fast (< 10 ps). While this result is consistent with the predictions of a Förster excitation transfer mechanism, it is not possible from these data to evaluate the rate constant for this process. The energy dependent slow response at 10 K indicates the presence of several subtle conformers within the exciton envelope, and suggests that the energetic barriers between these conformers is < 0.5 kcal/mol.

Literature Cited

- 1. D. S. Chemla and Z. Zyss, eds., Nonlinear Optical Properties of Organic Molecules and Crystals, Vol. 2, Academic Press, New York, 1987.
- 2. G. J. Blanchard, J. P. Heritage, A. C. Von Lehmen, M. K. Kelly, G. L. Baker and S. Etemad, *Phys. Rev. Letters*, 63, 887(1989).
- 3. G. J. Blanchard and J. P. Heritage, J. Chem. Phys., 93, 4377(1990).
- 4. M. E. Morrow and C. J. Eckhardt, Chem. Phys. Letters, 144, 65(1988).
- 5. L. Sebastian and G. Weiser, Phys. Rev. Letters, 46, 1156(1981).
- 6. L. Sebatian and G. Weiser, Chem Phys., 62, 447(1981).
- 7. R. J. Hood, H. Muller, C. J. Eckhardt, R. R. Chaance, and K. C. Yee, *Chem. Phys. Letters*, 54, 295(1978).
- 8. S. A. Hambir, T. Yang, G. J. Blanchard and G. L. Baker, Chem. Phys. Letters, 201, 521(1993).
- 9. T. S. Robinson, Proc. Phys. Soc. (London), **B65**, 910(1952).
- 10. T. S. Robinson and W. C. Price, Proc. Phys. Soc. (London), **B66**, 969(1953).
- 11. G. A. Anderson and W. B. Person, J. Chem Phys., 36, 62(1962).
- 12. Y. Jiang, S. A. Hambir and G. J. Blanchard, Opt. Commun., 99, 216(1993).
- G. J. Blanchard and M. J. Wirth, *Anal. Chem.*, 58, 532(1986); P. Bado, S. B. Wilson and K. R. Wilson, *Rev Sci. Instrum.*, 53, 706(1982); L. Andor, A. Lorincz, J. Siemion, D. D. Smith and S. A. Rice, *Rev. Sci. Instrum.*, 55, 64(1984).
- 14. D. N. Batchelder and D. Bloor, J. Phys. C, 15, 3005(1982).
- 15. G. J. Blanchard and J. P. Heritage, Chem. Phys. Letters, 177, 287(1991).
- 16. M. J. Nowak, G. J. Blanchard, G. L. Baker, S. Etemad, Z. G. Soos, *Phys. Rev.*, **B41**, 7933(1990).
- 17. D. Bloor and F. H. Preston, *Phys. Stat. Solidi* (a), 39, 607(1977).
- 18. M. Schott, F. Batallan and M. Bertaykt, Chem Phys. Letters, 53, 443(1978).
- 19. V. Enkelmann and G. Wegner, *Makromol. Chem.*, 178, 635(1977); V. Enkelmann, *Acta. Cryst.*, B33, 2842(1977).

- 20. V. Enkelman, R. J. Leyrer, G. Schleier, G. Wegner, J. Mat. Sci., 15, 168(1980).
- 21. S. A. Hambir, Y. Jiang and G. J. Blanchard, J. Chem. Phys., 98, 6075(1993).

CHAPTER 4

Disorder Induced Enhancement of the Third Order Optical Nonlinearity in a Conjugated Polymer

Abstract

The relationship between material disorder and nonlinear optical response for a conjugated polymer was investigated. Inverse Raman scattering, the technique used here, is sensitive to the transition cross sections of both the purely electronic $(S_1^{v=0} \leftrightarrow S_0^{v=0})$ and vibronic $(S_1^{v=0} \leftrightarrow S_0^{v=0})$ transitions accessed, and both of these quantities are related to the extent of disorder in the polymer backbone. These morphology dependencies were verified by using crystalline and amorphous samples of the polydiacetylene poly(4BCMU). The magnitude of the nonlinear response per backbone repeat unit in the amorphous material is comparable to that of the crystalline form because of the large potential well displacement between the ground and excited electronic states characteristic of the disordered material. This increased potential well displacement compensates for the nonlinear response lost to the reduced macroscopic polymer alignment associated with the 2-dimensionally isotropic spin cast film.

4.1. Introduction

The routing and storage of electronic signals is the fundamental action by which computing and related technologies operate. The properties intrinsic to semiconductor materials limit how fast electronic signals may be processed, and improvements beyond this point will require either new materials, new signal processing strategies, or a combination of the two. Replacing electrons with photons is a logical step in achieving faster information processing. Unfortunately, the technology and methodology for processing photonic signals, without first converting them into electronic signals, lags far behind the ability to send them over long distances. Advancing the field of photonic signal processing will require significant progress in both materials and switching strategies. If photon-based switching is to bear any resemblance to the architecture used for present-day electronic switching, which it must to ensure backward-compatibility, then materials that possess a large nonlinear optical response will be the cornerstone of this new technology. An all-optical switching material must change state or "turn on" rapidly without being excited directly, because the lifetime of a resulting excited state would limit its "turn off" time. A large nonresonant optical nonlinearity is therefore needed, and polydiacetylenes, because of their extensive conjugation, possess among the largest nonresonant third order optical nonlinearities known, $\chi^{(3)} \sim 10^{-9}$ esu.^[1,2] Despite this favorable optical property, most polydiacetylenes are available only as crystalline materials. While ideal for fundamental spectroscopic investigations, this structural property limits the potential utility of these materials for device applications. One family of polydiacetylenes, however, possesses urethane based side groups, and the labile nature of these side groups allows the

polymers to be synthesized and processed into a range of morphologies ranging from single crystals to amorphous films. The focus of this work is on determining the morphology-dependence of the nonlinear response for poly(4BCMU), a widely studied processable polydiacetylene (Figure 4.1).

Most device-oriented work aimed at exploiting $\chi^{(3)}$ has focused on conjugated polymers in waveguide formats because of the compatibility of this device structure with semiconductor electronics and optical fiber technology. [3-11] The preparation of waveguides and linear waveguiding have been demonstrated for both crystalline and amorphous thin films of polydiacetylenes. Nonlinear effects have been characterized as well, but the unambiguous demonstration of all-optical switching in waveguide devices has been elusive. [12,13] The fundamental limitation of such devices is the deleterious effects that both linear and nonlinear absorption have on waveguide performance. For example, linear losses not only reduce the intensity of the signal in the waveguide, but also lead to a slow, thermally-induced refractive index change that often overwhelms the nonlinear response and severely limits the duty cycle attainable for all-optical switching. [3,14] A further complication is that the nonlinear susceptibility contains both real and imaginary terms, and only the real part of the response (n₂) is useful for waveguide-based optical switching. The most significant contribution to the imaginary part of $\chi^{(3)}$ for this type of device is two-photon absorption. For crystalline polydiacetylenes waveguide-based switching is limited to wavelengths $\geq 1.3 \mu m$ with the low energy limit being determined by linear losses from overtone absorptions in the near-IR. [15] Switching strategies based on conjugated polymers in waveguide formats will be difficult to implement, and will be

Figure 4.1. Poly[5,7-dodecadiyne-1,12-diolsbis(n-butoxycarbonymethylurethane)] or Poly(4BCMU). The dashed lines indicates hydrogen bonding between the side groups.

impractical in the 0.7-1.3 µm wavelength range where many high powered solid state lasers are available. If these materials are to be useful for photonic signal processing applications, then alternative switching strategies will have to be employed.

Blanchard et. al. have reported on the inverse Raman scattering response of the polydiacetylene PTS, [16-18] a crystalline polydiacetylene (with rigid p-toluene sulfonate sidegroups) that possesses the same large nonlinear optical response as poly(4BCMU). The motivation for investigating poly(4BCMU) using inverse Raman scattering is to determine the effect(s) of structural disorder within the nonlinear chromophore on its optical response. This question is central to determining the ultimate utility of these materials for applications as photonic logic gates. The focus here is on the fundamental relationship between polymer morphology and nonlinear optical response in this material. The inverse Raman response of polydiacetylenes can be modeled quantitatively as a strongly coupled three level system, and the transition cross sections for the transitions accessed depend on the morphology of the polymer. The data presented here demonstrate that the deterministic transition cross section for the inverse Raman process is larger for the disordered material than for the corresponding crystalline material. This is an expected result based on the shorter effective conjugation length characteristic of the disordered material, and the reasons for this enhancement in the nonlinear response of disordered poly(4BCMU) are detailed below.

4.2. Theory

In order to provide a frame of reference for the motivations behind this work, the sort of optical device for which these materials will be useful must be considered. While there are many possible optical switching schemes, perhaps one of the most conceptually straightforward is that of an ultrafast optically-triggered shutter. This shutter could operate in either of two modes; normally open or normally closed. This work will concentrate on the latter because, for such a device, high contrast is not necessary; the switched signal exists against a dark background. For this device, a "carrier" light pulse incident on the material would be in resonance with the (excitonic) electronic transition and is either absorbed or reflected except when a "trigger" light pulse is coincident with the carrier pulse. The trigger pulse perturbs the excitonic absorption band in such a way as to allow the transmission of the carrier pulse. Only when both the trigger and carrier pulses are present does the material transmit at the carrier pulse frequency. Such a device is the optical analogue of a digital AND gate. The mechanism of the nonlinear response used as a "shutter" effect is stimulated inverse Raman scattering, [19] one of a family of nondegenerate four wave mixing processes. A significant reason for using nondegenerate, instead of degenerate, wavemixing spectroscopy is that, for nondegenerate processes, the detected optical response depends critically on the nuclear, i.e. vibrational, as well as electronic response of the system. For a coupled three level system (Figure 4.2), the third order susceptibility describing inverse Raman scattering is given by [20]

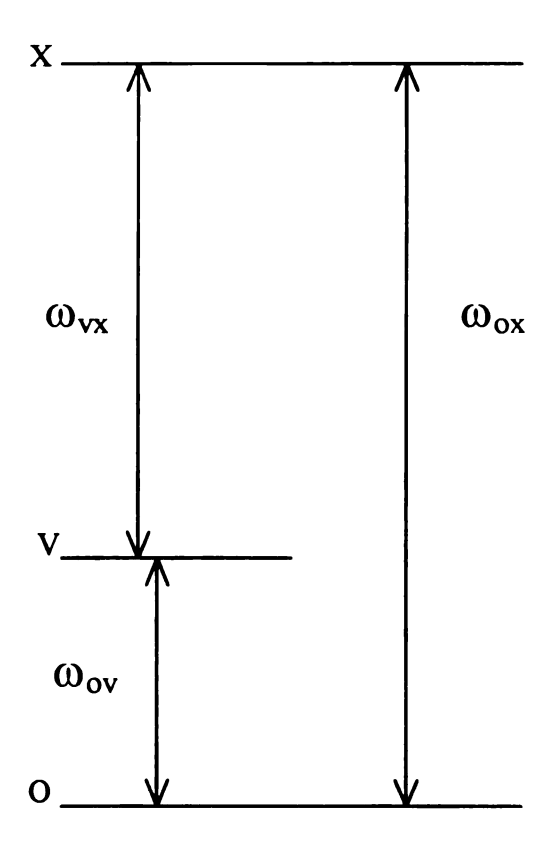


Figure 4.2. Schematic three level system.

$$\chi^{(3)}(\omega_t) = \frac{|\mu_{0x}|^2 |\mu_{vx}|^2}{\hbar^3} \bullet \frac{1}{(\omega_{0x} - \omega_t - i\gamma_{0x})^2 (\omega_{0y} - \omega_t + \omega_p - i\gamma_{0y})}$$
[1]

where the terms μ are dipole moments for the appropriate transitions, ω 's are frequencies and γ 's are linewidths. The subscripts refer to the levels shown in Figure 4.2, "t" is for "test" (= carrier) and "p" is for "pump" (= trigger), where the test and pump electric fields are provided by two independently tunable lasers. The important features in the inverse Raman response, including the phonon-mediated optical Stark effect, [16,20-22] arise from interference between the two complex terms in the denominator of Equation 1.

The relationship between polymer morphology and inverse Raman response is straightforward and is determined largely by the numerator terms in Equation 1. $\chi^{(3)}$ is related to the square of the dipole moments for both the purely electronic $X \leftrightarrow 0$ and the vibronic $X \leftrightarrow v$ transitions. The square of the transition dipole moment is related to the transition cross-section, [23]

$$\sigma_{ab} = \frac{8\pi^3 N_b \omega_{ab}}{3hc} \left| \int \psi_a \mu_{ab} \psi_b d\tau \right|^2$$
 [2]

where a and b are the two states involved in the transition. $\chi^{(3)}$ is proportional to the transition cross-sections and therefore the overlap integrals for those transitions, and the

$$\chi^{(3)} \propto \sigma_{0x} \sigma_{vx} \propto \langle 0|x \rangle^2 \langle v|x \rangle^2$$
 [3]

overlap integral for a transition is a function of the displacement between the ground and excited electronic state potential wells. The potential well displacement can be controlled by macroscopic polymer processing techniques. For identical ground and excited state harmonic oscillators, the displacement is expressed in terms of the dimensionless quantity $z_1^{[24]}$

$$z = \left(2\pi^2 \frac{mf}{h}\right)^{1/2} D \tag{4}$$

where m is the effective mass of the system, f is the vibrational frequency and D is the well displacement. Blanchard *et. al.* have shown that polydiacetylenes can be treated to excellent approximation using this harmonic oscillator model. The harmonic oscillator overlap integrals and resultant $\chi^{(3)}$ are (for a $\nu = 1 \text{ mode})^{[24]}$

$$\langle 0|0\rangle = \exp\left(-z^{2}/2\right) \qquad \langle 1|0\rangle = -z \, \exp\left(-z^{2}/2\right)$$

$$\chi^{(3)} \propto z^{2} \exp\left(-2z^{2}\right)$$
[5]

The dependence of $\chi^{(3)}$ on the potential well displacement is shown in Figure 4.3. For the polydiacetylene PTS the largest value of z, for the backbone C=C stretch, is ~0.5. [17,24] The magnitude of the two-color nonlinear response of a polydiacetylene can be increased by almost a factor of two if D can be optimized. The experimental data, described below, demonstrate that inducing disorder in poly(4BCMU) can serve to optimize D.

4.3. Experimental

4.3.1. Laser Spectroscopy. Stimulated inverse Raman spectroscopy is performed using a pump-probe laser spectrometer. [16-18,25] For these measurements an intense "pump" pulse provides sub-resonant excitation and a weak "test" pulse approximately one vibrational resonance higher in energy than the pump pulse interrogates the result of the excitation. The spectrometer used to generate these pulses has been described in detail in chapter 1, and only a brief synopsis is provided in here. The source laser is a mode-locked CW Nd:YAG laser (Coherent Antares 76-S) that produces 3W (average) at the second harmonic wavelength, 532 nm, and 1W (average) at the third harmonic, 355 nm. The repetition rate of this laser is ~76 MHz and the pulsewidth is ~100 ps FWHM. The output from this laser is used to excite two cavity dumped dye lasers (Coherent 701-3). The pulsewidths output from these lasers are 5 ps FWHM and the cross correlation between the two dye lasers is ~10 ps FWHM. For experiments on the crystalline polymer, the pump laser wavelength was varied between 730 nm and 680 nm (LDS 698 dye, Exciton) and the probe (test) laser tuned over the range of 670 nm to 635 nm (Kiton Red, Exciton). For experiments on the spin cast polymer film, the pump laser wavelengths

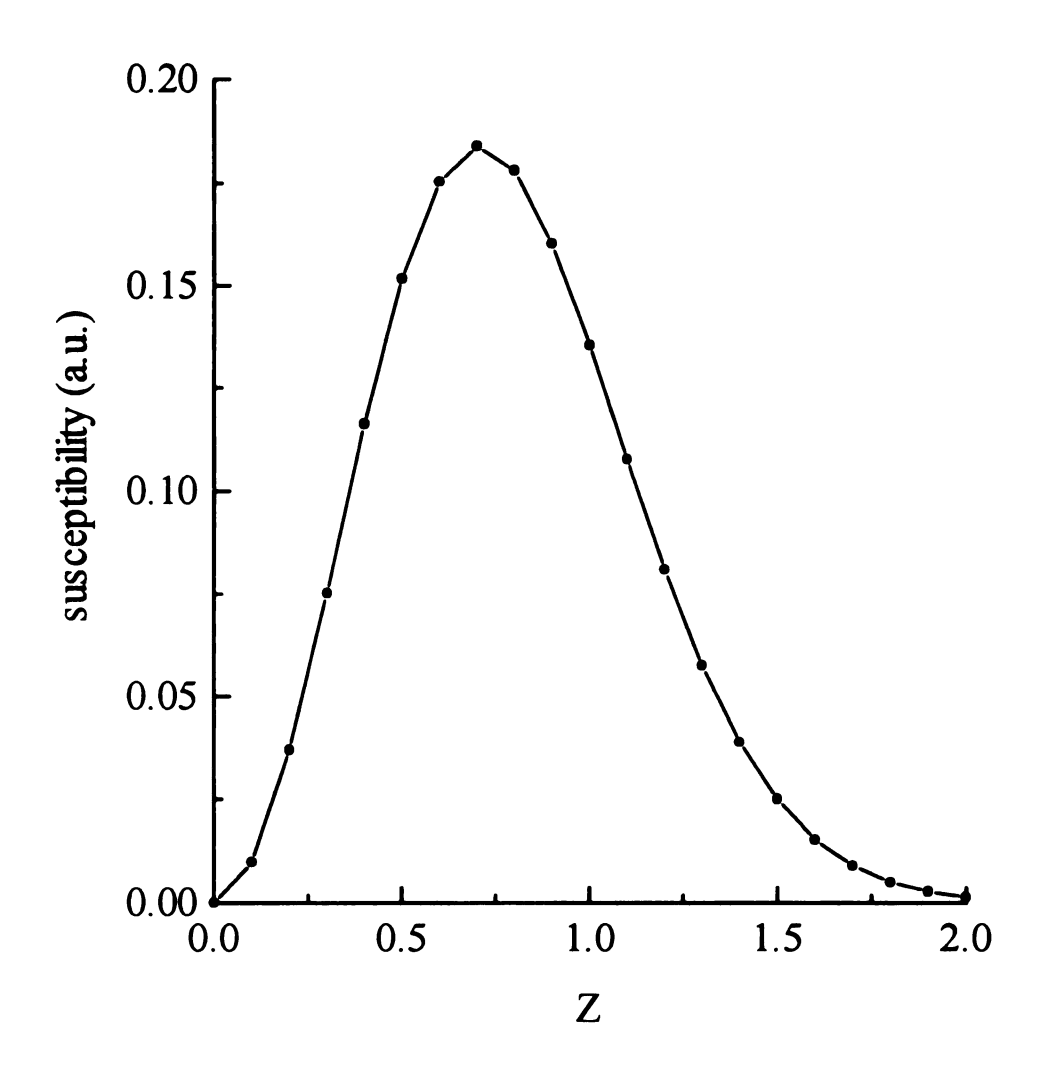


Figure 4.3. Nonlinear susceptibility as a function of potential well displacement.

were set between 627 nm and 579 nm (Rhodamine 6G, Rhodamine 610, Exciton) and probe laser wavelengths were tuned over the range of 565 nm to 520 nm (pyromethene 567 and coumarin 500, Exciton). The pump-probe signals are detected using radio- and audio-frequency triple modulation signal encoding with synchronous demodulation detection, allowing shot noise limited sensitivity and at least 4 orders of magnitude of linear dynamic range. This wide dynamic range is necessary for the quantitative measurement of the subtle features present in inverse Raman data.

Experimental stimulated inverse Raman spectra are obtained for a particular pump energy through a series of time scans at different probe frequencies. Though tedious, this technique measures signal intensities quantitatively because of its combined high time and frequency resolution. Families of inverse Raman spectra, taken at a progression of pump energies, are fit to calculated spectra to obtain σ_{vX} .

4.3.2. Materials processing. The synthesis of poly(4BCMU) can yield either the crystalline (blue phase) form of the material or, subsequent to polymerization, can be dissolved in an appropriate solvent and spin coated onto rigid substrates. For the preparation of the spin cast film, the polymer was mixed 5% by weight with cyclopentanone and dissolved by heating at 35°C and stirring. The resulting solution was spin coated at 1000 rpm for 60 seconds onto a quartz substrate. These two forms of poly(4BCMU) represent the extrema in the extent of disorder attainable in this material.

4.4. Results and Discussion

The magnitude of $\chi^{(3)}$ in polydiacetylenes is related to the oscillator strength of the exciton that dominates the absorption edge, and optical pumping schemes that couple vibrational modes to the exciton (e.g. the phonon mediated dynamic Stark effects)^[16,21,22] can be used to effect a nonlinear switching response that is not hindered by linear losses. These dynamic Stark effects have been measured and modeled quantitatively in crystalline forms of polydiacetylenes. [16-18] The exciton-phonon coupling that determines the efficiency of these Stark effects is intimately related to polymer ordering through the exciton line shape $(\gamma_x \text{ in Equation 1})$ and potential well displacement, D. [17] Poly(4BCMU) is the most widely studied member of a family of poly(nBCMU) polydiacetylenes^[29,30] whose macroscopic crystallinity is determined by the hydrogen bonded network formed by the urethane-based side groups (indicated by dashed lines in Figure 4.1). Disruption of this hydrogen bonded network reduces local order, interrupting the conjugation of the polymer backbone, thereby causing a dramatic change in the linewidth and energy of the excitonic response. [31] The position of the excitonic transition is remarkably sensitive to changes in polymer morphology, a ~300 meV blue shift and broadening of the excitonic resonance is observed on solvent disordering of crystalline poly(4BCMU) (Figure 4.4). For crystalline poly(4BCMU) the excitonic transition occurs at 1.96 eV and for the spin cast film, the transition is found to be centered at 2.29 eV. Both the shift and the transition line width can be used to characterize disorder in these materials. Poly(4BCMU) is processable into

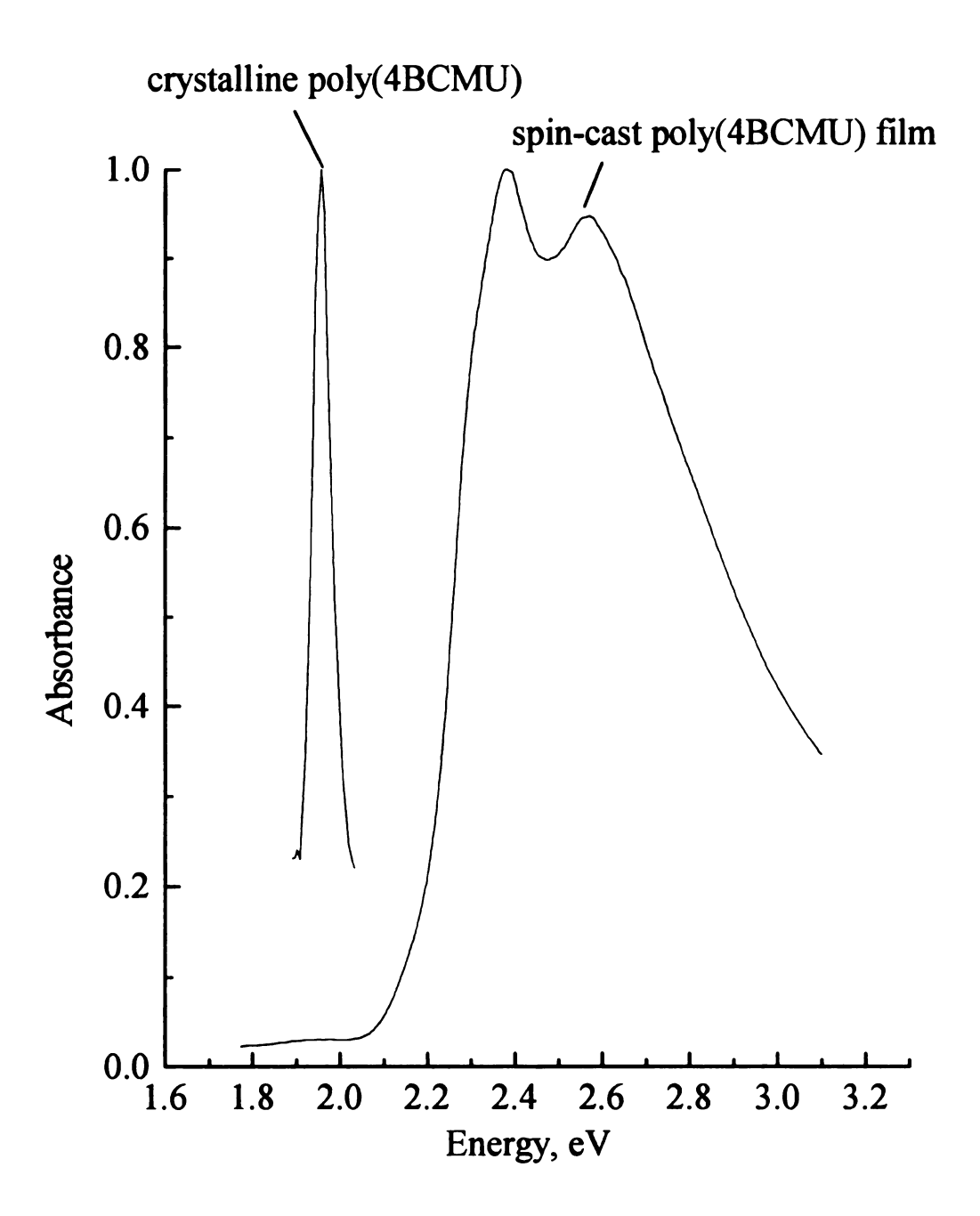


Figure 4.4. Linear absorption spectra of crystalline and spin cast film forms of poly(4BCMU). For the crystalline polymer, $\omega_{ox} = 1.96$ eV and for the spin cast film, $\omega_{ox} = 2.29$ eV.

morphologies ranging from single crystals to films that are isotropic in two dimensions. [7,32]

To understand the relationship between polymer disorder and the excitonic transition energy and linewidth, it is useful to consider the optical response of polydiacetylenes in the context of a one-dimensional particle in a box. For such a system the energy level spacing, ΔE, depends on the inverse of the square of the length of the "box", L,

$$\Delta E = \frac{h^2}{8mL^2} \tag{6}$$

Equation 6 implies that, for an infinite polymer chain, the energy gap should tend to zero. This clearly does not correspond to experimental data, and the practical limit to this interpretation lies in the characteristic length of the exciton, which is determined by the coulombic and correlation forces intrinsic to the conjugated backbone π system. If the spacing between interruptions in conjugation along the polymer backbone is greater than the characteristic exciton length plus the distance the exciton can migrate during its ~2 ps lifetime, [33] then the chain appears "infinite" to the excitation. Introducing disorder into the polymer reduces the effective length of the conjugated segment, thereby increasing ΔE . The presence of disorder also implies a distribution of conjugation lengths because the location of defects along the backbone is necessarily statistical. A distribution of conjugation lengths will result in a distribution of transition energies, $\Delta(\Delta E)$. The

introduction of disorder in polydiacetylenes has two measurable effects on the linear optical response of these materials - a spectral shift and an increase in the measured linewidth of the excitonic resonance.

Figures 4.5 through 4.8 show inverse Raman optical responses of both crystalline and spin cast poly(4BCMU). The intrinsic nonlinear response that gives rise to the inverse Raman spectra can be modeled qualitatively using Equation 1 in the small signal limit. The Schmitt-Rink model^[34] used in this calculation is more complete, and its application to experimental data has been described in the paper by Blanchard *et.al.*^[16-18] The signal detected experimentally is related to $Im\{\chi^{(3)}\}$ through the complex dielectric response of the polymer. In the limit of a small signal and a thick sample,

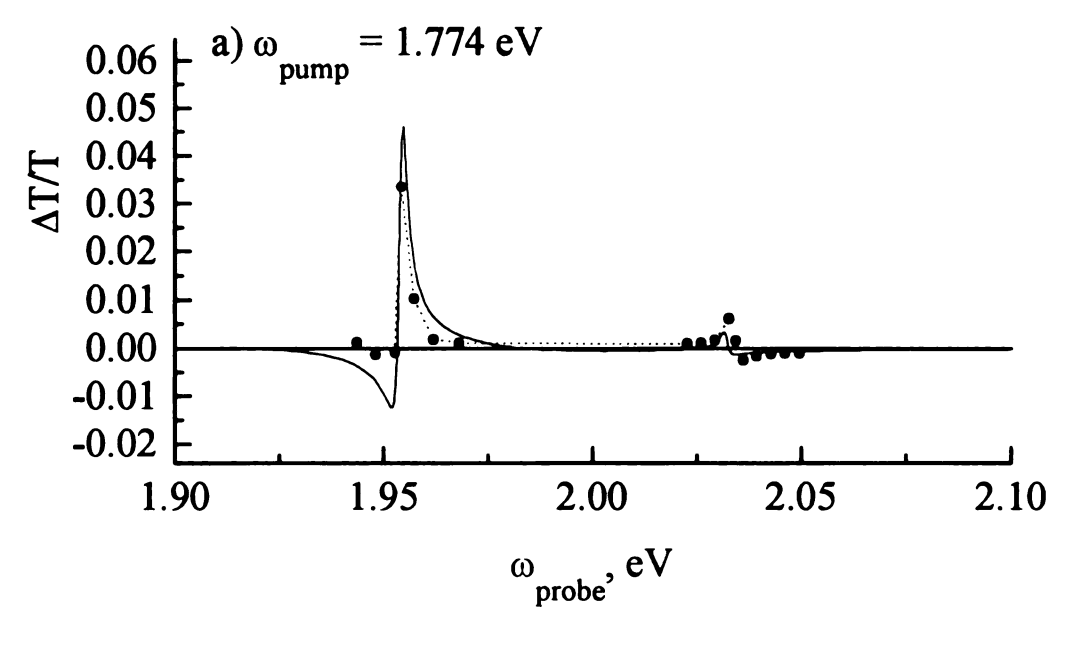
$$\frac{\Delta T}{T} \approx \Delta \alpha \ell = \left(\frac{2\omega \ell}{c}\right) \Delta k$$
 [7]

 $\Delta k = k(pump \ on) - k(pump \ off)$, ℓ is the material thickness, ω is the probe laser frequency and α is the material absorptivity at frequency ω . Δk is related to $\chi^{(3)}$ through the complex dielectric response of the material.

$$\Delta k = \left[\left(\Delta \varepsilon_1^2 + \Delta \varepsilon_2^2 \right)^{\frac{1}{2}} - \Delta \varepsilon_1 \right]^{\frac{1}{2}}$$

$$\Delta \varepsilon_1 = 1 + 4\pi \operatorname{Re} \left\{ \chi^{(3)} \right\}$$

$$\Delta \varepsilon_2 = 4\pi \operatorname{Im} \left\{ \chi^{(3)} \right\}$$
[8]



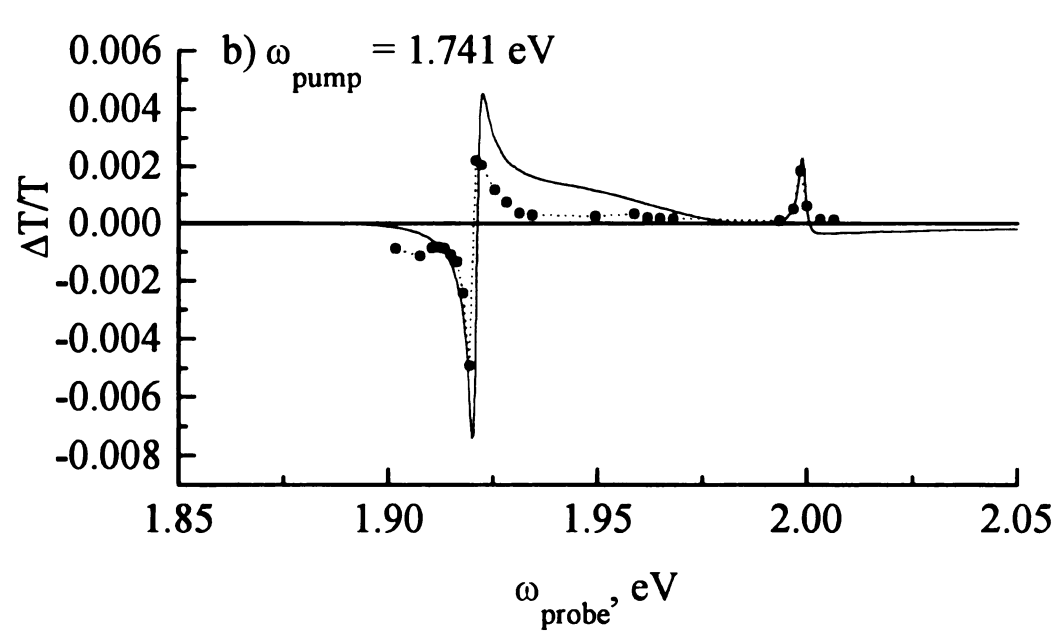


Figure 4.5. Experimental data points and calculated fit (solid line) for a) stimulated inverse Raman spectrum of crystalline poly(4BCMU) for $\omega_p = 1.774 eV$ and b) for $\omega_p = 1.741 eV$.

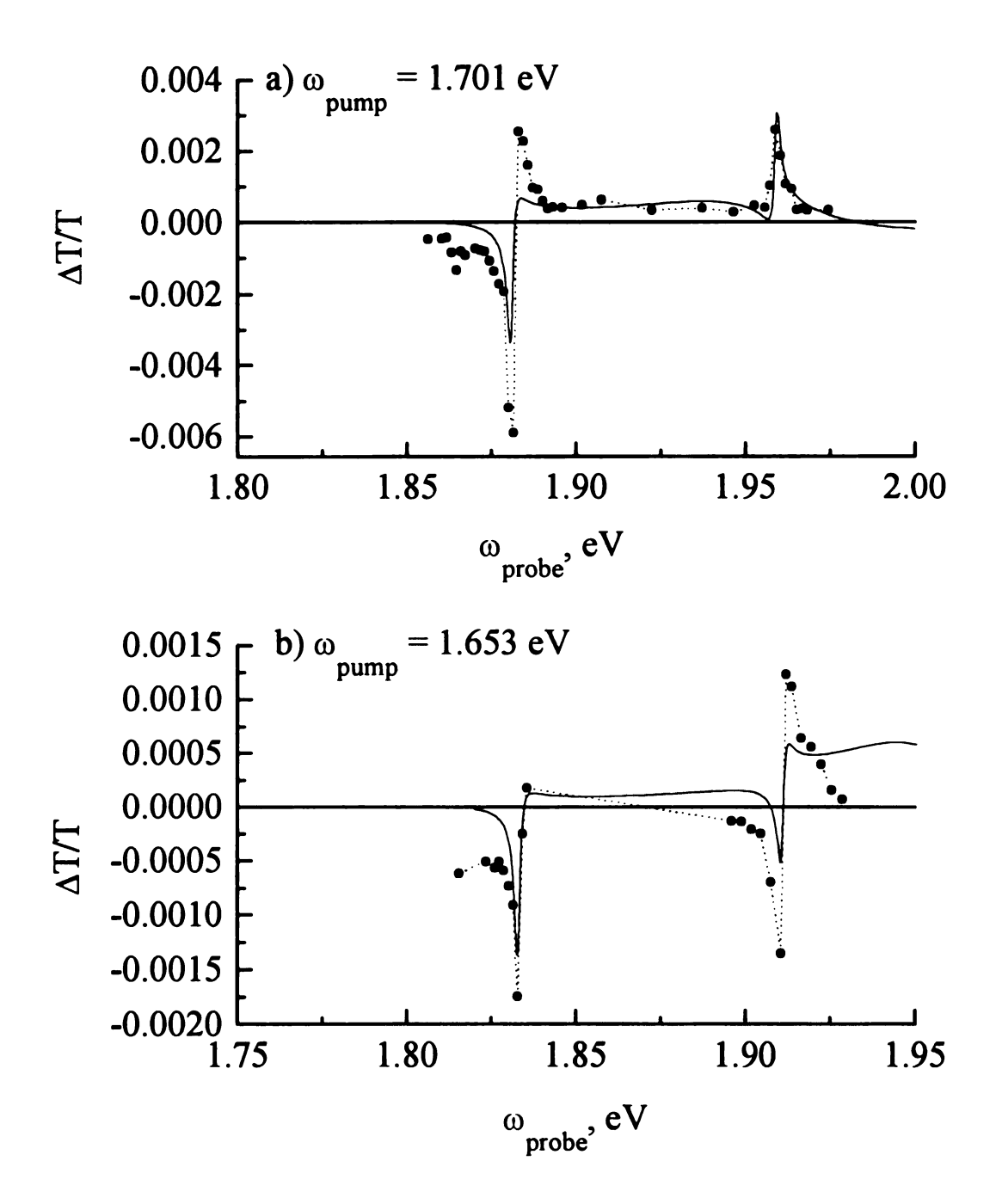


Figure 4.6. Experimental data points and calculated fit (solid line) for a) stimulated inverse Raman spectrum of crystalline poly(4BCMU) for $\omega_p = 1.701 eV$ and b) for $\omega_p = 1.653 eV$.

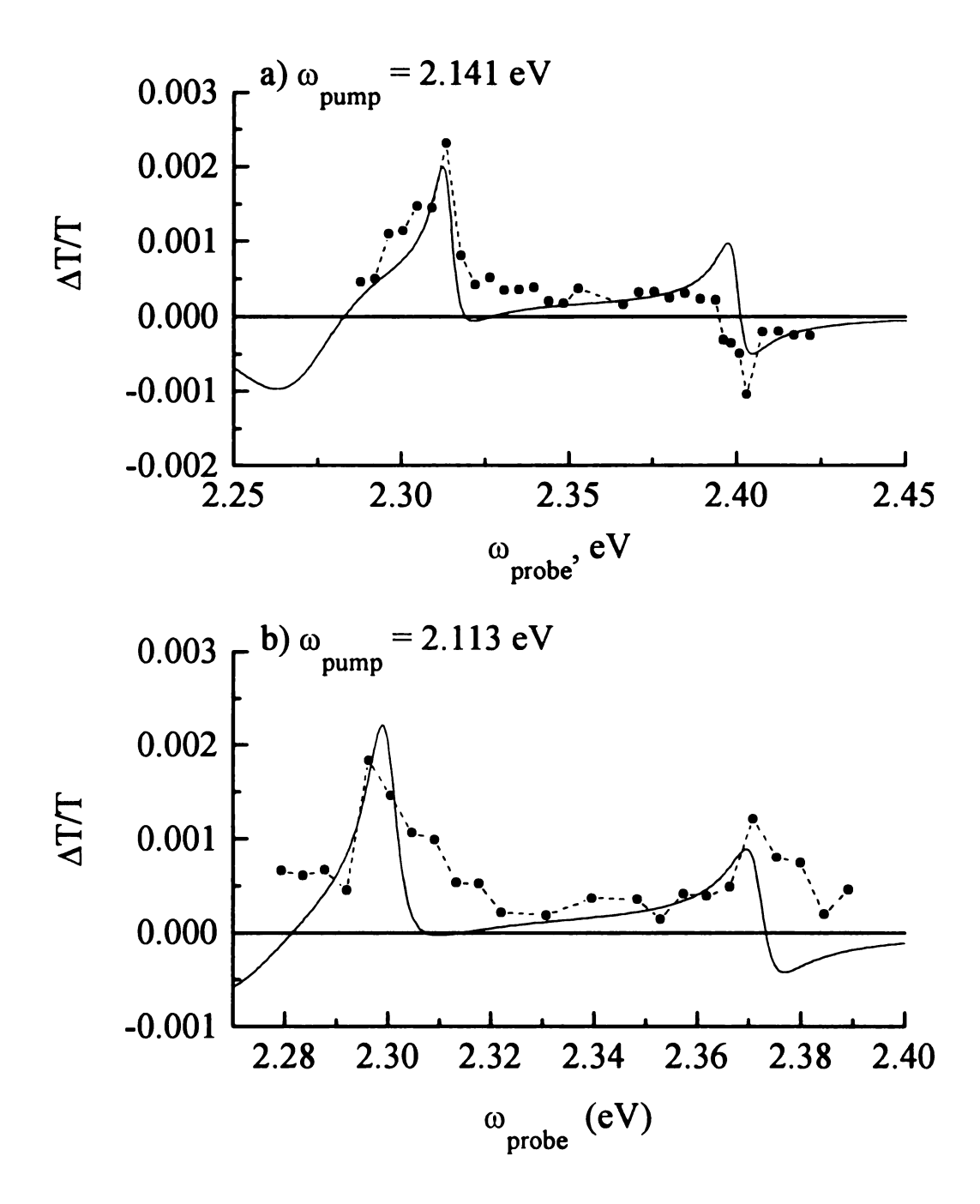


Figure 4.7. Experimental data points and calculated fit (solid line) for a) stimulated inverse Raman spectrum of spin cast poly(4BCMU) for $\omega_p = 2.141eV$ and b) for $\omega_p = 2.113eV$.

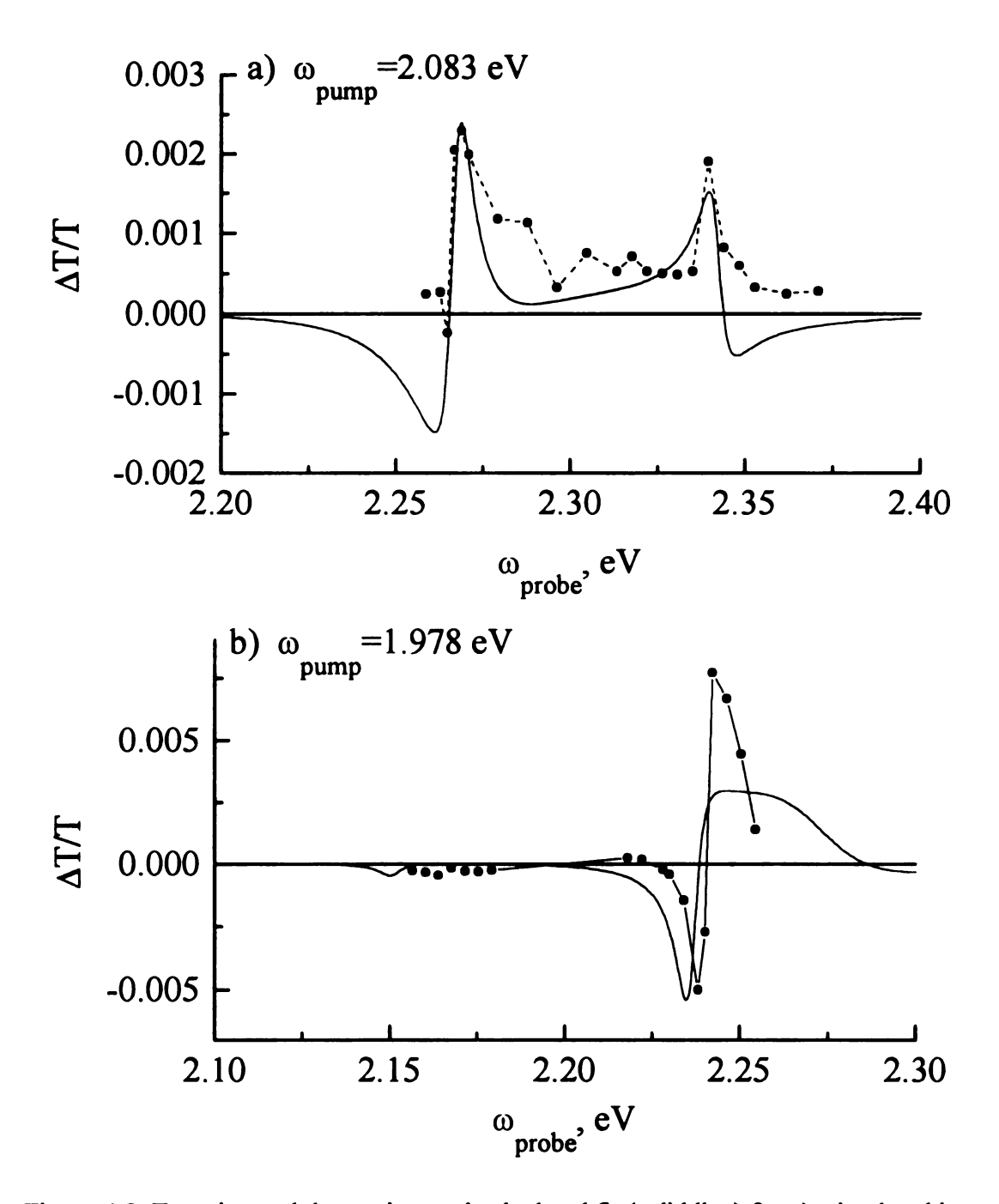


Figure 4.8. Experimental data points and calculated fit (solid line) for a) stimulated inverse Raman spectrum of spin cast poly(4BCMU) for $\omega_p = 2.083 \, \text{eV}$ and b) for $\omega_p = 1.978 \, \text{eV}$.

For materials with a large energy-dependent dielectric response, such as conjugated polymers, the difference between $\Delta T/T$ and $Im\{\chi^{(3)}\}$ can be significant. Using the relationships shown in Equations 8, virtually quantitative agreement between theory and experiment for both crystalline and spin-cast poly(4BCMU) has been achieved. Any slight differences between experiment and calculation can be traced to the use of a Lorentzian lineshape function in the theory and the experimental deviations from this lineshape assumption.

Figures 4.5-4.8 contain both the calculated and experimental inverse Raman spectra for crystalline and spin cast poly(4BCMU). The signal size increases as the overlap between the vibrational resonance and the electronic resonance is increased. As can be seen from the linear responses for the two forms of the polymer (Figure 4.4), the linewidth of the electronic transition changes significantly with disorder. What is not apparent from the linear responses, however, is that the effective linewidth of the exciton in the spin cast film is similar to that for the crystalline polymer, $(\gamma_x \sim 50 \text{ meV})$ with the vibrational linewidth for the spin cast films being significantly wider than for the crystals ($\gamma_v^{film} \sim 9 \text{ meV}$). This finding indicates that, while the shift in the excitonic transition energy is due to change(s) in the conjugation length, the majority of the spectral broadening in the film arises from the distribution of conjugation lengths present in the film, as discussed above. This finding also implies that the cross section for the dominant excitonic transition, σ_{0X} , in the film is diminished to only a small extent on disordering. This point is discussed below. For the calculations reported in Figures 4.5-4.8, the linewidth ratio $(\gamma_{0X}/\gamma_{0v}) = 17$ and 5.5 for crystalline and spin cast polymers, respectively, were found to be the best fits to the

experimental data. The value of the linewidth ratio affects the size and shape of the inverse Raman response. For off resonance conditions, where $\omega_p + \omega_{ov} >> \omega_{ox}$ and $\omega_t >>$ ω_{ox} , the Raman response is primarily absorptive and the sign of $\Delta T/T$ changes from positive to negative as ω_t increases through ω_{ox} . This sign change at the excitonic resonance is a blue-shift of the electronic transition caused by both the electronic and phonon-mediated optical Stark effects. The contribution to the $\Delta T/T$ response from these Stark effects increases as the linewidth ratio decreases. On resonance, where the pump energy is exactly $\hbar\omega_{0v}$ lower in energy than the electronic resonance and at $\omega_t = \omega_{ox}$, a transmissive (positive $\Delta T/T$) response with absorptive side bands is observed. These features are the result of splitting of the excitonic transition due to the resonant phononmediated optical Stark effect. The "hole" centered at ω_{ox} is larger than the absorptive inverse Raman response, and a transmissive feature is observed. The spectral width of the hole is determined by the electronic and vibrational linewidths and the Rabi frequency, R = $\mu_{0X}E_{p}$. The details of this transmissive feature are sensitive to higher order nonlinearities, χ $\chi^{(7)}$, etc.. [34] but these effects will be negligible for realistic experimental conditions. Between these two extremes, the inverse Raman response appears dispersive due to interference between the vibrational and electronic resonances, i.e. the denominator terms in Equation 1.

The experimental data show that the nonlinear optical response from unaligned spin cast films compares favorably with the response from crystalline poly(4BCMU). The primary difference between the nonlinear response of a crystal and a spin-cast film of

poly(4BCMU) lies in the absolute size of the response. The qualitative nature of the signal is largely unaffected by modest changes in line widths and variations in the linear dielectric response, although the quantitative details of the lineshapes and intensities depend critically on the cross sections and linewidths. Indeed, it is this quantitative information that is important in elucidating the role that polymer disorder plays in affecting the nonlinear response. For a spin cast film, there are two competing factors that serve to approximately cancel one another. A reduction in the intensity of the nonlinear response is expected solely because of inefficient alignment of the nonlinear chromophore(s) with the incident electric field. Compensating for this reduction is an increase in the magnitude of the nonlinear response per chromophore due to a reduction in effective conjugation length of the nonlinear chromophore. By fitting the experimental data to the Schmitt-Rink model, and using dielectric corrections, the transition cross sections, σ_{vX} , for the C=C and C=C stretching resonances in both crystals and films were obtained (Table 4.1). In these fits to the data, it was determined that the optimum sample thickness and transition cross section consistent with all of the spectra taken for a given type of sample, either crystalline or spin cast film. For a given set of calculations there are no adjustable parameters. The sample thickness (l = 700 Å for crystalline poly(4BCMU) and l = 300 Å for the spin cast film) and transition cross sections (Table 4.1) were held constant for all calculations of the spin cast film spectra, and a different set of optimized values were used for the calculation of crystalline polymer spectra. The way to determine the optimum values of σ and l has been described by Blanchard et. al. [16-18] and we will not detail this procedure here. From these fits to the data the cross sections σ_{vX} for the double and triple bond resonances were

determined and are almost a factor of two *larger* for the spin cast film than for the crystalline polymer.

Table 4.1. Experimental v-X transition cross-sections and maximum ΔT/T values for backbone double and triple bond stretching resonances in crystalline and spin cast films of poly(4BCMU).

	C=C stretch		C≡C stretch	
	σ _{vX} (eV)	$(\Delta T/T)_{max}$	σ _{vX} (eV)	$(\Delta T/T)_{max}$
crystal	0.15	0.014	0.07	0.0023
spin cast film	0.26	0.0021	0.15	0.0019

This is an expected result based on the information presented in the theory section. The dependence of the nonlinear response on polymer disorder can be understood at an intuitive level. Both the ground state and excitonic equilibrium internuclear distances, r_e , depend on the π electron density of the conjugated system over the exciton coordinate. On excitation, the electron density of the π system is reduced by one electron, and hence, the strength of the π bonds decreases, making r_e^* larger than r_e . This reduction in electron density is distributed over the effective conjugation length of the system. The longer the conjugation length, the smaller the change in electron density per bond on excitation. Thus a disordered material, having a displacement larger than that for the corresponding crystalline material partially compensates for the loss of nonlinear response associated with a processing-induced loss of anisotropy. These experimental data demonstrate that σ_{vx} for the C=C and C=C backbone stretching resonances are almost a factor of two larger for the

spin cast film than for the crystalline polymer. This model predicts that with the increase in σ_{vX} there will be a corresponding decrease in σ_{0X} . Because of the functionality of the overlap integrals, however, (see Equations 5) an increase in potential well displacement results in an increase in $\chi^{(3)}$.

The data presented in Figures 4.5-4.8 also provide structural information analogous to that available from spontaneous resonance Raman measurements. The frequencies of the C=C and C=C backbone stretching resonances in poly(4BCMU) are sensitive to disorder in the system. Zheng et al. [35] have found that the spontaneous resonance Raman response of spin cast films of poly(4BCMU) exhibits a significant excitation energy dependence. Specifically, the energies of both the C=C and C=C vary according to the excitation energy, and the variation does not depend in a simple way on the excitation frequency (Table 4.2). Zheng et al. concluded from this work that different excitation wavelengths

Table 4.2. Experimental frequencies of C=C and C=C stretching resonances for spin cast film poly(4BCMU) as a function of excitation energy.

	C=C stretch	C≡C stretch	
ω_p (eV)	ω _v (eV)	ω _v (eV)	
2.141	0.173	0.254	
2.113	0.184	0.258	
2.083	0.184	0.258	
1.978	0.190	0.256	
	1		

selected regions with a characteristic extent of disorder, or a particular conjugation length.

Different excitation wavelengths selected different subsections of the cast film, and

because the C=C and C=C resonances are isolated to the polymer backbone, it is not surprising that their center frequencies depend critically on the extent of backbone order in the system. The inverse Raman data on poly(4BCMU) films also exhibit an excitation energy dependence, and we believe the origin of this effect is the same as that for the spontaneous resonance Raman data.

As mentioned earlier, while the nonlinear response of spin cast films of poly(4BCMU) is enhanced per backbone nonlinear chromophore unit compared to the crystalline material, the magnitude of the signal (for the same sample thickness) is close to the same for the two systems due to the orientational disorder intrinsic to the spin cast film. Disorder induced enhancement of $\chi^{(3)}$ in poly(4BCMU) can be increased further by controlling the macroscopic backbone orientation within the spin cast polymer film. The backbone orientation of the polymer can be controlled by stretch alignment. This processing technique optimizes the long range orientation of the polymer while maintaining the short range disorder that serves to enhance $\chi^{(3)}$. For thin polymer films, interactions between the poly(4BCMU) film and the substrate can also influence the nonlinear response of the system. These processing-related effects are described in the next chapter. [36]

4.5. Conclusion

Stimulated inverse Raman scattering has been used to examine the dependence of $\gamma^{(3)}$ on material disorder. The data on crystalline and spin cast films of poly(4BCMU) show that little if any effective nonlinear response is lost in the amorphous material (Table 4.1). The enhancement of nonlinear response in a disordered polymer can be accounted for by the large displacement between the ground and excited state equilibrium distance which partially restores the nonlinear response. The magnitude of the $\Delta T/T$ signal is modest in the experiments reported in here because the measurements were made in the small signal limit, but the observed transient change in transmission of ~1% for the ~10 nJ pulse energies used indicates that this method of accessing $\chi^{(3)}$ is extremely efficient and that, ultimately, this optical signal processing strategy will prove successful for photonic logic device applications. These data also demonstrate that there is a significant opportunity to enhance the $\chi^{(3)}$ response in processed films compared to the corresponding crystalline polymer because stretch alignment will return a portion of $\chi^{(3)}$ lost to macroscopic alignment while maintaining the enhancement in $\chi^{(3)}$ arising from microscopic disorder.

Literature Cited

- 1. C. Sauteret. J. P. Hermann, R. Frey, F. pradere, J. Ducuing, R. H. Baughman and R. R. Chance, *Phys. Rev. Lett.*, **36**, 956(1976).
- 2. P. W. Smith, Bell System Tech. Journal, 61, 1975(1982).
- 3. G. I. Stegeman, A. Miller in *Photonics and Switching*, Ed. J. E. Midwinter, Academic Press, London, 1994.
- 4. G. L. Baker in *Contemporary Topics in Polymer Science*, Vol. 7, Ed. by J. C. Salamone and J. Riffle, Plenum Press, New York, 1992, pp. 269-277.
- 5. G. I Stegeman, E. M. Wright, Opt Quant. Elect., 22, 95(1990).
- 6. S. R. Friberg, Y. Silberberg, M. K. Oliver, M. J. Andrejco, M. A. Saifi and P. W. Smith, Appl. Phys. Lett., 51, 1135(1987).
- 7. P. D. Townsend, G. L. Baker, N. E. Schlotter, C. F. Klausner and S. Etemad, Appl. Phys. Lett., 53, 1782(1988).
- 8. P. D. Townsend, G. L. Baker, N. E. Schlotter, C. F. Klausner and S. Etemad, Synth. Met., 28, D633(1989).
- 9. W. Krug, E. Miao, M. Derstine and J. Valera, J. Opt. Sco. Am. B, 6, 726(1989).
- 10. T. Kaino, K. Jinguji and S. Nara, Appl. Phys. Lett., 41, 802(1982)
- 11. N. E. Schlotter, J. L. Jackel, P. D. Townsend and G. L. Baker, Appl. Phys. Lett., 56, 13(1990).
- 12. D. M. Krol and M. Thakur, Appl. Phys. Lett., 56, 1406(1990).
- 13. M. C. Gabriel, N. A. Whitaker, C. W. Dirk, M. G. Kuzyk and M. Thakur, *Opt. Lett.*, **16**, 1334(1991).
- 14. P. D. Townsend, J. L. Jackel, G. L. Baker, J. A. Shelburne, III and S. Etemad, *Appl. Phys. Lett.*, **55**, 1829(1989).
- 15. A. Tanaka, H. Sawada, T. Takoshima and N. Wakatsuki, Fiber Integ. Opt., 7, 139(1988).
- 16. G. J. Blanchard, J. P. Heritage, A. C. Von Lehmen, M. K. Kelly, G. L Baker and S. Etemad, *Phys. Rev. Lett.*, 63, 887(1989).
- 17. G. J. Blanchard and J. P. Heritage, J. Chem. Phys., 93, 4377(1990).

- 18. G. J. Blanchard and J. P. Heritage, Chem. Phys. Lett., 177, 287(1991).
- 19. W. J. Jones and B. P. Stoicheff, Phys. Rev. Lett., 13, 657(1964).
- 20. S. Saikan, N. Hashimoto, T. Kushida and K. Namba, J. Chem. Phys., 82, 5409(1985).
- 21. M. Yoshiuzawa, Y. Hattori and T. Kobayashi, Phys. Rev. B, 47, 3882(1993).
- 22. T. Kobayashi, M. Yoshizawa, M. Hasegawa and M. Taiji, J. Opt. Soc Am B, 7, 1558(1990).
- 23. G. Herzberg, *Molecular Spectra and Molecular Structure*, Vol. 1, Van Nostrand, New York, 1950, p.383.
- 24. D. N. Batchelder and D. Bloor, J. Phys. C, 15, 3005(1982).
- 25. Y. Jiang, S. A. Hambir and G. J. Blanchard, Opt Commun., 99, 216(1993).
- 26. G. J. Blanchard and M. J. Wirth, Anal. Chem., 58, 532(1986).
- 27. P. Bado, S. B. Wilson and K. R. Wilson, Rev. Sci. Intrum., 53, 707(1982).
- 28. L. Andor, A. Lorincz, J. Siemion, D. D. Smith and S. A. Rice, *Rev. Sci. Instrum.*, 55, 64(1984).
- 29. T. Kobayashi, J. Lumin., 58,117(1994).
- 30. S. Molyneux, A. K. Kar, B. S. Wherrett, T. L. Axon and D. Bloor, *Opt Lett.*, 18, 2093(1993).
- 31. M. J. Nowak, G. J. Blanchard, G. L. Baker, S. Etemad and Z. G. Soos, "Slow Relaxations in PDA-4BCMU: From Crystals to Films", in *Conjugated Polymeric Materials: Opportunities in Electronics, Opto-Electronics and Molecular Electronics*, Ed. by J. L. Breda and R. R. Chance, NATO ASI Series E, Vol. 182, Kluwer Academic Publishers, Dordrecht, 1990, 421-427.
- 32. G. N. Patel, Polym. Prepr., ACS Div. Polym. Chem., 19(2), 155(1978).
- 33. G. M. Carter, M. K. Thakur, Y. J. Chen and J. V. Hryniewicz, *Appl. Phys. Lett.*, 47, 457(1985).
- 34. B. I. Greene, J. F. Mueller, J. Orenstein, D. H. Rapkine, S. Schmitt-Rink and M. Thakur, *Phys. Rev. Lett.*, **61**, 325(1988).
- 35. L. X. Zheng, R. E. Benner, Z. V. Vardeny and G. L. Baker, *Physical Review B*, 42, 3235(1990).
- 36. S. A. Hambir, D. Wolfe, G. J. Blanchard and G. L. Baker, in preparation.

CHAPTER 5

The Effect of Stretch Orientation on the Linear and Nonlinear Optical Response of Poly(4BCMU) Films

Abstract

The effect of stretching-induced alignment on the third order nonlinear optical response of thin films of the processable polydiacetylene poly(4BCMU) has been investigated. Modest enhancement of the nonlinear response in the stretch-aligned material compared to the non-aligned material was observed. The enhancement was limited by the extent to which the nonlinear polymer and supporting substrate can be stretched. In the stretch-aligned poly(4BCMU) films, two electronic resonances, centered at 2.02 eV and 2.29 eV, were detected by using stimulated inverse Raman scattering. The 2.02 eV electronic transition arises either from crystallinity induced in the spin cast poly(4BCMU) film by alignment or from an interaction between the substrate and the poly(4BCMU) backbone. The possible molecular origins for these data are discussed.

5.1. Introduction

Conjugated polymers have attracted significant attention as candidate materials for photonic signal processing applications. For a material to be suitable for photonic signal processing, it must possess a large nonlinear optical response and also be processable. Many materials satisfy either one of these criteria, but fail to fulfill both. Polydiacetylenes are one class of polymers that possesses a characteristically large third order $(\gamma^{(3)})$ nonlinear optical response. [1,2] and many members of this family of polymers can be synthesized as high quality single crystals. The availability of polydiacetylenes in this structural motif has allowed the unambiguous separation of inter-chain optical effects from those intrinsic to single polymer chains. [3-6] The ability to effect this separation is uncommon in most polymeric materials, and the spatial separation of adjacent polymer backbones by the sidegroups in many crystalline polydiacetylenes has allowed a substantial level of understanding to be achieved. There have been a large number of nonlinear optical effects demonstrated in crystalline polydiacetylenes, with several showing promise for photonic signal processing applications. While crystalline forms of polydiacetylenes are invaluable for understanding the spectroscopic processes intrinsic to strongly coupled three level systems, [7-9] it is unlikely that these materials will be used for practical device applications because of the difficulties associated with crystal growth as well as the inability to process these comparatively intractable crystals into useful device formats. The production of large-area thin polymer films is a well developed technology^[10-12] and is inexpensive compared to large scale crystal growth. Making thin films of polydiacetylenes requires that the polymer sidegroups be large and labile enough to allow the polymer to be

soluble in organic solvents. Highly uniform thin films of the polydiacetylene poly(4BCMU) have been demonstrated, [9,11] making this particular polymer a logical choice for further development. In chapter 4 it was shown that the disorder induced in poly(4BCMU) as a result of the film formation process served to enhance its inverse Raman^[13] nonlinear switching response per unit length of the polymer. [9] The magnitude of the inverse Raman response in thin films of poly(4BCMU) was the same as that for the crystalline polymer despite the loss of signal in the film associated with the unavoidable misalignment between the polymer nonlinear chromophore and the incident electric fields. The focus of this chapter is on efforts aimed at recovering that portion of the nonlinear response in films by using stretch alignment techniques. We found that this strategy is successful and, in this initial demonstration, is limited by both the elasticity of the supporting substrate and molecular interactions between the poly(4BCMU) nonlinear chromophore and the substrate.

5.2. Experimental

5.2.1. Nonlinear laser spectroscopy. A pump-probe laser spectrometer was used for our stimulated inverse Raman scattering measurements.^[14] An intense "pump" laser pulse provides sub-resonant excitation and a weak "probe" laser pulse, approximately one vibrational resonance higher in energy than the pump pulse, interrogates the result of the excitation. The spectrometer used for these measurements produces two trains of picosecond pulses which are independently frequency-tunable and have a well defined temporal relationship. The source laser is a mode-locked CW Nd:YAG laser that

produces 3 W average power at 532 nm and > 1 W average power at 355 nm. The repetition rate of this laser is ~76 MHz and the pulsewidth is ~100 ps FWHM. The output of this laser was used to excite synchronously two cavity-dumped dye lasers. The dye laser pulsewidths were typically 5 ps FWHM and the cross correlation between the two dye lasers was ~10 ps FWHM. For these experiments the pump laser wavelength was varied between 579 and 627 nm (Rhodamine 590 and Rhodamine 610, Exciton) and the probe laser was varied over the range 512 nm to 575 nm (Coumarin 500 and Pyromethene 567, Exciton). The pump-probe signals were detected using radio- and audio-frequency triple modulation signal encoding with synchronous demodulation detection, allowing shot noise limited sensitivity and at least 4 orders of magnitude of dynamic range. This wide dynamic range is necessary for the quantitative measurement of the subtle features present in inverse Raman data. [7,8]

- **5.2.2. Linear spectroscopy**. The absorption data for spin coated and stretch-aligned films of poly(4BCMU) were recorded with ~1 nm resolution using a Hitachi U4001 absorption spectrophotometer.
- **5.2.3. Material processing**. Macroscopic chain alignment of spin cast poly(4BCMU) films was enhanced using stretch-orientation. A 5 wt. % solution of poly(4BCMU) in cyclopentanone was used for spin coating (1000 rpm, 60 sec.) onto the optically transparent polymer substrate. After drying, the poly(4BCMU)/substrate composite was annealed at 100° C for two hours and stretched to the desired elongation ratio (ℓ/ℓ_0) using an in-house apparatus.

5.2.4. Substrate. The substrate support material used in this work was a copolymer poly(tetrafluoroethylene-co-hexafluoropropylene) (FEP). This polymer was chosen as the substrate material because it is amorphous, thereby avoiding Rayleigh scattering interference to the nonlinear response associated with the processing-induced formation of microcrystalline domains. Because of the nearly complete fluorination of this polymer, it possesses a low surface tension and thus does not adhere efficiently to poly(4BCMU). The surface of the FEP copolymer was modified using a method similar to that used by Bening and McCarthy^[16] and Dwight and Riggs.^[17] The copolymer substrate was treated with benzophenone and metallic sodium in cyclopentanone at 60°C for 24 hr under N₂ atmosphere and was subsequently rinsed with water, acetone and hexane, in that order. The purpose of this treatment is to abstract fluorine from the FEP copolymer surface and create carbon-carbon double bonds so that poly(4BCMU) can interact with the polymer substrate. Spontaneous resonance Raman spectra of the modified substrate exhibited a resonance at ~1560 cm⁻¹ which was assigned to the C=C stretching mode. The untreated substrate did not exhibit this resonance. Poly(4BCMU) adheres to the modified FEP substrate.

5.3. Results and Discussion

One of the primary limitations to progress in optical signal processing lies in the ability to control and process candidate nonlinear materials. To advance this field to the point of demonstrating practical devices, it will be necessary to effect optical switching in processable, predominantly non-crystalline materials. While such materials can be made with comparative ease, understanding their local structure is a substantially more difficult task. It is this local structure, however, that, to a large extent, determines the nonlinear optical response(s) of the candidate materials. The relationship between polymer morphology and nonlinear optical properties must be understood from a fundamental perspective to gain predictive control over the processing of these materials.

For practical applications, photonic materials should ideally combine the required optical properties with favorable mechanical properties, such as rigidity and strength, required for processability. The most common processing method for poly(4BCMU) is film deposition onto a polymer, glass, or semiconductor substrate by spin coating. The substrate provides the necessary mechanical characteristics to an otherwise fragile organic polymer. The thickness of the polymer film can be controlled through the spin coating rate and the amount of material deposited on the substrate. Because of the comparatively robust nature of the substrate, it is possible to perform macroscopic stretch alignment operations on this system in order to optimize the optical response of the photonic material.

In previous work on optical waveguiding in spin cast poly(4BCMU) films, high laser fluence at 1.06 µm was shown to change the steady state optical response of the polymer. This effect is not due to photochemical degradation, but instead to local heating resulting from the small, but finite linear absorption in poly(4BCMU) at 1.06 µm. While optical switching in poly(4BCMU) is not performed at 1.06 µm, it is necessary to consider thermally mediated optical processes. To make useful films, they have to be processed in such a way as to minimize their near-IR absorption tail. The extent of this tail is determined by local disorder in the polydiacetylene backbone. One important means of processing poly(4BCMU) is annealing. Differential scanning calorimetry (DSC) traces of spin-cast poly(4BCMU) films show two broad transitions; one beginning just above room temperature and extending to 110°C, and a second endothermic transition at 165°C. [18] The first transition is associated with melting of the hydrogen-bonded lattice formed within the side chains of poly(4BCMU), while the second transition reflects gross disordering of the polymer backbone. Annealing poly(4BCMU) films at ~100°C sharpens the first DSC transition and causes a corresponding increase in the intensity of the excitonic transition. Annealing allows the chains to relax locally and enables reformation of the hydrogen-bonded lattice. For annealing at $T > 110^{\circ}$ C, the hydrogen-bonded lattice "melts" and the chains rearrange to form ordered domains that scatter light.

Heat, solvent, and pressure cause backbone conformational changes in poly(4BCMU) and these changes are manifested as thermo-, solvato-^[19], and piezochromism.^[20] Particularly striking are chromic effects that reflect conformational disorder on length scales shorter than the size of a relaxed exciton on a polydiacteylene chain. For example, blue single

crystals of poly(4BCMU) turn red on exposure to solvent vapors,^[21] and form yellow solutions in good solvents.^[19] Similarly, heating poly(4BCMU) crystals yields first a red phase, and then a tacky orange-yellow solid at higher temperatures. In both cases, the red phase materials are less ordered than the single crystals, and yellow phase materials correspond to the most extensively disordered polydiacteylene chains.

The linear vibrational and electronic responses of polydiacetylenes provide important information on the conformation and orientation of the polymer backbone and side groups. Both the center frequency and the bandwidth of the $\pi \to \pi^*$ electronic transition. localized on the polymer backbone, depend on the processing history of the material and this relationship can be exploited to characterize and quantitate the extent of backbone disorder in the polymer. [21] Anisotropy in the electronic response can be used to infer the extent of backbone ordering in stretch aligned poly(4BCMU). While stretching clearly improves the overall alignment of the chains, the local environment can remain disordered because of twists in the polymer backbone, kinks, and side chain disorder. Spectra of stretch-aligned poly(4BCMU) show a higher optical dichroism than unstretched spin cast films (vide infra), but the shape of the absorption band for light polarized along the polymer backbone is largely unchanged from that of unstretched film cast onto the same substrate (Figure 5.1). A particularly sensitive marker for local disorder in poly(4BCMU) is the relative intensity of the exciton in polydiacetylenes. In addition, the energy of the excitonic transition depends sensitively on polymer morphology. For single crystals, the excitonic resonance appears at ~1.96 eV and dominates the optical properties of polydiacetylenes. For spin cast poly(4BCMU) films, the exciton appears at ~2.29 eV in

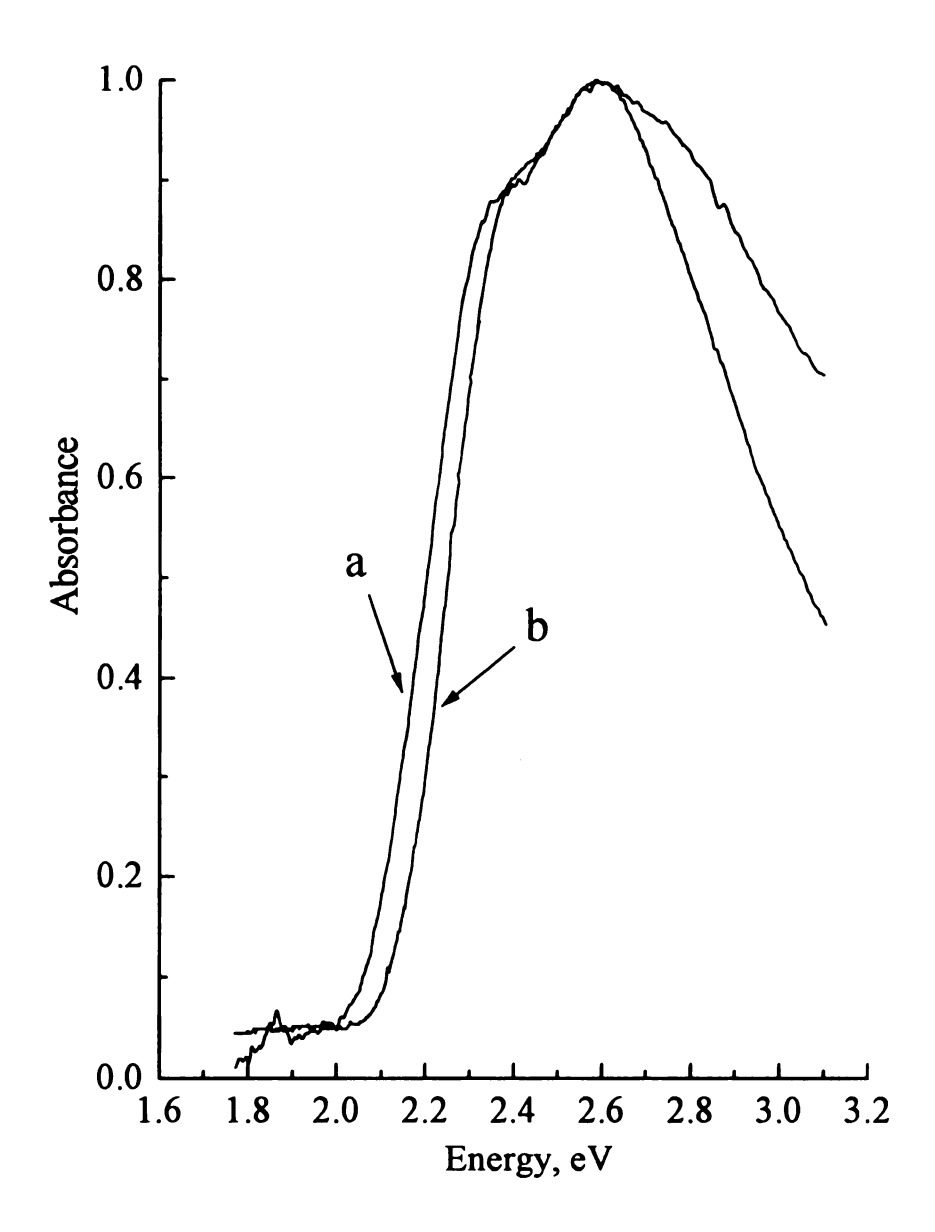


Figure 5.1. Linear absorption of a poly(4BCMU) film cast on FEP for elongation ratio: (a) $\ell/\ell_o = 5$ (b) $\ell/\ell_o = 1$.

accord with the increased disorder seen for films (Figure 5.2). The excitonic transition localized on the polymer backbone has been studied extensively in crystalline polydiacetylenes because it dominates their optical response. In these materials the exciton is one dimensional to within the width of the backbone π system, with a characteristic length of ~38 Å.^[22] The observed exciton binding energy of 400 meV and very large transition cross-section are direct results of its one-dimensional character and make this resonance useful for room temperature nonlinear optical signal processing applications. Both the shift and the transition line width can be used to characterize disorder in these materials.

As discussed above, the linear response of polydiacetylenes is known to depend on disorder in the polymer backbone. The inverse Raman scattering measurements on poly(4BCMU) films^[9] spin cast on a quartz substrate demonstrate that the nonlinear response of this material is also quite sensitive to polymer morphology, and in a manner that is advantageous for photonic signal processing applications (Figures 5.3-5.4). While aging of the spin-cast films shows a significant effect on the linear response of this material (Figure 5.2), its nonlinear inverse Raman response is largely unaffected, implying long-term stability of this material for photonic signal processing applications. Inverse Raman measurements on the crystalline polydiacetylene PTS show that the nonlinear optical response of polydiacetylenes can be modeled effectively in the context of a strongly coupled three level system.^[7,8] For crystalline poly(4BCMU), the inverse Raman scattering response is virtually identical to that for PTS, while for spin cast films of poly(4BCMU), the vibronic transition cross sections, resonance energies and linewidths all

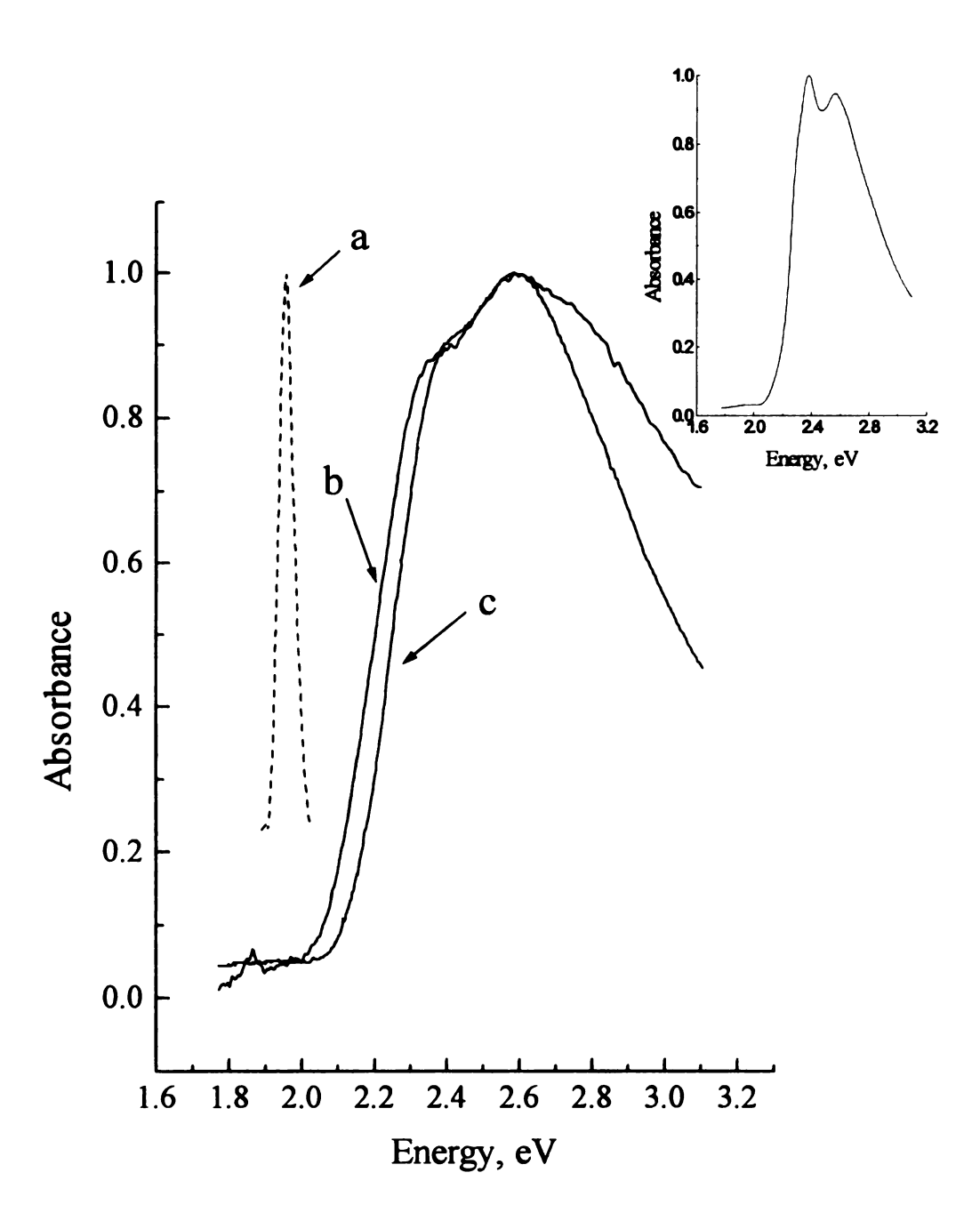


Figure 5.2. Linear absorption of (a) crystalline poly(4BCMU) (b) elongation to $\ell/\ell_0 = 5$ for a poly(4BCMU) film cast on FEP copolymer substrate and (c) freshly prepared spin cast poly(4BCMU) on a quartz substrate. Inset shows linear absorption of a four year old spin cast poly(4BCMU) on a quartz substrate.

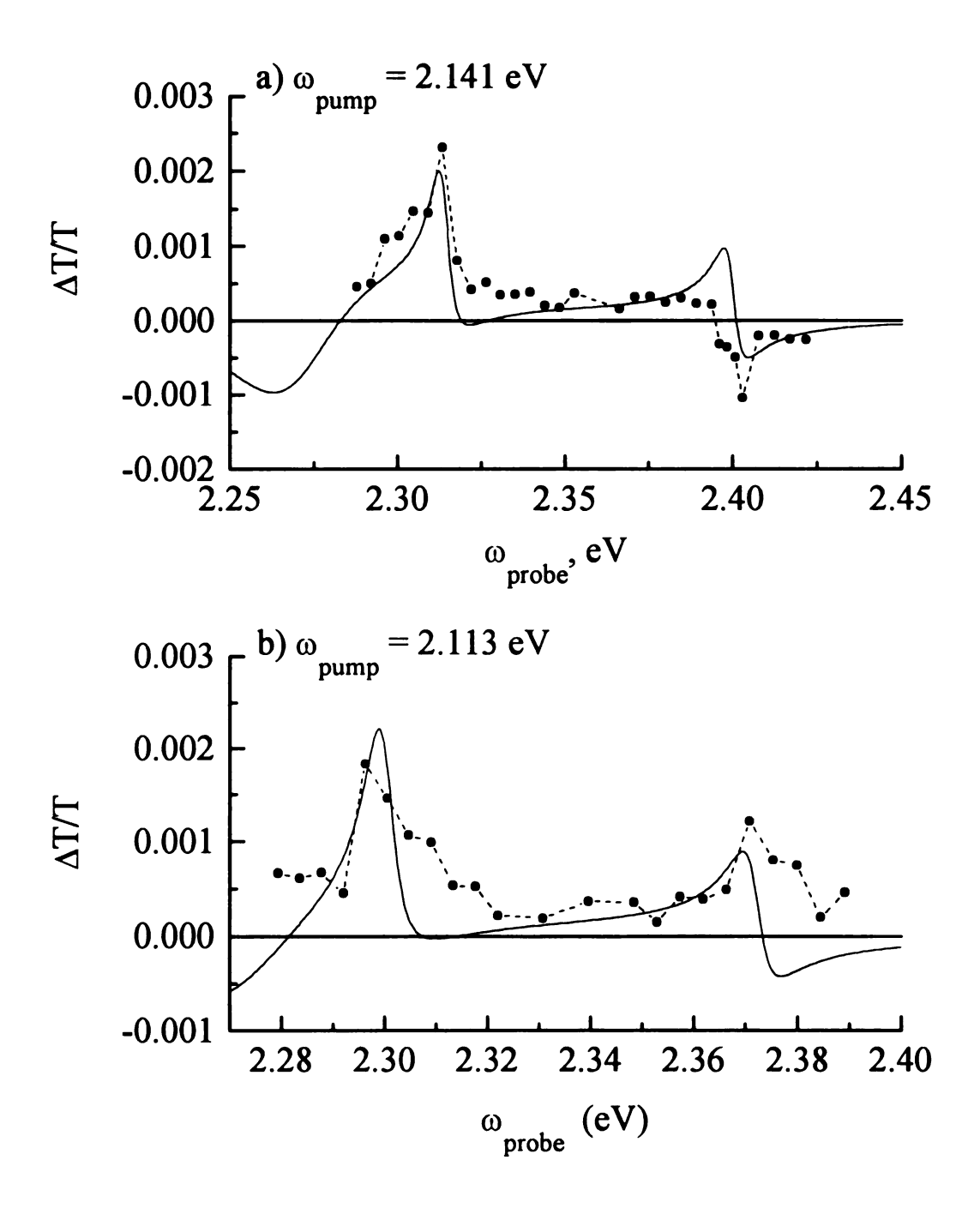


Figure 5.3. Experimental data points and calculated fit (solid line) for a) stimulated inverse Raman spectrum of spin cast poly(4BCMU) for $\omega_p = 2.141 eV$ and b) for $\omega_p = 2.113 eV$.

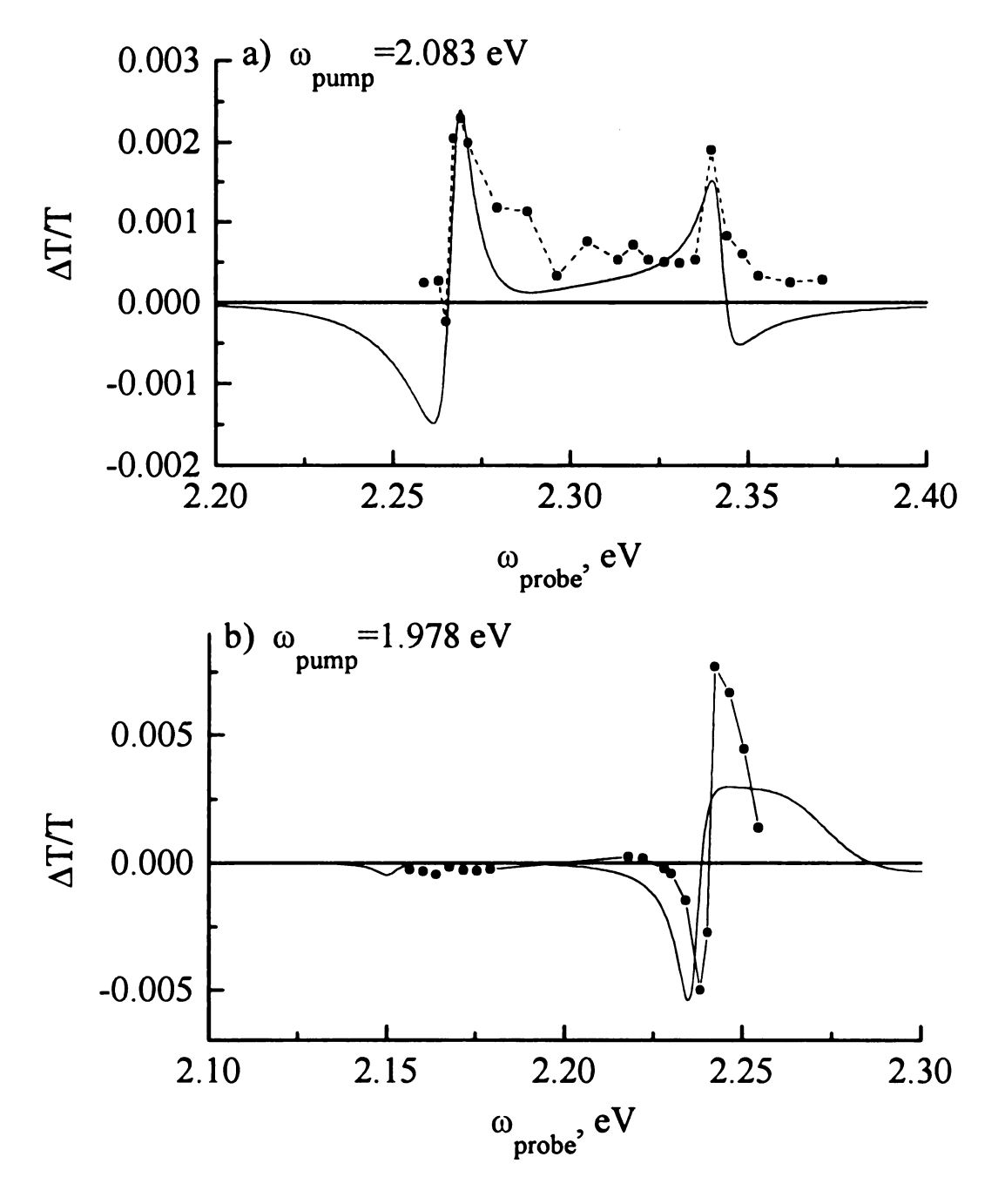


Figure 5.4. Experimental data points and calculated fit (solid line) for a) stimulated inverse Raman spectrum of spin cast poly(4BCMU) for $\omega_p = 2.083 eV$ and b) for $\omega_p = 1.978 eV$.

differ from those for the crystalline material and depend sensitively on the morphology of the polymer.^[9]

Figures 5.5-5.12 show the stimulated inverse Raman responses of stretch-aligned poly(4BCMU) films supported on FEP copolymer substrates. These responses, as for the inverse Raman spectra shown in chapter 4, are characteristic of a system with strong electronic-vibrational coupling. In the small signal limit, the nonlinear response induced in the material at a (probe) frequency ω_t by the action of an intense (pump) electric field at ω_p , the inverse Raman response, can be modeled qualitatively using Equation $1^{[23]}$

$$\chi^{(3)}(\omega_t) = \frac{|\mu_{0x}|^2 |\mu_{vx}|^2}{\hbar^3} \cdot \frac{1}{(\omega_{0x} - \omega_t - i\gamma_{0x})^2 (\omega_{0v} - \omega_t + \omega_p - i\gamma_{0v})}$$
[1]

where the terms μ are transition dipole moments and ω_{0v} , ω_{0x} , ω_{p} and ω_{t} are vibrational, excitonic and pump (p) and probe (t) laser frequencies, the terms γ are the linewidths for the indicated transitions, where 0, x and v are ground, excitonic and vibrational energy levels, respectively.^[7,8] The transition dipole moments and the linewidths both depend on the morphology of the material. The signal detected experimentally is related to the change in linear absorption through Equation 2.

$$\frac{\Delta T}{T} \cong \Delta \alpha \ell \tag{2}$$

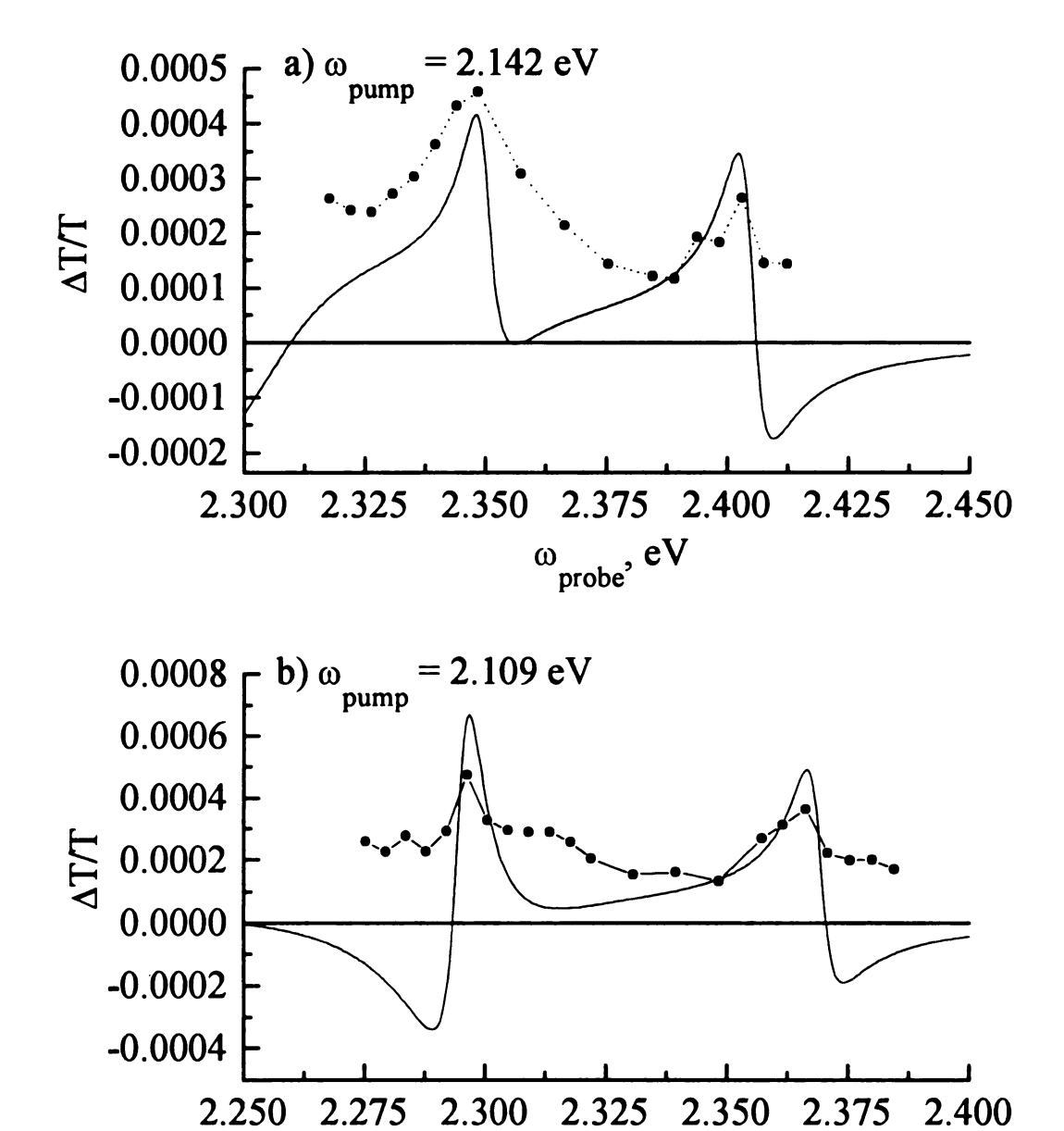


Figure 5.5. Experimental data (points) and calculated fit (solid line) of the stimulated inverse Raman spectrum of a spin cast film poly(4BCMU) on a FEP copolymer substrate, $\ell/\ell_0=1$, for (a) $\omega_{pump}=2.142$ eV and (b) $\omega_{pump}=2.109$ eV.

 $\omega_{\text{probe}},\,eV$

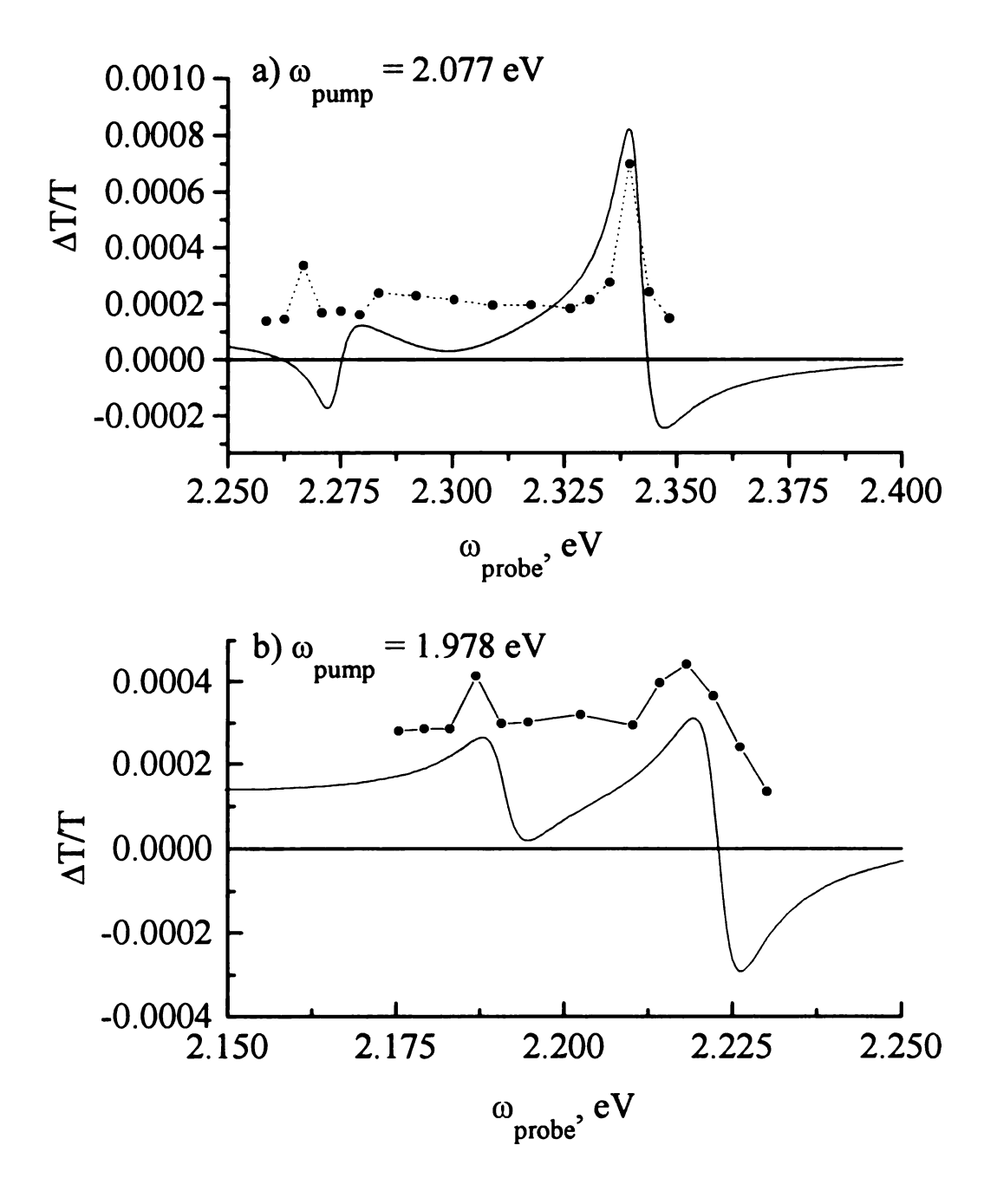


Figure 5.6. Experimental data (points) and calculated fit (solid line) of the stimulated inverse Raman spectrum of a spin cast film poly(4BCMU) on a FEP copolymer substrate, $\ell/\ell_0=1$, for (a) $\omega_{pump}=2.077$ eV and (b) $\omega_{pump}=1.978$ eV.

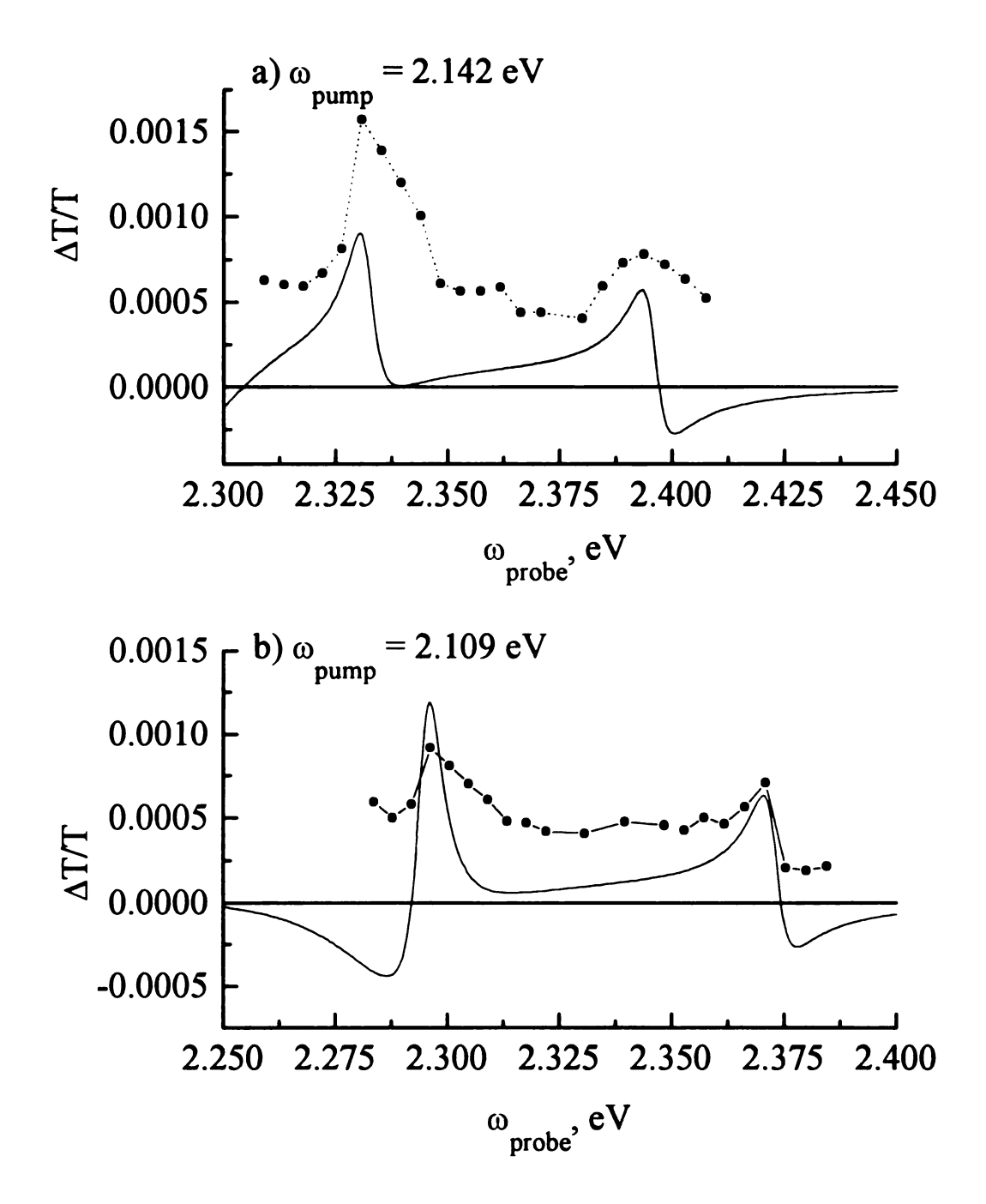


Figure 5.7. Experimental data (points) and calculated fit (solid line) of the stimulated inverse Raman spectrum of a spin cast film poly(4BCMU) on a FEP copolymer substrate, $\ell/\ell_0=1.5$, for (a) $\omega_{pump}=2.142$ eV and (b) $\omega_{pump}=2.109$ eV.

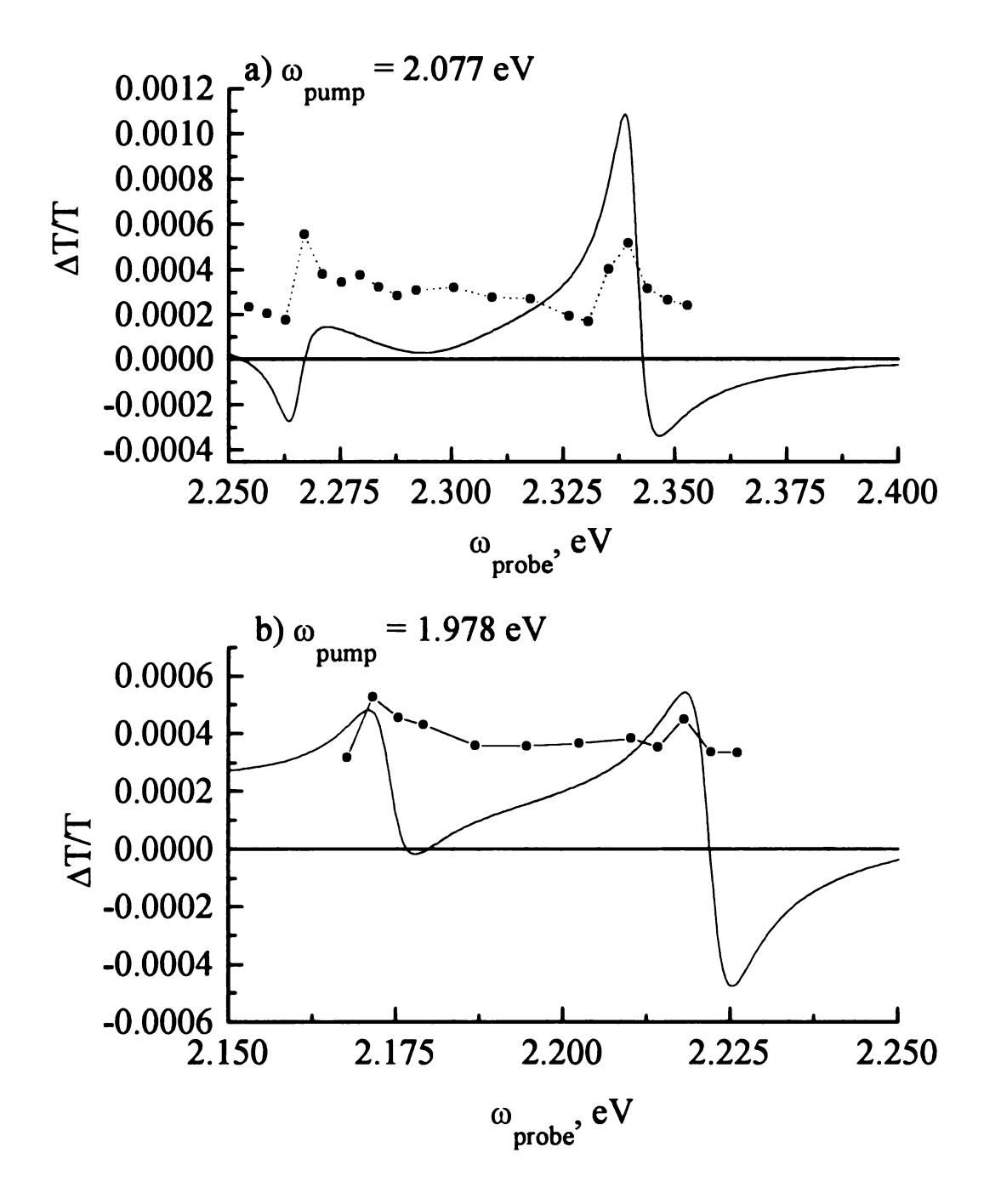


Figure 5.8. Experimental data (points) and calculated fit (solid line) of the stimulated inverse Raman spectrum of a spin cast film poly(4BCMU) on a FEP copolymer substrate, $\ell/\ell_o=1.5$, for (a) $\omega_{pump}=2.077$ eV and (b) $\omega_{pump}=1.978$ eV.

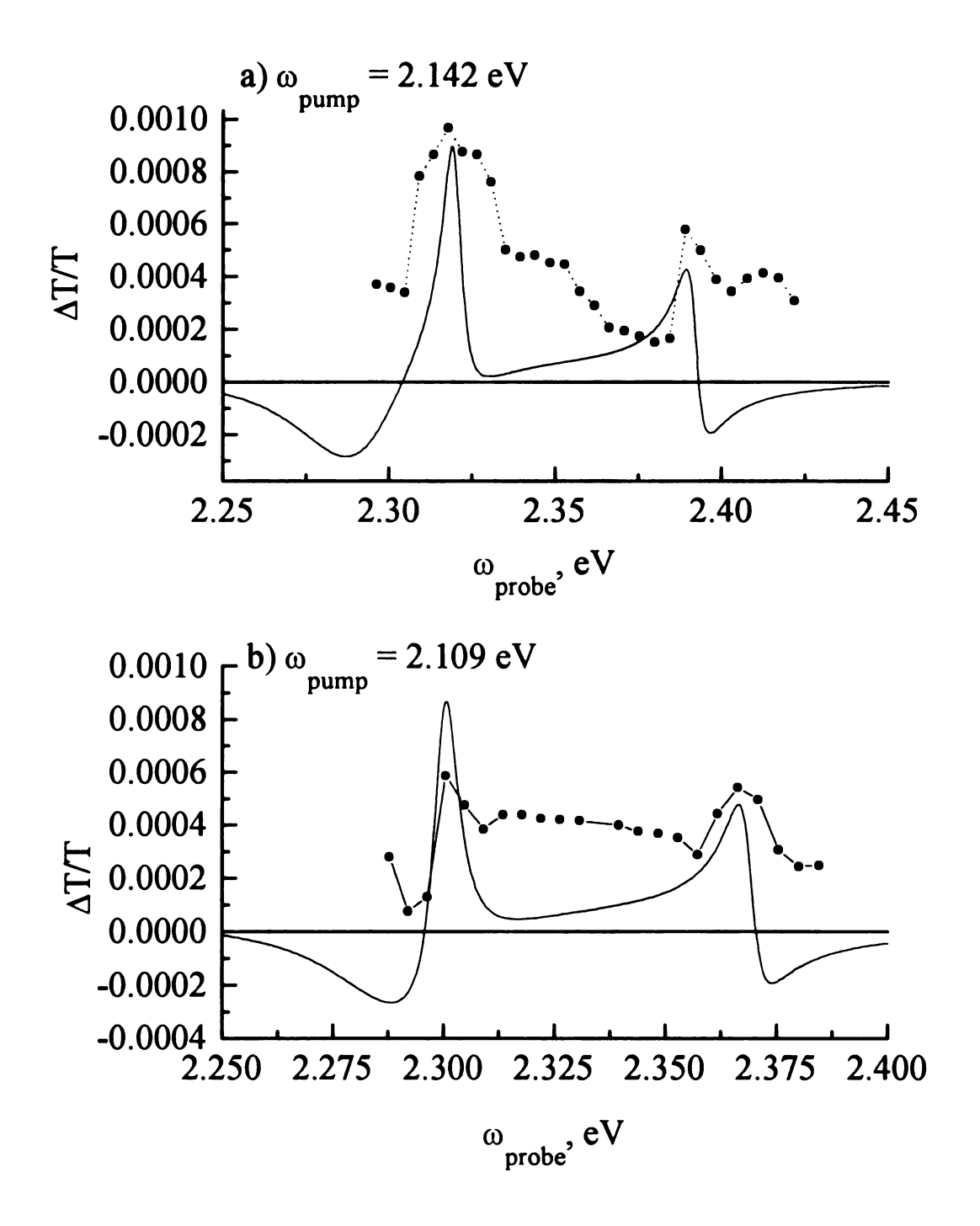


Figure 5.9. Experimental data (points) and calculated fit (solid line) of the stimulated inverse Raman spectrum of a spin cast film poly(4BCMU) on a FEP copolymer substrate, $\ell/\ell_0=3$, for (a) $\omega_{pump}=2.142$ eV and (b) $\omega_{pump}=2.109$ eV.

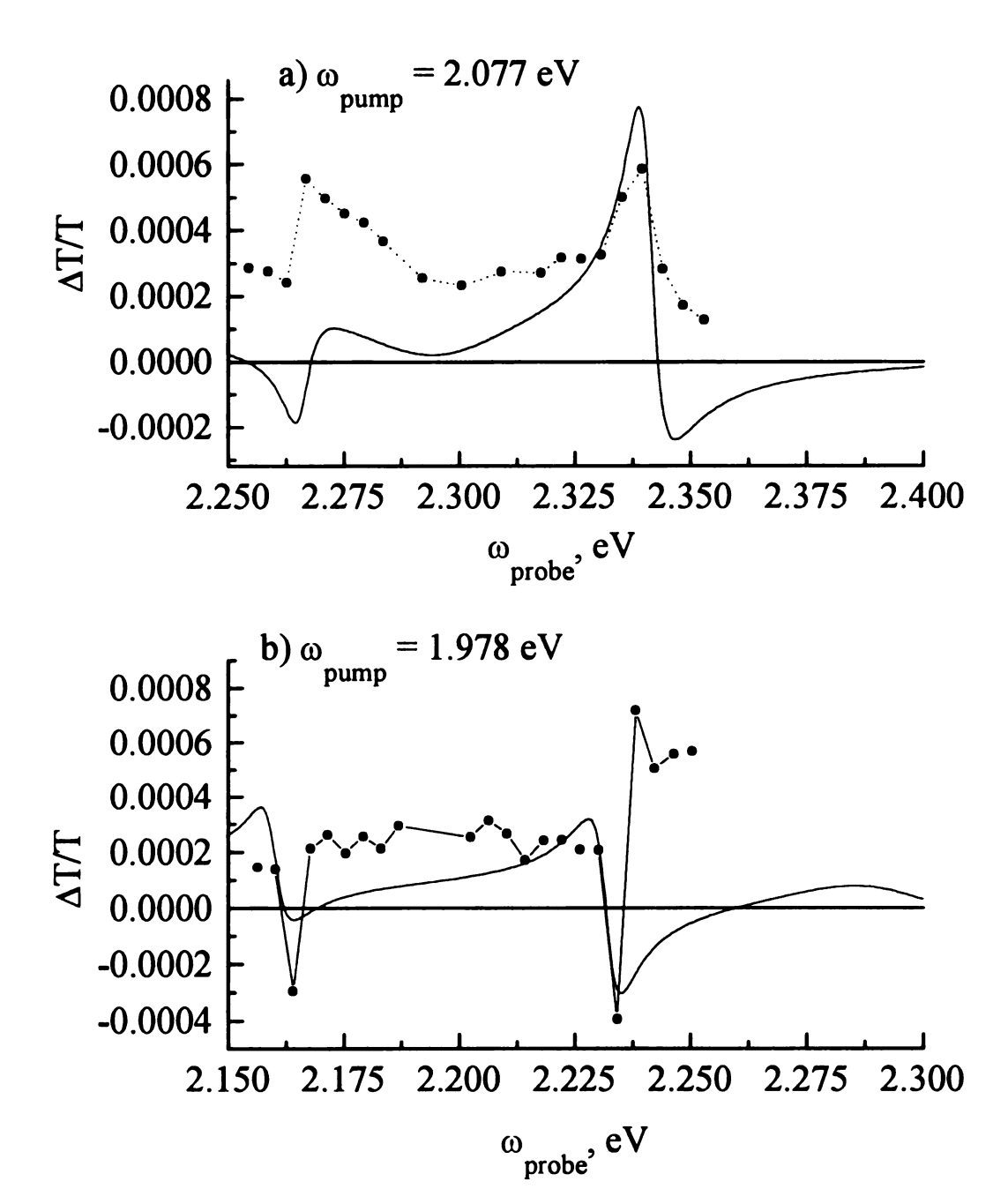


Figure 5.10. Experimental data (points) and calculated fit (solid line) of the stimulated inverse Raman spectrum of a spin cast film poly(4BCMU) on a FEP copolymer substrate, $\ell/\ell_0=3$, for (a) $\omega_{pump}=2.077$ eV and (b) $\omega_{pump}=1.978$ eV.

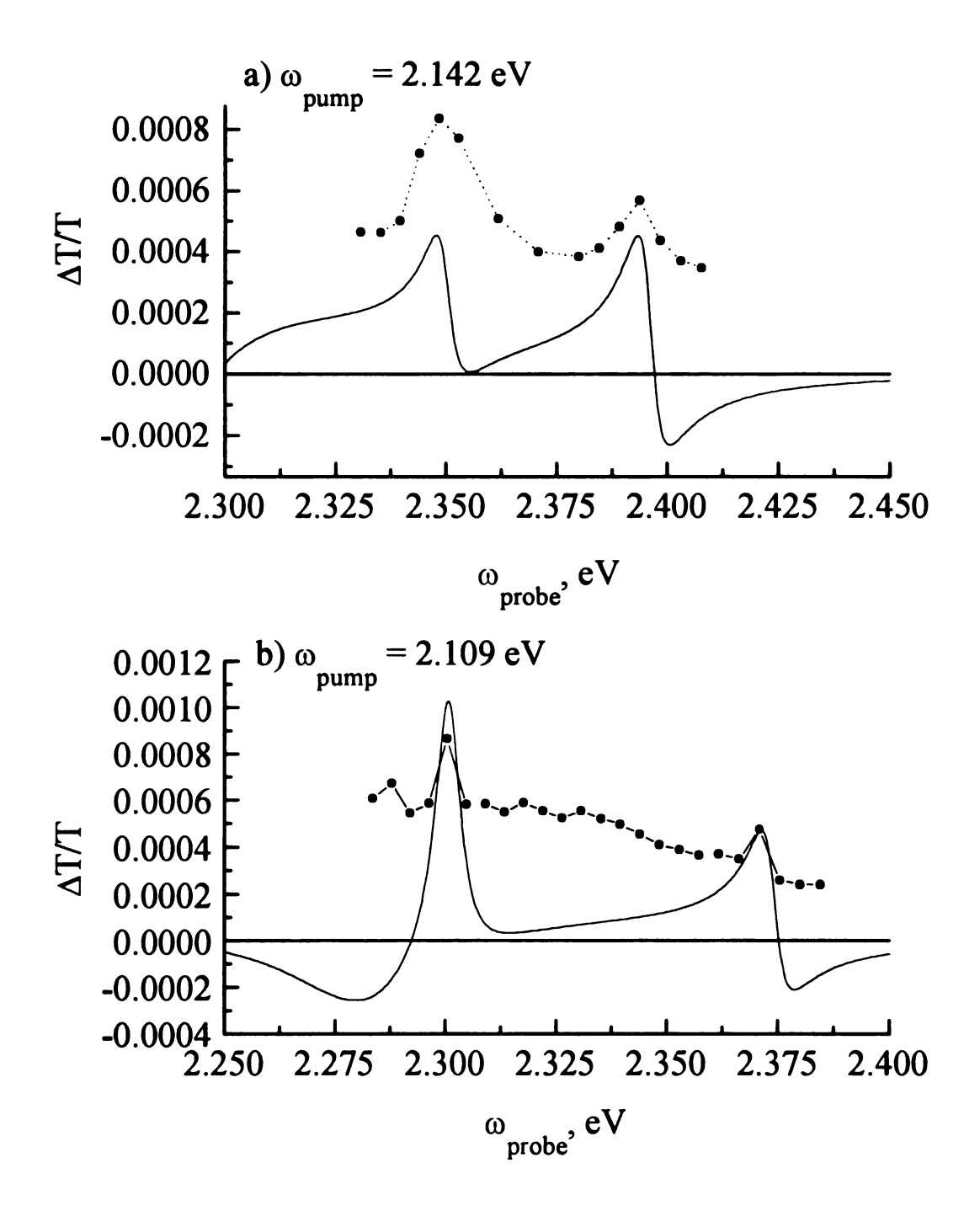


Figure 5.11. Experimental data (points) and calculated fit (solid line) of the stimulated inverse Raman spectrum of a spin cast film poly(4BCMU) on a FEP copolymer substrate, $\ell/\ell_0=5$, for (a) $\omega_{pump}=2.142$ eV and (b) $\omega_{pump}=2.109$ eV.

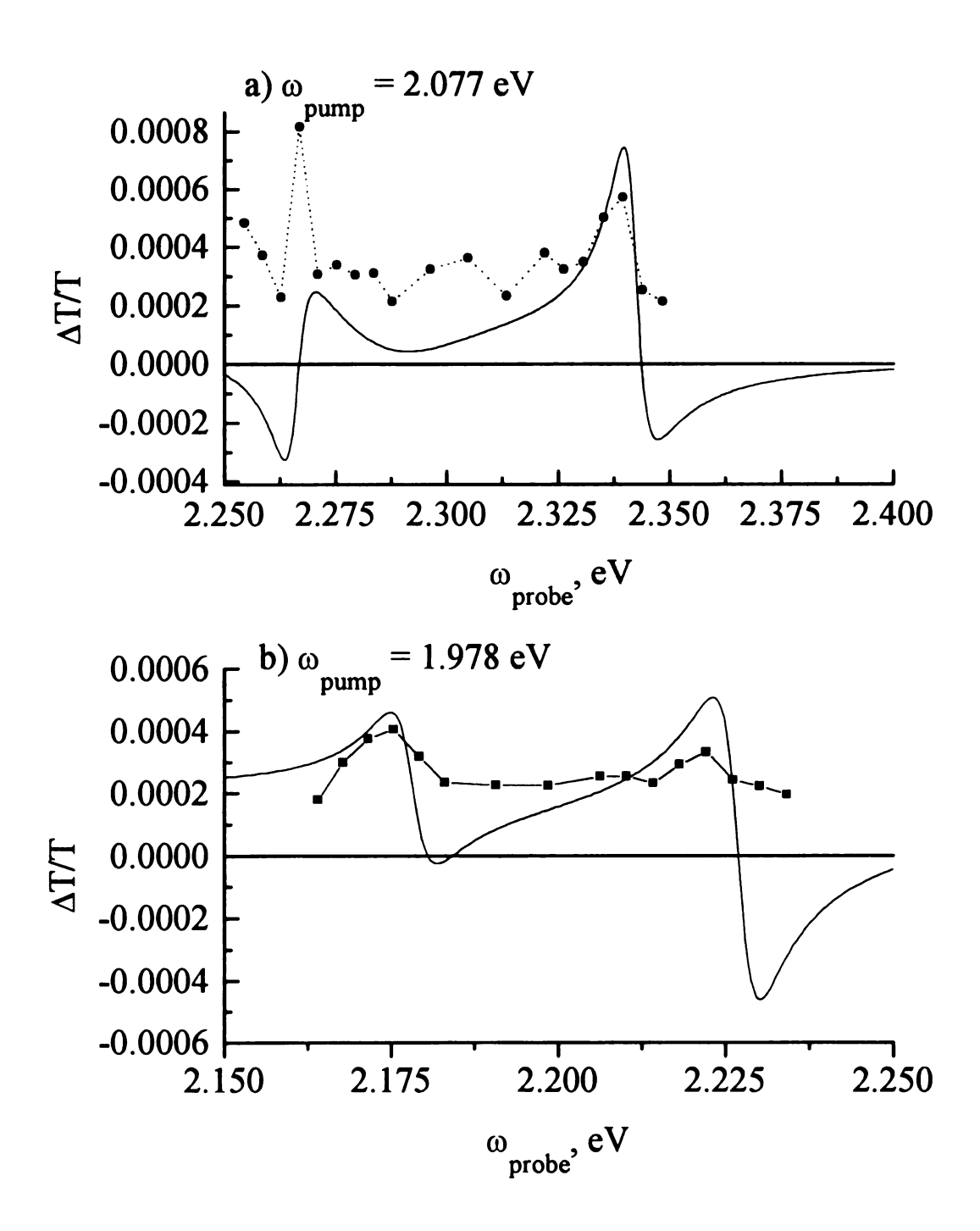


Figure 5.12. Experimental data (points) and calculated fit (solid line) of the stimulated inverse Raman spectrum of a spin cast film poly(4BCMU) on a FEP copolymer substrate, ℓ/ℓ_0 =5, for (a) ω_{pump} = 2.077 eV and (b) ω_{pump} =1.978 eV.

 $\Delta\alpha\ell$ is related to Im $\{\chi^{(3)}\}$ through the dielectric response of the material. By taking the dielectric response of the polydiacetylenes into account in the calculation of the expected signal, virtually quantitative agreement between theory and experiment for spin-cast and stretch-aligned poly(4BCMU) films has been achieved. In all of the inverse Raman measurements on the poly(4BCMU)/modified FEP system, a positive ($\Delta T/T>0$) displacement of the experimental data from the calculated responses has been observed. This slight difference between the experimental and calculated responses results from two factors. First, in the development of the theory, Lorentzian lineshape functions were used, and this is likely not an accurate representation of the experimental lineshapes. previous stimulated inverse Raman scattering data on crystalline polydiacetylenes show that, even for these highly ordered materials, a Lorentzian lineshape does not represent the actual resonances accurately. [5,7,8] In addition, the uniform background signal observed, only for the poly(4BCMU) films on polymer substrates, is due either to a coherent response from the substrate or from an induced spectroscopic feature arising from interactions between the substrate and the poly(4BCMU). Spontaneous Raman scattering from the substrate shows a vibrational resonance at 1560 cm⁻¹ superimposed on a broad background. The background signal in the inverse Raman spectra of the poly(4BCMU)/FEP system might be of the same origin as that of the broad background observed in spontaneous Raman scattering data on the modified FEP substrate.

There are two distinct classes of stimulated inverse Raman data that are presented here.

The first set of data is for spin-cast poly(4BCMU) on a quartz substrate annealed at room temperature for more than four years (Figures 5.3-5.4) and for a freshly prepared

poly(4BCMU) spin cast on a quartz substrate (Figure 5.13). These data can be interpreted in the context of the poly(4BCMU) film not interacting significantly with the substrate, and only one electronic resonance (2.29 eV) was required to achieve excellent agreement between experiment and calculation. For these data there is no anomalous offset of the signal, indicating that there was no detectable response attributable to interactions between the polymer nonlinear chromophore and the silica substrate.

The second set of data is for poly(4BCMU) spin cast on the modified FEP copolymer substrate (Figures 5.5-5.12). For these data, in addition to the constant offset to the signal discussed above, the agreement between experiment and theory was achieved only when two excitonic resonances were included in the calculation. In correspondence with the quartz substrate data, one excitonic resonance was centered at 2.29 eV ($\gamma_x \cong 50$ meV). The second excitonic resonance, required to achieve agreement with the data, appears at 2.02 eV ($\gamma_v \cong 50$ meV). There are two possible reasons for the presence of this additional electronic resonance, and based on the information at hand, it cannot be unambiguously determined which explanation is correct. One possibility is that the modification of the FEP copolymer substrate has introduced sites that interact strongly with the poly(4BCMU) backbone chromophore. Indeed, the removal of fluorine and introduction of C=C and C=C bonds onto the substrate surface presents an opportunity for strong π - π interaction between the two polymers. Although the characteristics of the modified FEP surface are not understood completely at the molecular level, the introduction of C=C and C=C bonds into the FEP substrate produces a material that can be considered to be composed of, at least in part, methyl-polyacetylene moieties. It is also possible that other

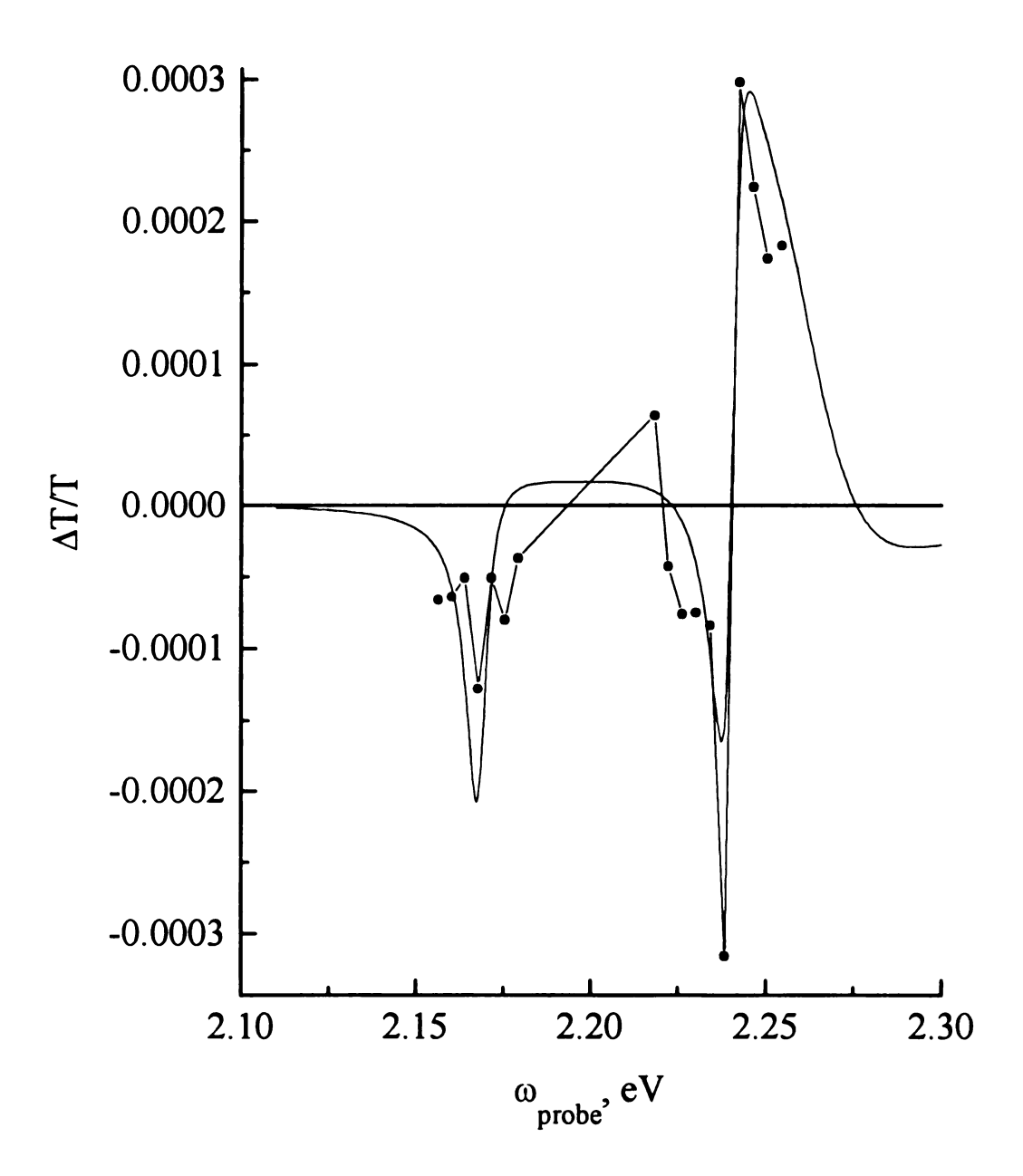


Figure 5.13. Experimental data (points) and calculated fit (solid line) of the stimulated inverse Raman spectrum of a freshly prepared spin cast poly(4BCMU) on quartz substrate for $\omega_{pump} = 1.978$ eV including in the calculation single excitonic resonance ($\omega_x = 2.29$ eV).

types of chemical interaction could be present in this polymer system.

Bening and McCarthy^[16] have shown that oxygen is introduced during rinsing of the FEP copolymer to form C=O moieties. Blanchard et. al. in their work on the polydiacetylene PTS have demonstrated the important role that oxygen interactions with the polydiacetylene backbone can have on the inverse Raman response. [5] For PTS, an excitonic resonance at ~2.39 eV (~400 meV higher in energy than the excitonic resonance) is associated with molecular oxygen adsorbed onto the backbone double bond. The second electronic resonance observed in poly(4BCMU) film could have a similar origin, with some oxygen-containing moiety (likely C=O) existing at the interface between the substrate and the poly(4BCMU), although the energy of the additional resonance observed in this work is ~270 meV below that of the 2.29 eV exciton. It is also possible, given the energy of the additional excitonic resonance, that small crystalline domains of poly(4BCMU) could be re-established in the films as a result of the annealing and stretching processes. The energy of this additional electronic resonance (2.02 eV) is within approximately one linewidth of the ~1.96 eV excitonic resonance seen in blue phase crystalline poly(4BCMU). The transition cross sections for the electronic-to-vibrational transitions we have measured provide some insight into the origin of this additional resonance (Table 5.1). The work of Blanchard et. al. on adsorption of oxygen to PTS showed transition cross sections of $\sigma \sim 1$ eV for the adsorbate-induced electronic state-topolymer backbone C=C stretch. [5] For crystalline polydiacetylenes, it was measured that $\sigma_{C=C} \cong 0.07~eV$ and $\sigma_{C=C} \cong 0.10$ - $0.15~eV,^{[7-9]}$ depending on the polydiacetylene. For spin cast films of poly(4BCMU), it was found that $\sigma_{C=C} \cong 0.15$ eV and $\sigma_{C=C} \cong 0.25$ eV, with

the enhancement compared to the crystalline material being attributable to disorder in the polymer backbone. For the stretch-aligned films reported here, it was observed that $\sigma_{C=C} \cong 0.25$ eV and $\sigma_{C=C} \cong 0.15$ eV

Table 5.1. Cross sections for ground state vibration-to-excited electronic state transitions in poly(4BCMU).

	Crystal	Spin-cast on	Spin cast on modified FEP		
		quartz	substrate		
			$1 \le \ell/\ell_0 \le 5$		
					
	$\omega_{\rm X} = 1.96 {\rm eV}$	$\omega_X = 2.29 \text{eV}$	$\omega_{\rm X} = 2.02 {\rm eV}$	$\omega_{\rm X} = 2.29 {\rm eV}$	
$\sigma_{C=C}$ (eV) $\sigma_{C=C}$ (eV)		$\omega_{X} = 2.29 \text{eV}$ 0.26	$\omega_{\mathbf{X}} = 2.02 \text{eV}$	$\omega_{\mathbf{X}} = 2.29 \text{eV}$	

for coupling to the 2.29 eV exciton. For the 2.02 eV electronic transition detected in the stretch-align films, best-fit values of $\sigma_{C=C} \cong 0.45$ eV and $\sigma_{C=C} \cong 0.25$ eV were obtained. The cross sections for the 2.02 eV resonance are significantly larger than those for the crystalline polymer, but are also much less than those observed for the adsorbate-induced electronic state in PTS. Based on these data, it appears that the 2.02 eV electronic transition seen in stretch-aligned films arises from an interaction of the poly(4BCMU) backbone with the substrate, where the interacting substrate moiety was not oxygen. X-ray diffraction data on these films might aid in determining the origin of this additional electronic resonance, but such measurements were not feasible on the materials at hand.

It is also possible that the additional excitonic resonance at 2.02 eV was intrinsic to poly(4BCMU) and its relative contribution to the nonlinear response depends on the

annealing history of the polymer. To evaluate this possibility, the inverse Raman scattering response of both freshly deposited and annealed samples of poly(4BCMU) cast on quartz substrates were examined. As discussed above, the inverse Raman scattering response of fresh and four year old poly(4BCMU) samples were identical to within the uncertainty of the measurements, suggesting the absence of an annealing without stretching-related origin of the 2.02 eV excitonic resonance seen for the FEP-supported films. The observed agreement between theory and experiment for calculations with two excitonic resonances (2.02 eV, 2.29 eV) was poor (Figure 5.14a). The corresponding calculation, where only the 2.29 eV resonance was included, provides excellent agreement with the experimental data (Figure 5.14b). For poly(4BCMU) spin cast on a quartz substrate, only a single excitonic resonance was required to achieve excellent agreement between theory and experiment. This result demonstrates that the 2.02 eV excitonic resonance seen for poly(4BCMU) spin cast on the FEP copolymer substrate arises from the interaction between the two polymers and was not intrinsic to poly(4BCMU).

An underlying assertion in the work presented here is that stretch alignment of poly(4BCMU) introduces some amount of macroscopic orientation into a material that is, before processing, isotropic in two dimensions. In order to demonstrate the validity of this assertion, the linear response of the stretch aligned films parallel and perpendicular to the stretch alignment axis has been compared. These results are shown in terms of the anisotropy ratio $\alpha_{\parallel}/\alpha_{\perp}$ for the supported poly(4BCMU) films stretched to different elongation ratios (Table 5.2). For the different elongation ratios, $\alpha_{\parallel}/\alpha_{\perp}$, increases with elongation, but comparison of these values with the experimental value of $\alpha_{\parallel}/\alpha_{\perp} \sim 50$ for

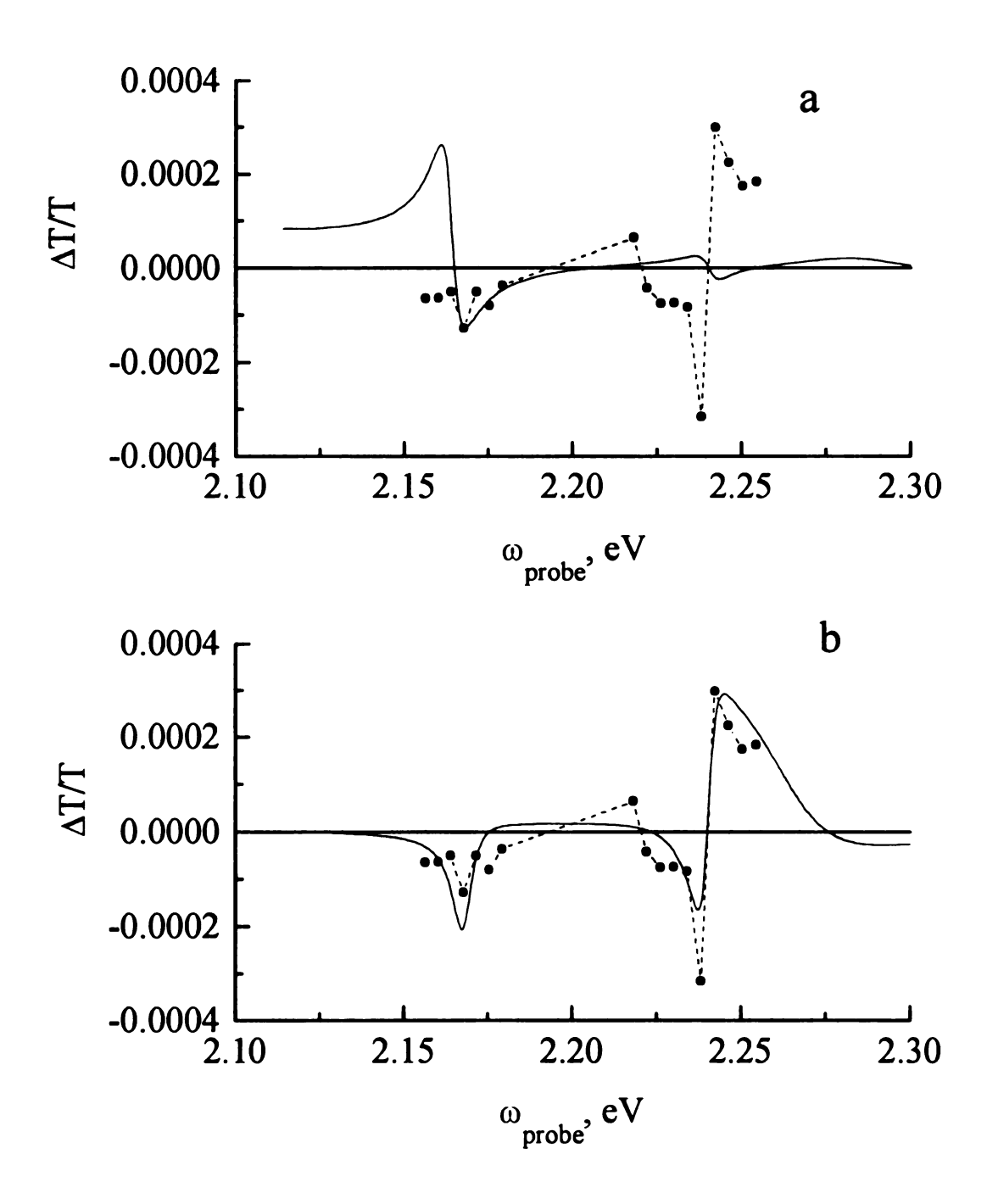


Figure 5.14. Experimental data (points) and calculated fit (solid line) of the stimulated inverse Raman spectrum of a freshly prepared spin cast poly(4BCMU) on quartz substrate for $\omega_{pump} = 1.978$ eV including in the calculation (a) two excitonic resonances ($\omega_x = 2.02$, 2.29 eV) (b) single excitonic resonance ($\omega_x = 2.29$ eV).

crystalline poly(4BCMU) demonstrates that the extent of alignment was modest with the modified FEP substrate. For the elongation ratio, ℓ/ℓ_0 , spanning the range of 1 (unstretched) to ~5, measured a corresponding variation in $\alpha_{\parallel}/\alpha_{\perp}$ from 1 to 2.5. To put these values in perspective, disordering a single crystal with $\alpha_{\parallel}/\alpha_{\perp} \sim 50$ by exposure to solvent vapor reduces $\alpha_{\parallel}/\alpha_{\perp}$ to 5.^[21] Larger values of $\alpha_{\parallel}/\alpha_{\perp}$ in the stretch-aligned films require a significantly larger elongation ratio, although the exact value of ℓ/ℓ_0 required to

Table 5.2. Comparison of elongation ratio and optical dichroism at 2.29 eV.

elongation	dichroism			
ratio (ℓ/ℓ_0)	(α _{II} /α _⊥)			
1	1			
1.5	1.9			
3	2.2			
5	2.5			
	J			

achieve $\alpha_{\parallel}/\alpha_{\perp} > 10$ cannot be predicted because of the mechanical strain and stress limitations inherent to both the modified FEP substrate and poly(4BCMU) materials. The limiting factor to attaining a higher elongation ratio in this work lies with the FEP copolymer substrate. While other polymers possessing greater deformability could be used, the presence of crystalline domains precludes their use because of significant Rayleigh scattering losses and interference. These anisotropic linear response experiments serve to demonstrate that, with the appropriate substrate, a dichroism close to that of a crystalline material could ultimately be obtained.

It is important to understand quantitatively the enhancement in nonlinear response derived from stretch alignment of these films. Comparison of absolute $\Delta T/T$ quantities was not meaningful because of sample-to-sample variations in the thickness of the poly(4BCMU) films, and because elongation of the polymer/substrate system serves to thin the poly(4BCMU) film. As discussed above, the quantity determined experimentally, $\Delta T/T \sim$ $\Delta\alpha\ell$. By normalizing the data for film thickness (ℓ) and laser intensity (T=I/I₀), the quantity $\Delta\alpha$ was obtained, which was compared directly for all of the samples (Figure 5.15). There was a significant loss of nonlinear response in the spin-cast, non-aligned film compared to that of the crystalline polymer, and this was anticipated, at least in part to misalignment between the polymer backbone and the incident electric fields. alignment to an elongation ratio of $\ell/\ell_0 = 5$ returns the $\Delta\alpha$ value to that seen for the crystalline polymer. It is anticipated that greater elongation of the spin cast films will allow the realization of a nonlinear response in the disordered material that was significantly larger than that for the corresponding crystal. Even at this limited elongation ratio, however, a significant enhancement of the nonlinear response was observed in the spin cast and stretch aligned system. Because the nonlinear chromophore was substantially disordered over short (oligomer) length scales, the linear response is comparatively broad. Accordingly, the nonlinear response of the spin cast and aligned system exhibits a substantially weaker wavelength-dependence than that seen for crystalline poly(4BCMU) (Figure 5.15). Thus optical devices based on aligned, spin-cast films of poly(4BCMU) will exhibit the additional benefit of a comparatively broad operating frequency range.

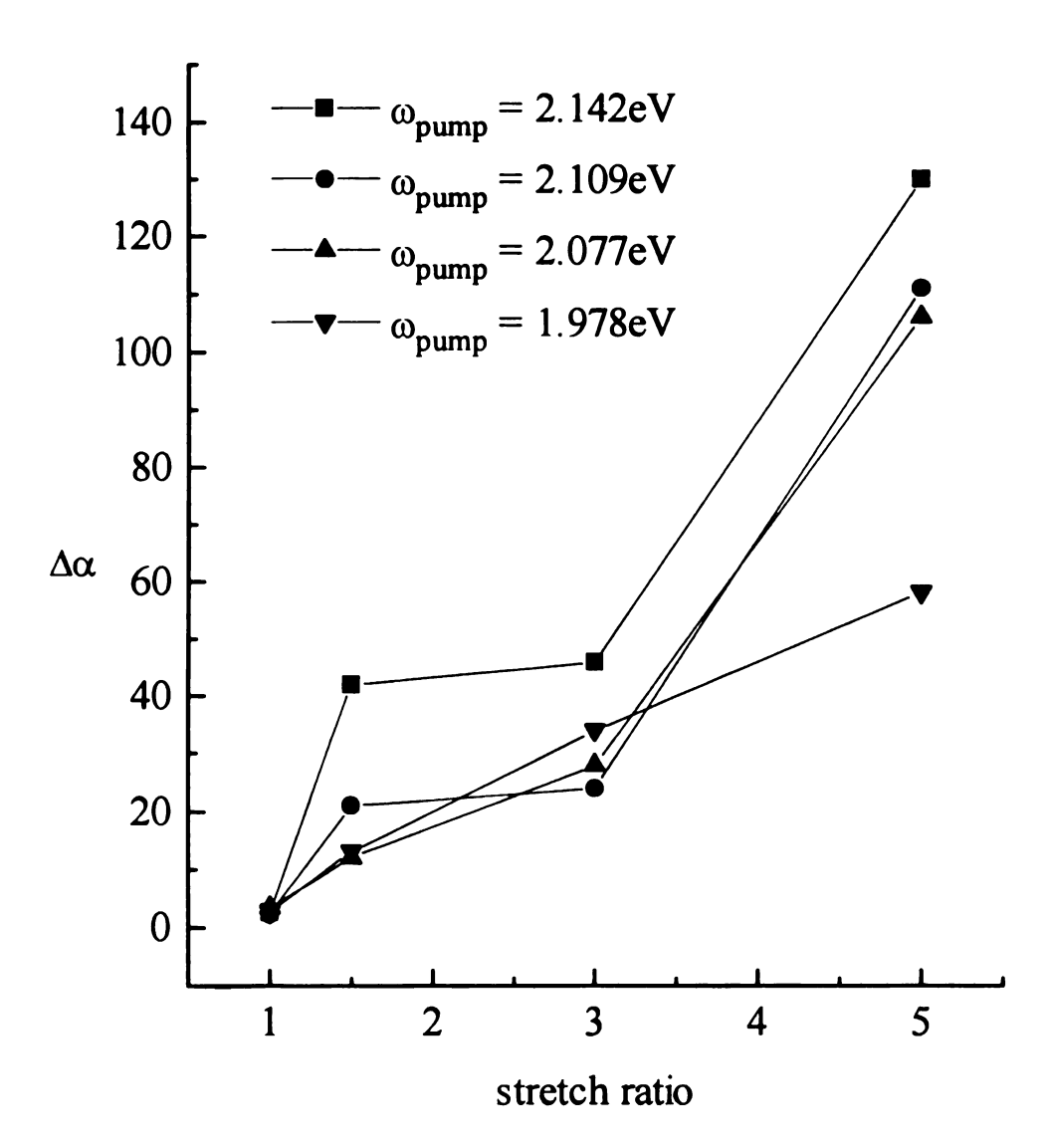


Figure 5.15. $\Delta\alpha$, the nonlinear response, normalized for sample thickness and laser intensities for the various forms of poly(4BCMU) as a function of stretching ratio for different excitation frequencies.

The data presented in Figures 5.5-5.12 contain information similar to that obtained from spontaneous resonance Raman scattering measurements. The polydiacetylene backbone C=C and C=C stretching resonance frequencies are sensitive to the disorder present in the stretch aligned films. The positions of both resonances depend on the excitation frequency (Table 5.3) but the relationship between these two quantities is not direct. The previous interpretation that the excitation energy-dependence of the vibrational resonances comes

Table 5.3. Excitation energy dependence of vibrational resonance frequencies of spin-cast and aligned poly(4BCMU) films.

	$\ell/\ell_0=1$		$\ell/\ell_0=1.5$	5	$\ell/\ell_0=3$		$\ell/\ell_0=5$	
ω_p (eV)	ω _{C=C}	ω _{C=C}	ω _{C=C}	ω _{C=C}	ω _{C=C}	ω _{C≖C}	ω _{C=C}	ω _{C≖C}
	(eV)	(eV)	(eV)	(eV)	(eV)	(eV)	(eV)	(eV)
1.978	0.213	0.245	0.196	0.244	0.182	0.254	0.200	0.249
2.077	0.197	0.265	0.186	0.264	0.187	0.264	0.189	0.265
2.109	0.186	0.260	0.186	0.264	0.191	0.260	0.192	0.265
2.142	0.208	0.263	0.190	0.254	0.178	0.250	0.208	0.254

about because different excitation frequencies access different regions of the stretch aligned film that possess a characteristic type or extent of disorder still holds true. Exactly analogous behavior has been measured in spin cast, unstretched films of poly(4BCMU).

5.4. Conclusion

The optical response of poly(4BCMU) thin films supported on a modified FEP copolymer substrate and processed to different elongation ratios has been investigated. An additional electronic resonance at 2.02 eV which is due either to crystallinity re-introduced by stretching and/or annealing or to a strong interaction between the poly(4BCMU) backbone and the modified FEP substrate has been detected. At this time the origin of this electronic feature can not be determined unambiguously. While the optical transparency of the stretch oriented FEP films were of high quality, the elongation ratio attainable for the substrate used was sufficient only to return the nonlinear response of the orientated poly(4BCMU) films to that of the crystalline polymer. The nonlinear response of this composite system could be enhanced by a more suitable choice of polymer substrate to achieve higher elongation ratios.

Literature Cited

- 1. C. Sauteret, J. P. Hermann, R. Frey, F. Pradere, J. Ducuing, R. H. Baughman and R. R. Chance, *Phys. Rev. Lett.*, **36**, 956(1976).
- 2. P. W. Smith, Bell System Tech. Journal, 61, 1975(1982).
- 3. G. J. Blanchard, J. P. Heritage, G. L. Baker and S. Etemad, *Chem. Phys. Lett.*, 158, 329(1989).
- 4. M. J. Nowak, G. J. Blanchard, G. L. Baker, S. Etemad and Z. G. Soos, *Phys. Rev. B*, 41, 7933(1990).
- 5. G. J. Blanchard, J. P. Heritage, Chem. Phys. Lett., 177, 287(1991).
- 6. S. A. Hambir, T. Yang, G. J. Blanchard and G. L. Baker, *Chem. Phys. Lett.*, 201, 521(1993).
- 7. G. J. Blanchard, J. P. Heritage, A. C. Von Lehmen, M. K. Kelly, G. L. Baker and S. Etemad, *Phys. Rev. Lett.*, 63, 887(1989).
- 8. G. J. Blanchard and J. P. Heritage, J. Chem. Phys., 93, 4377(1990).
- 9. S. A. Hambir, G. J. Blanchard and G. L. Baker, J. Chem. Phys., 102, 2295(1995).
- 10. N. E. Schlotter, J. L. Jackel, P. D. Townsend and G. L. Baker, Appl. Phys. Lett., 56,13(1990).
- 11. P. D. Townsend, J. L. Jackel, G. L. Baker, J. A. Shelburne, III, and S. Etemad, *Appl. Phys. Lett.*, **55**, 1829(1989).
- 12. P. D. Townsend, G. L. Baker, N.E. Schlotter, C. F. Klausner and S. Etemad, Appl. Phys. Lett., 53, 1782(1988).
- 13. W J. Jones and B. P. Stocheff, Phys. Rev. Lett., 13, 657(1964).
- 14. Y. Jiang, S. A. Hambir and G. J. Blanchard, Opt. Commun., 99, 216(1993).
- (a) P. Bado, S. B. Wilson and K. R. Wilson, Rev. Sci. Instrum., 53, 706(1982); (b) L. Andor, A. Lorincz, J. Siemion, D. D. Smith, and S. A. Rice, Rev. Sci. Instrum., 55, 64(1984); (c) G. J. Blanchard and M. J. Wirth, Anal. Chem., 58, 532(1986).
- 16. R. C. Bening and T. J. McCarthy, *Polym. Prepr.*, 29, 336(1988).
- 17. D. W. Dwight and W. J. Riggs, J. Coll. Interface Sci., 47, 650(1974).

- 18. G. L. Baker, J. A. Shelburne, III, and P. D. Townsend, *Inst. of Phys. Conf. Ser.*, 103, 227(1989).
- 19. R. R. Chance, M. W. Washbaugh, and D. J. Hupe, NATO Advanced Research Workshop; Polydiacetylenes, Synthesis, Structure and Electronic Properties, E102, 39(1985).
- 20. B. F. Variano, C. J. Sandroff and G. L. Baker, Macromolecules, 24, 4376(1991).
- 21. M. J. Nowak, G. J. Blanchard, G. L. Baker, S. Etemad and Z. G. Soos, in *Conjugated Polymeric Materials: Opportunities in Electronic, Opto-Electronics and Molecular Electronics*, Ed. by J. L. Bredas and R. R. Chance, NATO ASI Series E, 182, Kluwer Academic Publishers, Dordrecht, 421-427(1990).
- 22. B. I. Greene, J. Orensstein, R. R. Millard, and L. R. Williams, *Phys. Rev. Lett.*, 58, 2750(1987).
- 23. S. Saikan, N. Hashimoto, T. Kushida and K. Namba, J. Chem. Phys., 82, 5409(1985).
- 24. L. X. Zheng, R. E. Benner, Z. V. Vardeny and G. L. Baker, *Phys. Rev. B*, 42, 3235(1990).

Chapter 6

Feasibility Study of Degenerate Four Wave Mixing

This chapter describes an unsuccessful attempt to evaluate the electronic and vibrational contributions to the third order nonlinear optical response of polydiacetlyenes. We could not see the degenerate four wave mixing signal due to low laser power and scattering from the sample which results in a small signal to noise ratio. This experiment could be made successful by employing a powerful laser, where the peak power is very high, or by amplification of the laser pulses before they are used in the DFWM process.

6.1. Introduction

Degenerate four wave mixing (DFWM) is a widely used method of measuring $\chi^{(3)}$. The physical description of DFWM is that three spatially distinguishable electric fields $E_1(\omega, t)$, $E_2(\omega, t)$, $E_3(\omega, t)$ of the same frequency, ω , interact to generate a fourth wave $E_4(\omega, t)$ at the same frequency but with a different propagation direction. The equation for the output $E_4(\omega, t)$ will have the following form^[1,2]

$$\nabla^2 E_4 = -\frac{\varepsilon}{c^2} \left(\frac{\partial^2 E_4}{\partial r^2} \right) - \frac{4\pi}{c} \left(\frac{\partial^2 P}{\partial r^2} \right)$$
 [1]

in which the nonlinear polarization is given by

$$P = \chi^{(3)} E_1 E_2 E_3 \tag{2}$$

Many different beam geometries have been used for DFWM. The two common geometries are forward-wave geometry. (also known as folded boxcars geometry) and the counter propagating, backward-wave geometry. Figure 6.1 shows the schematic of the forward-wave geometry. The three input beams labeled 1,2 and 3 are incident on the sample, with the beam labeled 4 being the output beam, generated by the input beams according to the susceptibility of the material $\chi^{(3)}$. One of the incident beams is time delayed relative to the other beams which are coincident in time. The four beams shown in Figure 1 are emerging

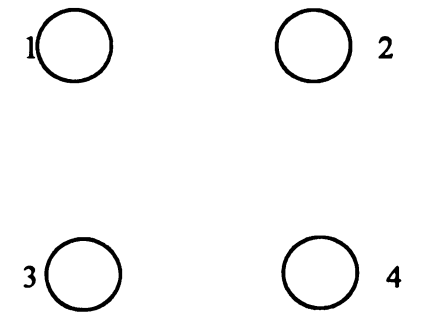


Figure 6.1. Schematics of the optical beam geometry in the plane of the sample for the folded boxcars geometry.

from the sample. The generated beam 4 is spatially separated from the intense incident beams and subsequently detected.

In the backward-wave geometry two beams called the forward (E_f) and backward (E_b) are counter propagating and the third beam called the probe (E_p) is incident on the sample at small angle θ with respect to E_f . For a pulsed laser experiment the pulses are split, each passing through a separately adjustable delay line, and meet at the sample in a backward-wave geometry. Beams E_f and E_p are synchronized in time by their cross correlation. Then the DFWM signal is studied as a function of time delay of the backward beam E_b . The DFWM signal obtained from the sample is compared with that obtained from CS_2 or some other reference by using the same power level. The $\chi^{(3)}$ value is then obtained by using the following equation for the case of a nonabsorbing sample^[1]

$$\frac{\chi_{sample}^{(3)}}{\chi_{reference}^{(3)}} = \left(\frac{\eta_{sample}^{o}}{\eta_{reference}^{o}}\right) \frac{\ell_{reference}}{\ell_{sample}} \sqrt{\frac{I_{sample}}{I_{reference}}}$$
[3]

where $\eta_{reference}$ and η_{sample} are the linear refractive index of reference and sample, respectively; $\ell_{reference}$ and ℓ_{sample} are the path lengths of reference and sample, respectively; $I_{reference}$ and I_{sample} are DFWM signal of reference and sample, respectively.

6.2. Experimental

The laser system employed in this experiment is a cavity dumped dye laser pumped by the second harmonic of Quantronix CW mode locked Nd:YAG laser. To cover the spectrum below the excitonic resonance in PDAs, the laser dyes DCM, LDS698, and LDS 722 were used which provide a tuning range from 650 to 750nm. The pulse width of the dye laser is ~5ps. The output of the laser was used as described in the introduction in a folded boxcars configuration. One of the three beams was chopped at a frequency of about 2KHz. The signal generated from DFWM would be detected with a photodiode or a photomultiplier and the output sent to a lock in amplifier.

6.3. Discussion

Many DFWM investigations of nonresonant $\chi^{(3)}$ are based on pumping the ground state to some virtual state. Pictorially this can be described as in Figure 6.2. If ΔE can be made

equal to the energy difference between the vibrational ground state and the excited state (Figure 6.2) it is possible to observe coupling between the vibrational and electronic

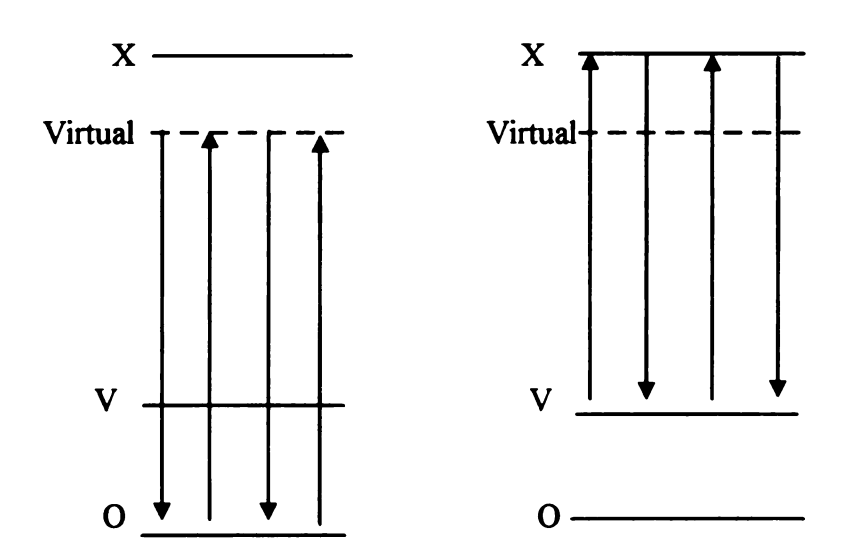


Figure 6.2. DFWM schematic energy level for the experiments.

resonance. It is expected that both the DFWM and the electronic-vibrational coupling would contribute to the observed $\chi^{(3)}$. That is

$$\chi_{observed}^{(3)} = \left| \chi_{DFWM}^{(3)} + \chi_{e-v}^{(3)} \right|$$
 [4]

In this case $\chi_{e-v}^{(3)}$ would be resonant and would be given by

$$\chi_{e-v}^{(3)} = \frac{k}{\omega_p - (\omega_x - \omega_v) - i\gamma_{ov}}$$
 [5]

where
$$k \propto \langle v | \mu^2 | x \rangle^2$$

We expect the value of ω_p - (ω_x - ω_v) ≈ 0 , hence even small k would result in a big $\chi_{e-v}^{(3)}$. The transition cross section for the v-x transition can be measured experimentally using inverse Raman scattering. The nonresonant $\chi_{DFWM}^{(3)}$ would be given approximately by

$$\chi_{DFWM}^{(3)} = \frac{k'}{\omega_p - \omega_x - i\gamma_x}$$
 [6]

and $|\omega_p - \omega_x| >> 0$, hence even if k' is large the denominator is also big, the value of $\chi_{DFWM}^{(3)}$ is expected to be small.

6.3.1. Unit conversions: $\chi^{(3)}$ values are reported in the literature in esu, which are cm⁴/sC². In order to calculate an expected E₄ for this experiment, we convert $\chi^{(3)}$ to SI units. We include this information to serve as a useful guide in the conversion between the two systems.

$$\chi_{esu}^{(3)} = \frac{Cn^2}{32\pi^2} \left(\frac{\lambda_o \omega_o^2}{2a\ell} \right) \left(\frac{45}{8} \frac{1}{M} \frac{E_4}{E_1 E_2 E_3} \right)^{\frac{1}{2}}$$
 [7]

[8]

$$\chi_{SI}^{(3)} = [factor]\chi_{esu}^{(3)}$$

$$\frac{C^4 m}{J^3} = \left[factor\right] \frac{cm^4}{sC^2} \left(\frac{1m}{1000cm}\right)^4 \left(\frac{1sC}{5.336X10^{-10}C}\right)^2 \chi_{esu}^{(3)}$$

 $[factor] = (4\pi\varepsilon_o)^3 \left(\frac{C^2}{Jm}\right)^3$

$$\chi_{SI}^{(3)} = 4.84 X 10^{-20} \chi_{esu}^{(3)}$$

Table 6.1. Conversion table between $\chi_{esu}^{(3)} \left(\frac{cm^4}{sC^2} \right)$ and $\chi_{SI}^{(3)} \left(\frac{C^4m}{J^3} \right)$.

$\chi_{esu}^{(3)} \left(\frac{cm^4}{sC^2} \right)$	$\chi_{SI}^{(3)} \left(\frac{C^4 m}{J^3} \right)$
10 ⁻⁹	4.84 x 10 ⁻²⁹
10 ⁻¹⁰	4.84 x 10 ⁻³⁰
10 ⁻¹¹	4.84 x 10 ⁻³¹

6.3.2. Magnitude of the expected signal

The $\chi^{(3)}$ in SI units where all quantities are evaluated in SI units is given by

$$\chi_{SI}^{(3)} = (4\pi\varepsilon_o)^2 \frac{Cn^2}{32\pi^2} \left(\frac{\lambda_o \omega_o^2}{2a\ell}\right) \left(\frac{45}{8} \frac{1}{M} \frac{E_4}{E_1 E_2 E_3}\right)^{\frac{1}{2}}$$
[10]

where c is the speed of light (3 x 10⁸ ms⁻¹); n is the linear refractive index of our sample (n = 3); λ_o is the incident wavelength (650nm); ω_o is the beam waist at focus ($\approx 20 \text{ x } 10^{-6} \text{m}$); a is characteristic pulse width (0.2 x 10¹²s⁻¹); ℓ is the effective interaction length in the Crystal ($\approx 10^{-7} \text{m}$); M is a factor that corrects for reflection (M ≈ 1); E₁, E₂ and E₃ are the incident pulse energies ($\approx 1.25 \text{ x } 10^{-9} \text{ J/pulse}$, peak power). Substituting these values and rearranging the above equation to solve for E₄ would yield

$$E_4 = \left(2.71X10^{24} \chi_{SI}^{(3)}\ell\right)^2$$
 [11]

for $\ell=1000\text{\AA}\ (10^{-7}\text{m})$ and different values of $\chi^{(3)}$ the average and peak E₄ powers are given in Table 6.2.

Table 6.2. Average and peak E₄ values for $\ell = 10^{-7}$ m and different $\chi^{(3)}$ values.

$\chi_{SI}^{(3)} \left(\frac{C^4 m}{J^3} \right)$	ℓ (m)	E ₄ (J/pulse)	E ₄ (W)(peak power)
4.84 x 10 ⁻²⁹	1 x 10 ⁻⁷	1.72 x 10 ⁻²²	3.44 x 10 ⁻¹¹
4.84 x 10 ⁻³⁰	1 x 10 ⁻⁷	1.72 x 10 ⁻²⁴	3.44×10^{-13}
4.84 x 10 ⁻³¹	1 x 10 ⁻⁷	1.72 x 10 ⁻²⁶	3.44 x 10 ⁻¹⁵

6.3.3. Expected Signal to Noise ratio

Calculation of the signal to noise ratio for $\chi^{(3)} = 10^{-10}$ esu and film thickness 10^{-7} m is shown below.

Average power = 30 mW

Peak power = 750 W

 $E_4 = 3.44 \times 10^{-13} \text{ W}$ (peak power, signal from DFWM) (from table 6.2).

Thus, for 1sec integration time

Number of signal photons = 5.63×10^{-6} photons

Number of noise photons = 1.23×10^{10} photons (assuming noise is limited by shot noise on any of the incident lasers).

Noise =
$$\sqrt{1.23X10^{10}}$$

$$\frac{Signal}{Noise} = \frac{5.53X10^{-6}}{\sqrt{1.23X10^{10}}} = 5.07X10^{-11}$$

The main reason we could not see signal were attributable to the low laser power and very large scattering. This experiment could be made a success by using a powerful laser or by amplifying the laser pulse to make the peak power very large.

Literature Cited

- 1. P. N. Prasad, D. J. Williams, Introduction to Nonlinear Optical Effects in Molecules and Polymers, Wiley Interscience, 1991.
- 2. Y. R. Shen, Principles of Nonlinear Optics, Wiley Interscience, 1984.
- 3. J. S. Shirley, R. J. Hall, A. C. Eckbreth, Opt. Lett., 5, 380(1980).

Chapter 7

Suggested Future Studies

This dissertation has discussed the relevance of optical energy storage on the side groups of polymeric materials to act like an "optical capacitor". The energy deposited on the side groups was found to migrate to the polymer backbone in less than 10ps, our instrument response time. [1,2] Even though not successful in storing energy, this work has demonstrated that the side groups can be used for triggering the optical response of the polymer backbone. This project can be extended to investigate if the time required for the energy to migrate from the side group to the polymer backbone can be increased by increasing the number of CH₂ spacers between the side group and the polymer backbone. However, even though the time required for the energy to migrate would increase, this might be accompanied by the addition of a very large number of structural conformers when the crystal is formed. Such structural complexity could easily serve to obscure the desired goal of controlling excitation transport.

One of the main requirements for optical switching is a large third order nonlinearity. The material of choice was poly(4BCMU) as it can be prepared in wide range of morphologies varying from crystalline to amorphous material. The large $\chi^{(3)}$ requirement for optical switching can be superseded if an efficient switching scheme and a material that can be tailored easily to a specific switching application are found. In this dissertation, we have

shown that inverse Raman scattering (IRS) could be used as an efficient switching scheme as it is very sensitive to subtle structural changes of materials. ^[3] In addition, it was found that the change in the magnitude of $\chi^{(3)}$ in going from crystalline to spin cast material was small. This is due to the very large increase in the transition cross section in the spin cast film. This small decrease in the observed $\chi^{(3)}$ is due to the loss of alignment of the chromophores. The nonlinearity lost to the misalignment of chromophores can be largely restored by stretch alignment. We have investigated stretch alignment using a polymer substrate FEP. ^[4] Even though a portion of the nonlinearity was restored it is limited by the stretching ratio attainable with the FEP polymer. This project can be extended to investigate other polymer substrates with higher stretching ratios the best candidate being polyethylene terphthalate. To observe a substantial restoration of nonlinearity a stretching ratio of ~10 will likely be necessary. This project is underway in our laboratory.

Conjugated polymers have received much attention from nonlinear optics community for potential applications in optical switching. It is the delocalized electrons which are the basis for the observed nonlinearity. Buckminsterfullerenes (C_{60} and C_{70}) are similar materials containing highly delocalized electrons and so are also interesting candidates in view of their expected nonlinearity. The large number of papers appearing on the nonlinear behavior of C_{60} and C_{70} show that these materials are attracting attention in the nonlinear optics community. [5-10] The future success of $\chi^{(3)}$ nonlinear optical signal processing will, however, depend on the identification of viable switching strategies in concert with novel approaches that can use the modest $\chi^{(3)}$ nonlinear responses characteristics of organic materials.

Literature Cited

- 1. S. A. Hambir, T. Yang, G. J. Blanchard and G. L. Baker, *Chem. Phys. Lett.*, 201, 521(1993).
- 2. S. A. Hambir, G. J. Blanchard and G. L. Baker, Appl. Spec., 49, 374(1995).
- 3. S. A. Hambir, G. J. Blanchard and G. L. Baker, J. Chem. Phys., 102, 2295(1995).
- 4. S. A. Hambir, D. Wolfe, G. J. Blanchard and G. L. Baker, in preparation.
- 5. W. J. Blau, H. J. Byrne, D. J. Cardin, T. J. Dennis, J. P. hare, H. W. Droto, R. Taylor, and D. R. M. Walton, *Phys. Rev. Lett.*, 67, 1423(1991).
- 6. R. J. Knize and J. P. Partanen, Phys. Rev. Lett., 68, 2704(1992).
- 7. Z. H. Kafafi, F. J. Bartoli, J. R. Lindle, and R. G. S. Pong, *Phys. Rev. Lett.*, 68, 2705(1992).
- 8. Z. H. Kafafi, J. R. Lindle, R. G. S. Pong, F. J. Bartoli, L. J. Lingg, and J. Milliken, *Chem. Phys. Lett.*, 188,492(1992).
- 9. H. Hoshi, N. Nakamura, Y. Maruyama, T. Nakagawa, S. Suzuki, H. Shiromaru, and Y. Achiba, *Jpn. J. Appl. Phys.*, **30**, L1397(1991).
- 10. Z. Shang, D. Wang, P. Ye, Y. Li, P. Wu, and D. Zhu, Opt. Lett., 17, 973(1992).

